# Study on Solution-Based Formation of Device-Element Thin Films at Low Temperatures

**2012.09**

**Jinchun Piao**

# Contents

# Chapter 1
# General introduction

## 1.1 Large-area display development

Since the black and white CRT TV was invented in 1897, TV has been evolved into new formation with history over 100 years (as shown in Fig. 1.1). The history of TV is showing big changes of TV so far. TV evolved from black and white to full color, from small size to large, from analogue to digital, and from CRT to flat thin TV. Large area display has become thinner and larger.

The appearance of OLED (organic light emitting diodes) display has created new histories. Comparing with inorganic materials, organic materials in devices is not having long history. Since organic single crystals were reported in 1960s, electroluminescence from small molecule OLED was reported 49 years ago [1.1)] and that from polymer OLED 29 years ago [1.2)]. It was the development of thin film heterojunction devices using molecule materials that rekindled interest in the field in the late 1980s, and it was the ability to fabricate large area devices with high yields that led to the more recent widespread commercialization of OLED in displays. Fig. 1.2 shows the history of OLED displays. OLED displays were commercialized as MP3 and cell phone displays in the late of 1990s. As large area displays, i.e. TV displays were commercialized in 2000s.

The rapidly accelerating deployment of OLED displays in portable electronic devices

and the introduction of a 55-inch-diagonal, 1 mm thick OLED television indicate that many of the manufacturing issues are finally controlled [1.3)].

Fig. 1.3 shows this year's commercialized OLED TV. In this year's Consumer Electronic Show (CES 2012), LG's 55-inch 55EM9600 OLED TV wins best product. This OLED TV has wide viewing angles and lightning-fast response times, only 4 mm depth and boasts a bezel around the screen just 1 mm wide.

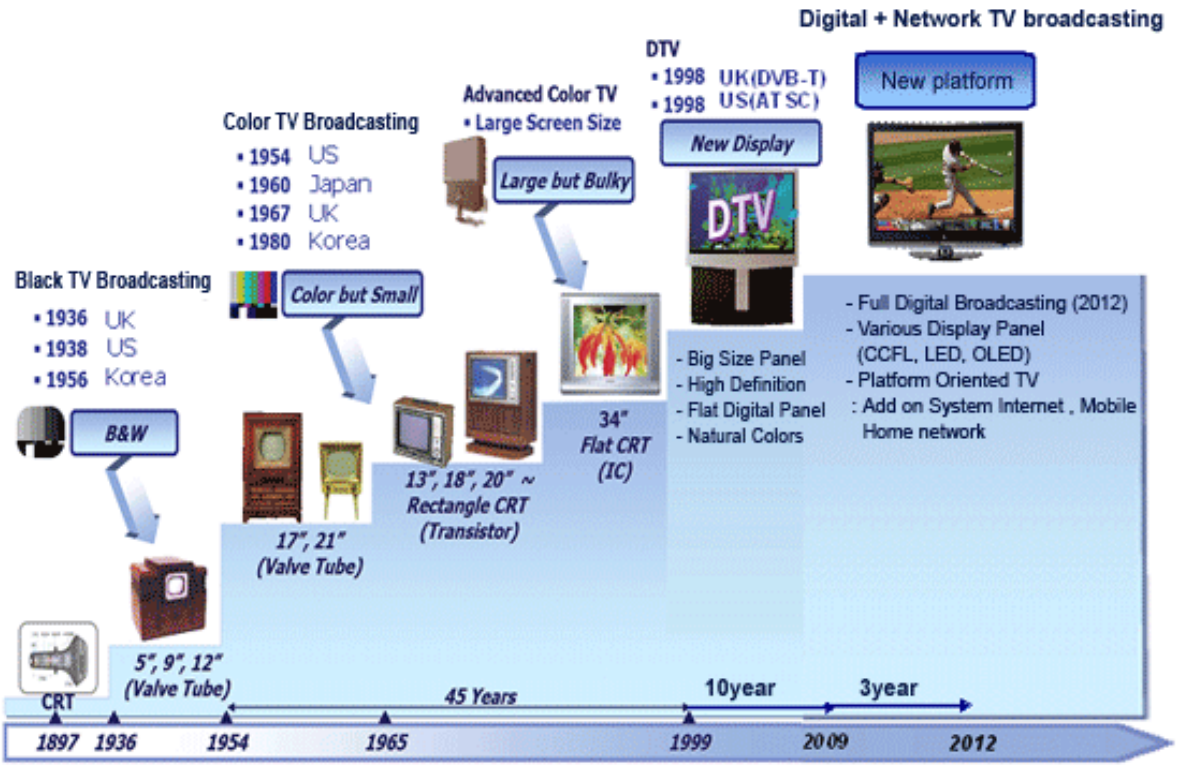


Figure 1.1 Large-area display histories.

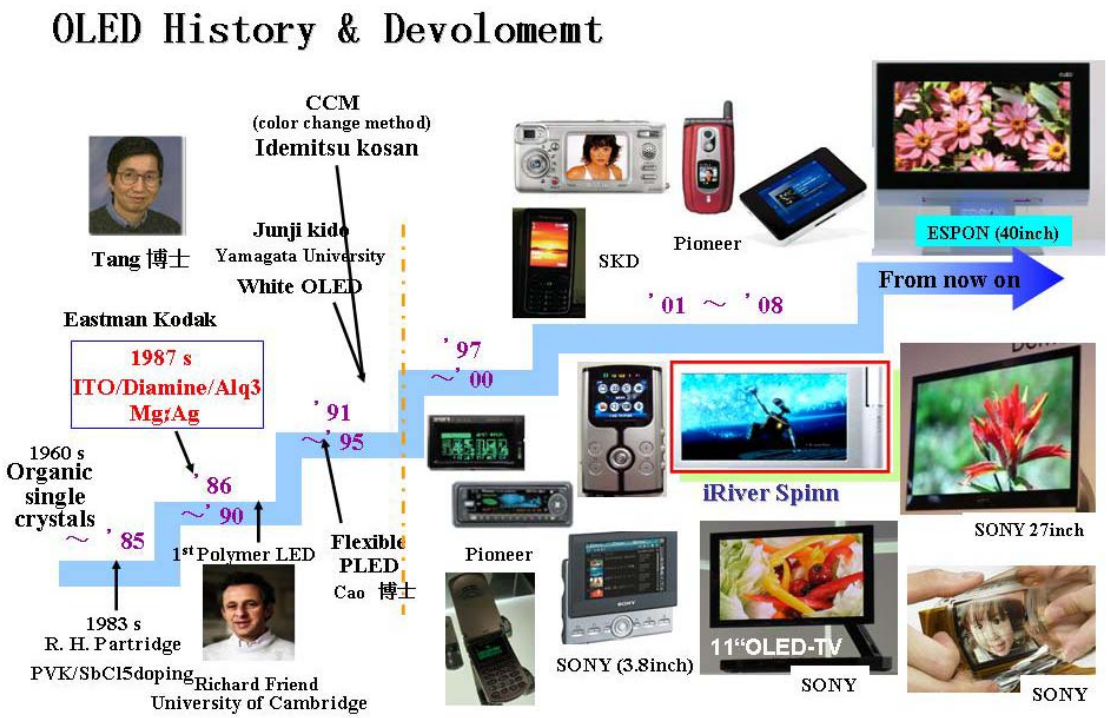


Figure 1.2 OLED display histories.

Figure 1.3 LG's 55-inch 55EM9600 OLED TV.

## 1.2 Pixels in organic displays

In organic displays, the pixels can be classified two parts: one is organic electroluminescence (EL); another one is organic thin film transistor (TFT) (as shown in Fig. 1.4). The emitting color was controlled by controlling RGB colors in pixels. In organic TFT, organic thin films were fabricated on insulator films, as example, deposited on silicon oxide thin films.

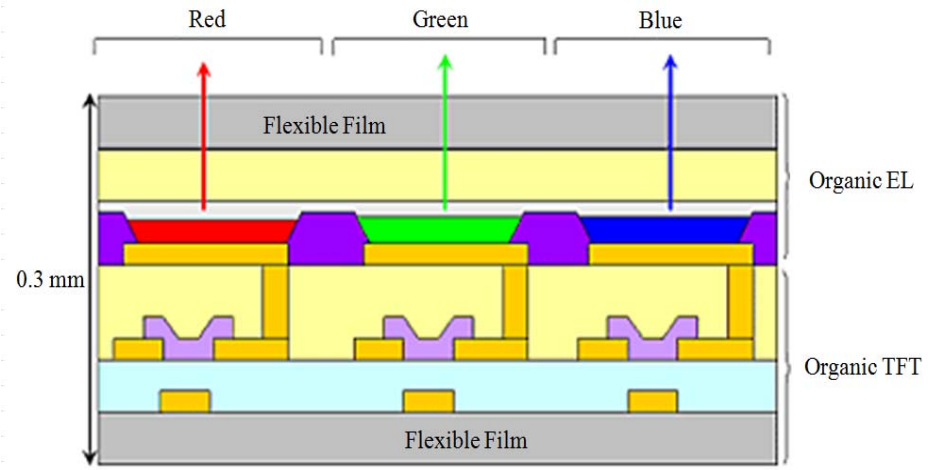


(a)

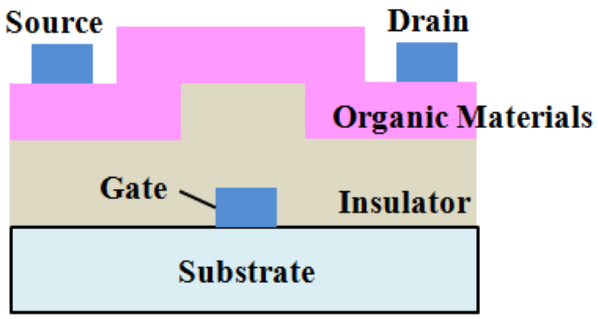


(b)

Figure 1.4 (a) Pixels in organic displays, and (b) schematic cross section of organic TFT.

### 1.2.1 Materials in organic EL

The device structure of OLED consists of several layers of organic materials sequentially deposited on glass substrate, each layer having a specific purpose that serves to enhance device quality and performance. The schematic representation of an ideal/standard OLED device is shown in Fig. 1.5.

Electron injection layer (EIL) creates a resistive contact between the metal and the organic layers. For example, when Aluminum was used as cathode materials, LiF generally was used as the EIL materials.

Electron transport layer (ETL) transports electrons, and tris (8-hydroxyquinolline) Aluminum ($Alq_3$) and bis (8- hydroxyquinolline) zinc ($Znq_2$) were well known as the ETL materials. To prevent diffusion of holes into the electron transport layer, hole blocking layer was sandwiched between ETL layer and Emission layer (EL). Poly ((((2-ethylhexyl) oxy) methoxy - 1, 4 -phenylene) -1, 2- ethenediyl) (MEH-PPV), $Alq_3$, $Znq_2$, bis (2- methyl -8- quinolinolato) – 4 - phenylphenolate aluminum ($BAlq_2$), 2, 9-dimethyl -4, 7- diphenyl-1, 10- phenanthroline (BCP), and 4, 4'- bis (2, 2-diphenylvinyl)-1, 1'- biphenyl (DPVBi) etc. were well known as the hole blocking materials.

In emission layer, electrons and holes were recombined and generate light to emit, and luminescent materials in electronically were used, such as $Znq_2$ (yellow), $Alq_3$ (green), tris (2-phenylpyridinato-C2, N) iridium ($Ir(ppy)_3$, green), tris (2-(4, 6-diflurophenyl) lpyridinato-C2, N) iridium (Ir $(Fppy)_3$, blue), and MEH-PPV (orange) etc.

Hole transport layer (HTL) transports holes to emission layer, and N, N' - bis

(3-methylphenyl)- N, N'- bis (phenyl)-benzidine (TPD), N, N'- bis (naphthalen-1-yl)-N, N'-bis (phenyl)- benzidine (α-NPB), 4, 4'- bis (carbazol-9-yl) biphenyl (CBP), N, N'-bis (3- methylphenyl)-N, N'-bis (phenyl)-9, 9- spirobifluorene (spiro-TPD), and 4, 4', 4''- tris (3- methylphenyl (phenyl)- amino) triphenylamine (m-MTDATA) were used as HTL materials.

In OLED structure, hole injection layer (HIL) controls injections of holes and smooth the anode surface. Copper phthalocyanine (CuPc), Titanyl phthalocyanine (TiOPc), and N-2-naphthalenyl-N, N- bis (4-(2-aphthalenyl phenyl amino) pheny) N-phenyl) N-phenyl -1, 4- benzenediamine (2-TNATA) were well known as HIL materials [1.4-1.26)]. Fig. 1.6 shows chemical structures for some OLED materials.

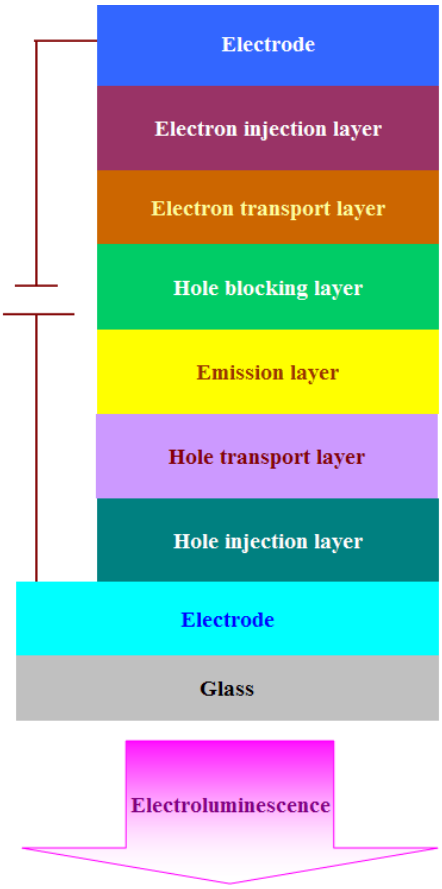


Figure 1.5 Schematic illustration of multi-layer structure of OLED.

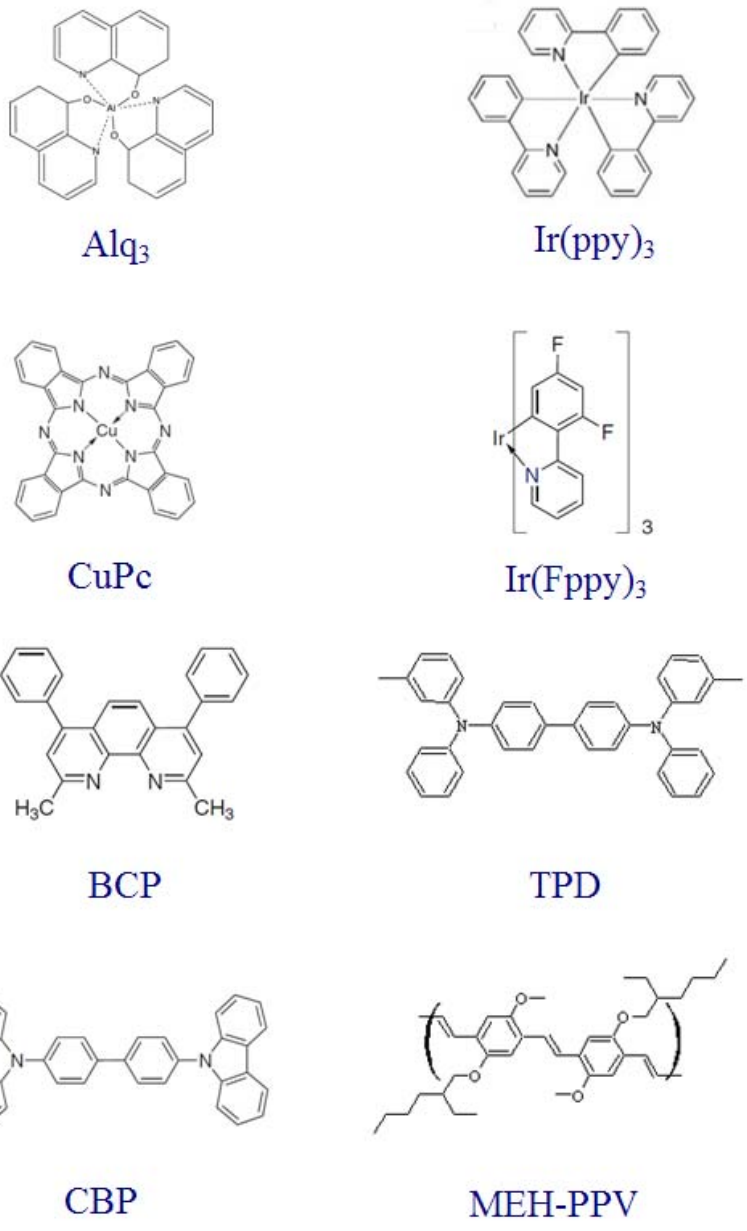


Figure 1.6 Chemical structures of some OLED materials.

### 1.2.2 Silicon oxide thin films

Over the past few decades, interest in transparent, thin silicon coatings have increasingly grown for several applications like optics, interlayer dielectrics, and barrier films for the food packaging and medical device industries. Silicon oxide thin films are undoubtedly the most important and widely used insulating films in modern electronic circuit devices. Excellent electrical insulating characteristics of silicon oxide thin films grown by thermal oxidation of silicon (Si) have supported high performance large scale integrated circuit (LSI) devices.

On the other hand recent demands for environmentally friendly, lightweight, and mobile devices require evolution of device processes at low temperature in order to meet the required use of plastic substrates or films. In addition, low temperature grown silicon oxide thin films are also highly expected as barrier films against gas and vapor diffusion for food-packaging and medical devices industries [1.27-1.30)] , owing to the transparency, recyclability, and microwave endurance of silicon oxide, as a candidate substituting thin metal (generally aluminum-based metals) coating.

For low temperature growth of silicon oxide thin films, vacuum based processes such as vacuum evaporation and sputtering have generally been used, but for electrical applications on large area substrates in mass production, especially on films by a continuous process flow like a roll-to-roll process, it is desirable to use vapor phase growth processes like chemical vapor deposition (CVD). In the CVD process, silane ($SiH_4$) and tetra ethyl ortho silicate (TEOS) have been the well known source materials for the growth of silicon oxide thin films. However, $SiH_4$ is flammable and dangerous in use, and TEOS, though it is a relatively inexpensive and safe source for

silicon, requires high temperature, for example, 600 $^{o}$C, which does not meet the growth on plastic substrates.

In our experiments we used polysilazane, inorganic polymer, as a source material for the CVD growth of silicon oxide. Focused on low temperature growth by using mist CVD process, without additional processes, we successfully fabricated silicon oxide thin films at low temperature.

## 1.3 Organic and inorganic materials in devices

Most interesting, and also wide spread, use of electronics is based on semiconductors. Materials in semiconductors are mainly classified two types, organic and inorganic materials. The nature of bonding in organic semiconductors is fundamentally different from their inorganic counterparts. Among the organic materials for electronic applications, we are mostly interested in that class which contain $\pi$ electrons. For example, consider ethylene ($C_2H_4$) molecule, in which the $sp^2$ hybridized carbon forms three co-planar $\sigma$ bonds; the carbon atom bonds with the other carbon and two hydrogen atoms. The fourth orbital ($p_z$) is perpendicular to the $sp^2$ hybridized orbital plane, and leads to additional $\pi$ bonding between the two carbon atoms. The molecular orbitals thus formed split into bonding and anti-bonding states, which commonly are also known as HOMO (highest occupied molecular orbital) and LUMO (lowest unoccupied molecular orbital), respectively (as shown in Fig. 1.7). These molecules form solids via a weak intermolecular bonding, clubbed under the name of “Van der Waal” bonds. On account of this weak bonding, although the HOMO and LUMO levels may take shape of an energy band, but the bands are rather narrow. Furthermore, consequent of

this weak intermolecular bonding is that the electronic properties of the organic solids are largely determined by the molecules themselves; role of the weak forces is only to hold the organic molecules together in a solid.

In inorganic system electronic conductivity is favored by a strong exchange interaction of atomic orbitals in a close-packed structure. A crystalline inorganic semiconductor with covalent/ionic inter-atomic bonding throughout the material, because of periodicity of the lattice, allows for a description of the electronic states in reciprocal space, k. Correspondingly, an inorganic semiconductor has an occupied valence band separated by an empty conduction band, as shown in Fig. 1.8 (a). Fig. 1.8 (b) shows simplified diagram of the electronic band structure of inorganic solids.

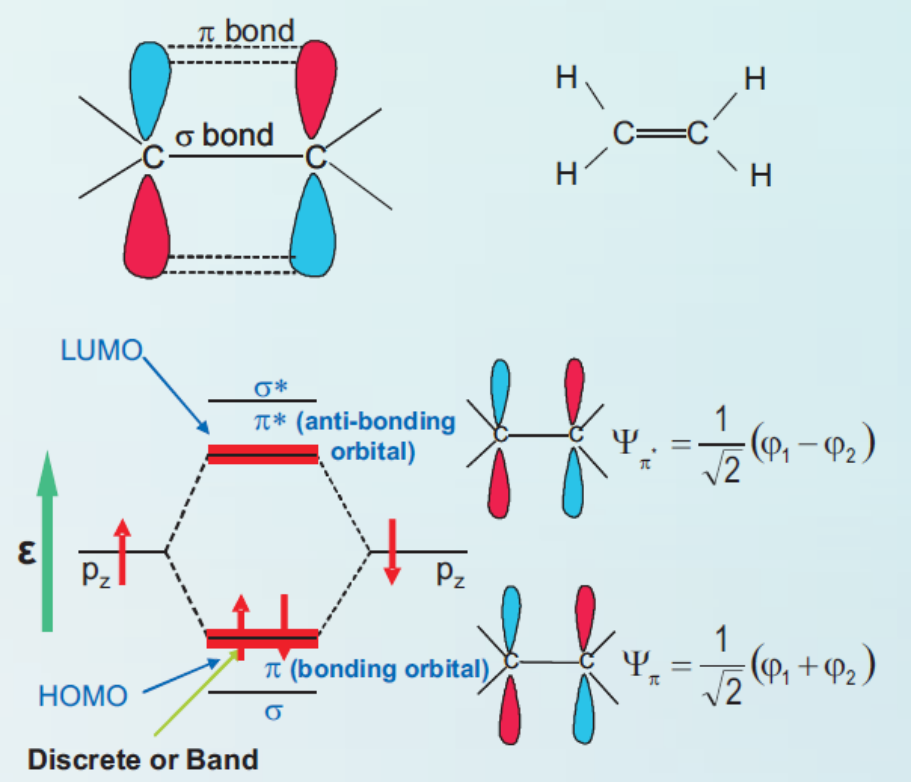


Figure 1.7 Ethylene molecule with σ and π bonds. Molecular bonding leads to bonding (occupied) and anti-bonding (empty) states, both corresponding to σ and π bonding orbitals. In solid form, the resulting HOMO and LUMO states take a form of bands, analogous to crystalline semiconductors, but the band-widths are significantly smaller.

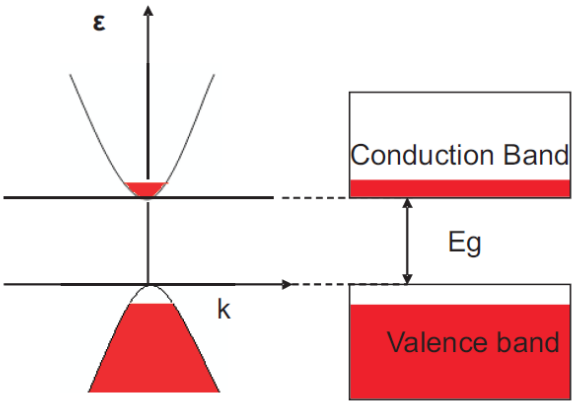


(a)

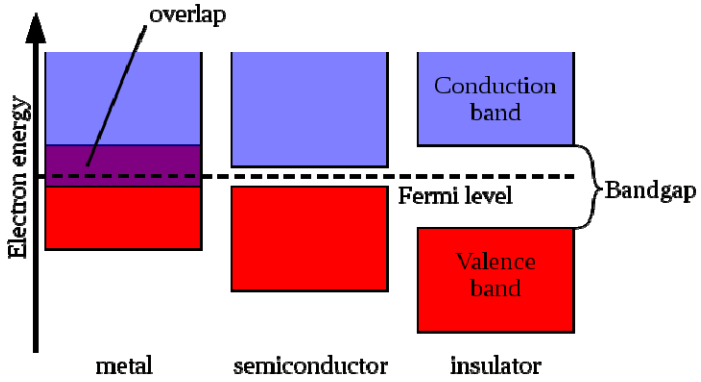


(b)

Figure 1.8 (a) Valence and conduction band in crystalline semiconductors. The valence band is completely occupied by electrons and conduction band is empty 0 K. At higher temperatures, some electrons from the valence band populate the conduction band. (b) Simplified diagram of the electronic band structure of inorganic solids.

## 1.4 Deposition process in fabrication of organic thin films

The first electroluminescence from small molecule organic light emitting diodes (OLED) was reported 49 years ago [1.1)] and that from polymer OLED 29 years ago [1.2)]. The controlled growth of highly ordered thin film either by vacuum deposition or solution process is till subject ongoing research. Owing to the strong demands from market to low cost and large area devices, together with severe competition with other physics based devices, simple, cost effective, and low energy consumption fabrication processes for EL material thin films and multilayered structures have attracted increased interest. Solution based deposition technology such as spin coating, dipping, spraying, and inkjet printing can meet the demand and marked progress has been continuing recently.

### 1.4.1 Quantum efficiency in organic materials

Because exciton formation under electrical exciton results in 25% singlet excitons and 75% triplet excitons, phosphorescent materials have been requisite for obtaining high electroluminescence (EL) efficiency in OLED. To increase internal EL efficiency, charge transfer transition in metal complexes were applied in OLED. MLCT (metal to ligand charge transfer) and/or LMCT (ligand to metal charge transfer) which transition occur in metal complexes. MLCT complexes experience a partial transfer of electrons from the metal to the ligand. Usually this occurs for metals with highly filled d orbitals capable of donating electrons into the anti-bonding orbitals of the ligand. The non-bonding d orbitals must match the anti-bonding orbitals in terms of size, shape, and

symmetry. Conversely, there can be excitation of an electron in a ligand based orbital into an empty metal based orbital LMCT. LMCT complexes experience a partial transfer of electrons from the ligand to the metal. With the controlling ligand structure or central metal atoms in metal complexes can control the color of emission. Table 1.1 shows chemical structure, absorption and emission spectrum, and emission color of Ir $(ppy)_3$ and their derivatives, $Alq_3$, and $Znq_2$ [1.4-1.17].

Heavy center metal in metal complexes can control singlet and triplet excitons, and improve the internal EL efficiency. In particular, devices containing metal complexes such as tris (2-phenylpyridinato) iridium (Ir $(ppy)_3$) and their derivatives have resulted in nearly 100% internal EL efficiency by harvesting both singlet and triplet excitons [1.31, 1.32]. Until now, phosphorescence has been considered the sole solution for high efficiency OLED. Adding phosphorescent dyes (metal complexes) or synthesizing organic molecular with relatively small energy band gap between its single and triplet excited states can improve the efficiency in OLED [1.33].

| Metal complexes | Chemical structure | Absorption spectrum (nm) | Emission spectrum (nm) | Emission color |
|---|---|---|---|---|
| tris(2-phenylpyridinato -C2,N)iridium $Ir(ppy)_3$ | 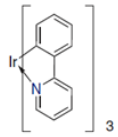 | 282 | 510 | Green |
| tris(2-(4,6-difluorophenyl) lpyridinato-C2,N)iridium $Ir(Fppy)_3$ | 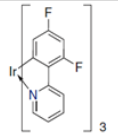 | 347 | 471 | Blue |
| tris(1-phenylisoquinolinato -C2,N)iridium $Ir(piq)_3$ | 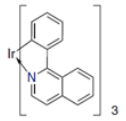 | 324 | 615 | Red |
| tris(8-hydroxyquinolline) Aluminum $Alq_3$ | 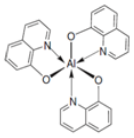 | 259 | 512 | Green |
| bis(8-hydroxyquinolline) zinc $Znq_2$ | 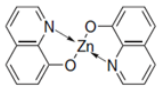 | 251 | 478 | Yellow |

Table 1.1 Chemical structure, absorption and emission spectrum, and emission color of Ir (ppy) $_3$, Ir (Fppy) $_3$, Ir (piq) $_3$, $Alq_3$, and $Znq_2$.

### 1.4.2 Solution process using small molecules

OLED have drawn intense attention during the past decades due to their potential applications in solid state lighting and flat panel displays [1.34-1.39]. Generally, there are two approaches to fabricate devices: for OLED based on small molecules, the standard fabrication method is vapor deposition under vacuum; for polymeric materials, simple solution process such as spin coating or inkjet printing can be utilized. Small molecules have advantages such as easy synthesis and purification, and the vapor deposition techniques allow the fabrication of complicated multiple layers with excellent device performance. However, thermal evaporation process under high vacuum increases fabrication complexity and makes the utilization of the expensive OLED materials very low (~20%) [1.40]. Additionally, pixilation using evaporation masks would limit its scalability and resolution.

The best way to improve the efficiency of the process and reduce the production cost is to use solution process for the fabrication of OLED. For example, inkjet printing can be effectively used to fabricate large area, high resolution, full color, and flat panel displays [1.41]. On the other hand, although light emitting polymers are considered to be suitable for solution process, their performances are lower than vacuum deposited small molecules. The efficiency and lifetime of polymer based devices need to be further improved for applications in commercial active-matrix OLED devices, while there are some intrinsic difficulties such as the control of batch-to-batch variations and the purification of the polymeric materials. Therefore, it is a good strategy to develop OLED based on solution process using small molecules, which would open up exciting possibilities for commercialization of printed OLED for displays and lighting.

However, unfortunately, a large majority of the small molecules designed for vacuum deposition are not suitable for the solution process, such as $Alq_3$.

About two decades have elapsed since $Alq_3$ appeared as a milestone for the development of OLED [1.42)]. $Alq_3$ still one of the most stable and fluorescent solid state materials, making it as the emitting material and electron transport layer (ETL). Subsequently, quinolate metal complexes have become a very important class of electroluminescent material in OLED [1.43-1.45)].

To fabricate OLED by solution process, the principal interest in the use of soluble $Alq_3$ complex derivatives lies in the scope for low cost manufacturing, such as spin coating. However, most structurally modified $Alq_3$ derivatives become less stable than $Alq_3$. Up to now, several attempts have been reported to dissolve $Alq_3$ complex and their derivatives in tetrahydrofuran (THF), dimethylforamide (DMF), or dimethylsulfoxide (DMSO) [1.46-1.48)]. However, these materials are not environmentally friendly materials. In our experiments, we used $Alq_3$ as materials and methanol as the solvents.

## 1.5 Deposition process in fabrication of silicon oxide thin films

Silica coating films have a variety of applications as electric insulating coatings, protective barriers against oxidation, corrosion, and scratching for metallic materials, passivation films for semiconductors, coatings on glass for preventing alkali-dissolution, and antireflection coatings. Various techniques have been used thus far in preparing silica coating films, such as vacuum deposition (CVD), sol-gel method using alkoxides, liquid phase deposition (LPD), and electrophoresis [1.49-1.63].

### 1.5.1 Materials in silicon oxide thin film fabrication

Generally, the silicon oxide films are deposited by thermal oxidation with a high temperature of nearly 1000 °C. An excessively high deposition temperature would lead to defect formation and diffusion, such as vacancies, self-interstitial atoms and dislocation. Therefore, it is necessary to applying low temperature deposition method for fabrication of silicon oxide films.

For low temperature growth of silicon oxide thin films, vacuum based processes such as vacuum evaporation and sputtering have generally been used, but for electrical applications on large area substrates in mass production, especially on films by a continuous process flow like a roll-to-roll process, it is desirable to use vapor phase growth processes like chemical vapor deposition (CVD). In the CVD process, silane ($SiH_4$) and tetra ethyl ortho silicate (TEOS) have been the well known source materials for the growth of silicon oxide thin films. However, $SiH_4$ is flammable and dangerous in use, and TEOS, though it is a relatively inexpensive and safe source for

silicon, requires high temperature, for example, 600 $^{o}$C, which does not meet the growth on plastic substrates.

Recently it becomes possible to fabricate silica glass coatings onto various kinds of materials by heating coated polysilazane films. To produce high quality silica glass coatings from the polysilazane precursor, heating processes above 600 $^{o}$C are necessary.

### 1.5.2 Deposition processes for silicon oxide thin film fabrication

As mentioned above, to produce high quality silica glass coating from the polysilazane precursors, heating processes above 600 $^{o}$C are necessary. Lowering of the process temperature is necessary for fabricating high quality silica glass coatings onto thermally unstable substrates such as plastics or semi-conductive devices.

C. Kato et al. successfully demonstrated a room temperature photochemical fabrication of silica glass coatings by utilizing a vacuum ultraviolet (VUV) light irradiation [1.63)]. V. S. Kortov et al. performed with $SiO_2$ samples through the thermal decomposition of polysilazane in air [1.64)]. In their reports, heating of polysilazane to T = 600 °C for 48 hours in air resulted in the chemical reaction and create silicon dioxide films. T. Kubo et al. reported that through soaking in hot water polysilazane films can be converted to silica films [1.65)]. From their paper, we can conclude soaking polysilazane films in 25 °C water for 24 hours can create silica films. Long fabrication time is not suitable for device process. In our experiments, a little arranged these fabrication methods. We shortened fabrication time to 1 hour and controlled growth temperature under 350 °C.

## 1.6 Objective and outline of this thesis

As mentioned earlier, organic materials and silicon oxides are very important materials in devices. Because of the strong market demands for low cost and large area devices, together with severe competition with other physics based devices, simple, cost effective, and low energy consumption fabrication processes for organic electroluminescence (EL) material thin films and multilayered structures have attracted increased interest. Solution based deposition technologies such as spin coating, dipping, spraying, and inkjet printing can meet the demands and their marked progress has been continuing recently.

However, solution based technologies require the materials to be dissolved in suitable volatile solvents such as alcohol. Actually, it is difficult to find novel solvents for many useful and conventional organic EL materials that are known to exhibit high efficiency and long term EL, such as $Alq_3$, and we must apply vacuum evaporation for the fabrication of their thin films even though it possesses several problems against large area, low cost, and flat panel devices. In our research, found the application of high ultrasonic power is effective to prepare a solution of $Alq_3$ in methanol.

This thesis consists of six chapters.

In chapter 1, the general introduction including the research background, motivation and purpose is presented; following a basic understanding of solution based thin film formation at low temperature.

In chapter 2, I will introduce two kinds of fabrication methods. One is ultrasonic spray-assisted vapor deposition method. This method can be used in the fabrication of organic thin films. Controlling the concentration of solution and scanning speed, can control the thickness of thin films. Another is mist CVD method. Carrier gas carried polysilazane particles to substrate area and react with ozone gas create silicon oxide thin films on substrates. Controlling ozone gas flow rates, growth temperature, and grown time can control the fabrication of silicon oxide thin films.

In chapter 3, I will present the preparation of $Alq_3$/methanol solution and polysilazane solution. When preparing $Alq_3$/methanol solution, we applied high ultrasonic power to the mixture of $Alq_3$ and methanol. Nuclear magnetic resonance (NMR) study of $Alq_3$/methanol solution means $Alq_3$ atoms have no serious damages even after high ultrasonic power. Because polysilazane, purchased from Exousia Inc., were diluted in oxylene, we have to pay attention to chemical reaction when choosing solvents. Considering solubility in oxylene and polysilazane, stability in solution, and environmentally friendly, we choose methyl acetate as the solvents.

In chapter 4, we firstly fabricated $Alq_3$ thin films on glass substrates in order to confirm the impact of making the $Alq_3$ containing solution. Secondly, we deposited $Alq_3$ thin films on indium tin oxide (ITO) to show the potential application of the mist deposition method for future device fabrication. Despite of the flat surface, the current density in $Alq_3$ thin films is low. Maybe it is caused by low carrier density, or maybe caused poor film structure originating from the mist deposition technology. To clear these reasons, we continued the two sets of experiments, that is, the fabrication and

electrical characterization of a MEH-PPV thin film and $Alq_3$/TPD structure.

In chapter 5, I will report the challenge to deposit SiOx thin films by using mist CVD method at low temperature. The source material is inorganic polymer, names polysilazane, $(R_1R_2Si\text{-}NR_3)_n$. Polysilazane can react with oxide atoms, making silicon oxide thin films on substrates. Comparing with $SiH_4$ and TEOS, polysilazane is a safe material and can be deposited at low temperature. We already deposited SiOx thin films on flexible polyimide (PI) substrates at 200 $^oC$. In order to decrease the refractive index, we applied annealing treatments, ozone annealing and hot water annealing treatments. Through annealing treatment, the refractive index has decreased from 1.48 to 1.45-1.46.

In chapter6, the conclusions of the study were summarized in details. In addition, the perspectives for extending the investigations of solution based thin film fabrication to large size flexible thin fabrication were given.

## References and notes


1.1) M. Rope, H.P. Kallmann, and P. Magnante: J. Chem. Phys. **38** (1963) 2042.

1.2) R.H. Partridge: Polymer **24** (1983) 733.

1.3) Fanky So, Junji Kido, and Paul Burrows: MRS Bulletin **33** (2008) 663.

1.4) V.R. Ricardo, N.Z. Francisco, and M. Emiliano: Org. Electron. **9** (2008) 625.

1.5) V.P. Barberis and J.A. Mikroyannidis: Synth. Met. **156** (2006) 865.

1.6) H. Wang, Q. Qian, K. Lin, B. Peng, W. Huang, F. Liu, and W. Wei: J. Poly. Sci. B-Poly. Phys. **50** (2012) 180.

1.7) V. Jankus, C. Winscom, and A.P. Monkman: Adv. Func. Mater. **21** (2011) 2522.

1.8) A. Endo, K. Suzuki, T. Yoshihara, S. Tobita, M. Yahiro, and C. Adachi: Chem. Phys. Lett. **460** (2008) 155.

1.9) M. Colombo, T. Brunold, T. Riedener, H. Gudel, M. Fortsch, and H. Burgi: Inorg. Chem. **33** (1994) 545.

1.10) C.H. Jonda, A. Mayer, U. Stolz, A. Elschner, and A. Karbach: J. Mater. Sci. **35** (2000) 5645.

1.11) C. Bae, S. Lee, S. Choi, and G. Kwag: Inorg. Chem. **44** (2005) 7911.

1.12) G. Xu, Y. Tang, C. Tsang, J. Zapien, C. Lee, and N. Wong: J. Mater. Chem. **20** (2010) 3006.

1.13) C. Tu, Y. Lai, and D. Kwong: IEEE Electron Device Lett. **27** (2006) 354.

1.14) Y. Okabayashi, T. Mitarai, S.Yamazaki, and R.Matsuyama: Appl. Surf. Sci. **244** (2005) 217.

1.15) T. Takayama, M. Kitamura, Y. Kobayashi, Y. Arakawa, and K. Kudo: Macromol. Rapid Commun. **25** (2004) 1171.

1.16) J. Lu, A.R. Hlil, Y. Meng, A.S. Hay, Y. Tao, M. D'Iorio, T. Maindron, J. Dodelet: J. Polymer Sci. Part A: **38** (2000) 2887.

1.17) Q. Mei, B. Tong, L. Liang, and M. Lua: J. Photochem. and Photobiology A: Chem. **191** (2007) 216.

1.18) S. Yang, Z. Xu, Z. Wang, and X. Xu: Appl. Phys. Lett. **79** (2001) 2529.

1.19) J. Wang, H. Wabg, H. Huang, and D. Yan: Appl. Phys. Lett. **87** (2005) 093507.

1.20) S. Takano, Y. Mimura, N. Matsui, K. Utsugi, T. Gotoh, C. Tani, K. Tateishi, N. Ohde: J. Imaging Tech. **17** (1991) 46.

1.21) M. Ishihara, K. Okumoto, and Y. Shirota: Org. Light-Emitting Mater. Dev. **5214** (2004) 133.

1.22) Y. Shirota, Y. Kuwabara, H. Inada, T. Wakimoto, H. Nakada, Y. Yonemoto, S. Kawami, and K. Imai: Appl. Phys. Lett. **65** (1994) 807.

1.23) TPI. Saragi, T. Fuhrmann-Lieker, and J. Salbeck: Synth. Met. **148** (2005) 267.

1.24) Y. Tao, E. Balasubra, A. Danel, B. Jarosz, and P. Tomasik: Chem. Mater. **13** (2001) 1207.

1.25) M. Carrard, S. Goncalves-Condo, L. Si-Ahmed, D. Ades, and A. Siove: Thin Solid Films **352** (1999) 189.

1.26) H. Mu, H. Shen, and D. Klotzkin: Solid State Electron. **48** (2004) 2085.

1.27) A. Erlat, R. Spontak, R. Cloarke, T. Robinson, P. Haaland, Y. Tropsha, N. Harvey, and E. Vogler: J. Phys. Chem. B **103** (1999) 6047.

1.28) K. Eun, W. Hwang, B. Sharma, J. Ahn, Y. Lee, and S. Choa: Modern Phys. Lett. B **26** (2012) 1250077.

1.29) B. Singh, J. Bouchet, Y. Leterrier, J. Manson, G. Rochat, and P. Fayet: Surf. Coat. Technol. **202** (2007) 208.

1.30) D. Howells, B. Henry, J. Madocks, and H. Assender: Thin Solid Films **516** (2008) 3081.

1.31) M.A. Baldo, D.F. O'Brien, Y. You, A. Shoustikov, M.E. Thompson, and S.R. Forrest: Nature (London) **395** (1998) 151.

1.32) C. Adachi, M.A. Baldo, M.E. Thompson, and S.R. Forrest: J. Appl. Phys. 90 (2001) 5048.

1.33) A. Endo, K. Sato, K. Yoshimura, T. Kai, A. Kawada, H. Miyazaki, and C. Adachi: Appl. Phys. Lett. **98** (2011) 083302.

1.34) C.W. Tang and S.A. VanSlyke: Appl. Phys. Lett. **51** (1987) 913.

1.35) J.H. Burroughes, D.D.C. Bradley, A.R. Brown, R.N. Marks, K. Mackay, R.H. Friend, P.L. Burns, and A.B. Holmes: Nature **347** (1990) 539.

1.36) U. Mitschke and P. Bauerle: J. Mater. Chem. **10** (2010) 1471.

1.37) R.H. Friend, R.W. Gymer, A.B. Holmes, J.H. Burroughes, R.N. Marks, C. Taliani, D.D.C. Bradley, D.A. Dos Santos, J.L. Bredas, M. Logdlund, and W.R. Salaneck: Nature **397** (1999) 121.

1.38) B.W. D'Andrade and S.R. Forrest: Adv. Mater. **16** (2004) 1585.

1.39) A. Misra, P. Kumar, M.N. Kamalasanan, and S. Chandra: Semicond. Sci. Technol. **21** (2006) R35.

1.40) H. Kim, Y. Byun, R.R. Das, B.K. Choi, and P. Ahn: Appl. Phys. Lett. **91** (2007) 093512.

1.41) T. Sonoyama, M. Ito, R. Ishii, S. Seki, S. Miyashita, S. Xia, J. Brooks, R. Kwong, M. Inbasekaran, and J.J. Brown: Idw '07 Proceedings of the 14$^{th}$ International Display Workshops **1** (2007) 241.

1.42) C.W. Tang and S.A. VanSlyke: Appl. Phys. Lett. **51** (1987) 913.

1.43) A. Curioni, M. Andreoni, and W. Andreoni: Chem. Phys. Lett. **294** (1998) 263.

1.44) F. Bai, M. Zheng, G. Yu, and D. Zhu: Thin Solid Films **363** (2000) 118.

1.45) D. Ma, G. Wang, Y. Hu, Y. Zhang, L. Wang, X. Jing, F. Wang, C. Lee, and S. Lee: Appl. Phys. Lett. **82** (2003) 1296.

1.46) J. Xie, Z. Ning, and H. Tian: Tetrahedron Lett. **46** (2005) 8559.

1.47) S. Liao, J. Shiu, S. Liu, S. Yeh, Y. Chen, C. Chen, T. Chow, and C. Wu: J. Am. Chem. Soc. **131** (2009) 763.

1.48) L. Duan, L. Hou, T. Lee, J. Qiao, D. Zhang, G. Dong, L. Wang, and Y. Qiu: J. Mater. Chem. **20** (2010) 6392.

1.49) A. Erlat, R. Spontak, R. Cloarke, T. Robinson, P. Haaland, Y. Tropsha, N. Harvey, and E. Vogler: J. Phys. Chem. B **103** (1999) 6047.

1.50) K. Eun, W. Hwang, B. Sharma, J. Ahn, Y. Lee, and S. Choa: Modern Phys. Lett. B **26** (2012) 1250077.

1.51) B. Singh, J. Bouchet, Y. Leterrier, J. Manson, G. Rochat, and P. Fayet: Surf. Coat. Technol. **202** (2007) 208.

1.52) D. Howells, B. Henry, J. Madocks, and H. Assender: Thin Solid Films **516** (2008) 3081.

1.53) S. Yang, P.T. Mirau, C. Pai, O. Nalamasu, E. Reichmanis, E. Lin, H. Lee, D.W. Gidley, and J. Sun: Chem. Mater. **13** (2001) 2762.

1.54) O.D. Sanctis, L. Gomez, N. Pellegri, C. Parodi, A. Marajofsky, and A. Duran: J. Non-Cryst. Solids **121** (1990) 338.

1.55) R.K. Brow and C.G. Pantano: in Better Ceramics through Chemistry, edited by C.J. Brinker, D.E. Clark, and D.R. Ulrich (Mater. Res. Soc. Symp. Proc. **32**, Pittsburgh, PA, 1984) 361.

1.56) K. Makita: New Ceramics **9** (1996) 33 [in Japanese].

1.57) K. Kintaka, J. Nishii, A. Mizutani, and H. Nakano: Opt. Lett. **26** (2001) 1642.

1.58) F. Roccaforte, S. Dhar, F. Harbsmeier, and K.P. Lieb: Appl. Phys. Lett. **75** (1999) 2903.

1.59) Y. Song, T. Sakurai, K. Maruta, A. Matsushita, S. Matsumoto, S. Saisho, and K. Kikuchi : Vacuum **59** (2000) 755.

1.60) M. Shirai, S. Umeda, M. Tsunooka, and T. Matsuo: Eur. Polym. J. **34** (1998) 1295.

1.61) J. Oh, H. Imai, and H.Hirashima: Chem. Mater. **10** (1998) 1582.

1.62) P.J. Mitcell and G.D. Wilcox: Nature **357** (1992) 395.

1.63) C. Kato, S. Tanaka, Y. Naganuma, and T. Shindo: J. Photopolymer Sci. Technol. **16** (2003) 163.

1.64) V.S. Kortov, A.F. Zatsepin, S.V. Gorbuno, and A.M. Murzakae: Phys. Solid State **48** (2006) 1273.

1.65) T. Kubo, E. Tadaoka, and H. Kozuka: J. Mater. Res. **19** (2003) 635.

# Chapter 2
# Mist vapor deposition method for solution based thin film fabrication

## 2.1 Introduction

Owing to the strong demands from market on low cost and large area devices, by simple, cost effective, and low energy consumption fabrication processes for thin films and multilayered structures have attracted increased interest. In organic thin film fabrication, solution based deposition technologies such as spin coating, dipping, spraying, and inkjet printing can meet the demand and they recently have shown marked progress recently [2.1-2.9]. In inorganic thin film fabrication, chemical vapor deposition (CVD) and sputtering have generally used.

In our experiments, two kinds of deposition methods were applied. One is called ultrasonic spray-assisted solution based mist deposition technology, mainly be applied to fabricate organic thin films; another is called mist chemical vapor deposition (mist CVD) method, be applied to deposit silicon oxide thin films.

## 2.2 Ultrasonic spray-assisted solution based mist deposition

### 2.2.1 Introduction

As a non vacuum and solution based vapor deposition technology, which can achieve good controllability of thin films like vapor phase deposition, we have developed a ultrasonic spray-assisted mist vapor deposition method originally developed for ferroelectric [2.10)] and zinc oxide (ZnO) [2.11-2.16)] thin films and later for organic thin films of poly (3,4- ethylenedioxythiophene) : poly (styrenesulfonate) (PEDOT : PSS) [2.17)].

The schematic system configuration for ultrasonic assisted mist deposition is shown in Fig. 2.1. As a precursor we prepared solution of target organic materials. Solvents, we chose, were the safe and environmentally friendly ones such as methanol and methylacetate rather than tetrahydrofuran and dichloroethane. Some materials, especially small molecule materials, were hard to be solved, and for these materials we added strong ultrasonic power of 20 kHz and 200 W to the solute-solvent mixture for, for example 1 hour, resulting in transparent solution [2.18-2.20)].

The solution was atomized by ultrasonic power applied to transducers (Honda Electronics HM2412), where the frequency, oscillator voltage, and current of an ultrasonic generator were set at 2.4 MHz, 26 V, and 1.3 A, respectively. The solution was atomized and mist particles consisted with the solution was generated. They were transferred by nitrogen carrier gas to the substrate area. Near the substrate surface solvent was vaporized by heat and solute deposits onto the substrate.

The mist particle size is being calculated from the empirical formula

$$d=0.34(8\pi\sigma/\rho f^2) \quad (2.1)$$

where $d$ is the number of median particle diameter in cm, $\sigma$ is the surface tension, $\rho$ is the liquid density, and $f$ is the frequency of the waves caused on the surface of liquid. When $f$ is 3 MHz, the same as that of applied ultrasonic power, then $d$ is about 2-3 μm [2.15, 2.21].

The mist particles can be flown in gas atmosphere, and are transferred with a carrier gas. This system is similar to a chemical vapor deposition (CVD) system, depositing after surface migration.

### 2.2.2 Comparison with spray deposition method

Some people confuse the mist deposition method with spray deposition method. Table 2.1 is comparing the general tendency of fundamental physics in mist deposition with spray deposition. Of course spray deposition is making marked progress overcoming the following disadvantages, but here the general tendencies are summarized.

In mist deposition, the mist particle size is about 2-3 μm. The mist particles can be flown in gas atmosphere, and are transferred with a carrier gas. This system is similar to a chemical vapor deposition (CVD) system, depositing after surface migration. In spray deposition, the particle size is typically about 10 μm and sprayed onto substrates at the velocity of 1-100 mm/s, which is too fast and there is no sufficient migration at the substrate surface. In mist deposition, most of solvents are evaporated before arriving to substrates. Deposited films can have flat surface, and this technology can

be applied to deposit layered structure. In spray deposition, droplets directly adhere to the substrates with high surface energy. The films tend to have rough surface. Mist deposition method is a good technology to control the formation of thin films.

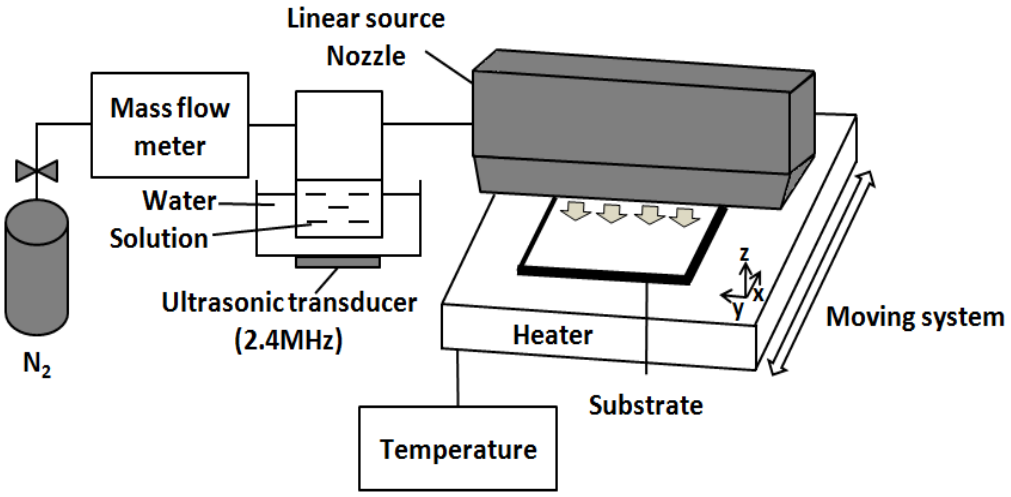


Figure 2.1 Schematic illustration of the mist deposition system.

| | **Mist deposition** | **Spray deposition** |
|---|---|---|
| Particle size | 2-3 μm | typically 10 μm |
| Particle velocity | Same as a carrier gas | 1-100 mm/s |
| Surface migration | Good | Poor |
| Multilayer deposition | Easy for successive deposition; Solvent may be the same for successive layer | Different solvents should be used for each layer in order to avoid affect on the underlying layer |
| Surface morphology | Smooth surface be expected; Owing to sufficient migration | Rough surface tends to be resulted; Owing to aggregation of incident source particles |

Table 2.1 Comparison of fundamental features of mist deposition in terms of spray deposition.

### 2.2.3 Organic thin film fabrication

In our experiments, we applied ultrasonic spray-assisted solution based mist deposition method to fabricate organic thin films. Using this technology, we successfully deposited aluminum tris (8- hydroxyquinoline) ($Alq_3$) [2.18, 2.19], and N, N' - bis (3 - methylphenyl) - N, N' - diphenylbenzidine) (TPD) [2.20] thin films. Among these materials, $Alq_3$ and TPD are key materials for organic electroluminescence (EL) devices and have not been successfully deposited by solution based processes because of their low solubility in safe organic solvents. We found that they can be solved in methanol under application of high ultrasonic power [2.18-2.20] keeping the original molecular structure [2.19]. This allowed the use of solution based vapor deposition technology, that is, mist deposition method, for the formation of their thin films, and actually uniform thin films with small root-mean-square (RMS) surface roughness of about 1 nm for the area of 500×500 nm derived by atomic force microscopy (AFM).

In chapter 4, I will discuss the details about organic thin films by using ultrasonic spray-assisted solution based mist deposition method.

## 2.3 Mist chemical vapor deposition method (mist CVD)

In fabrication of silicon oxide thin films, we used polysilazane as the reaction source. Since the vapor pressure of polysilazane is low, it cannot be transferred to the reaction area in gas phase, limiting the use as a CVD source. On the other hand, a mist CVD growth technology has been developed in order for using a variety of source materials even if the vapor pressure is too low to be transferred in gas phase [2.22)]. The key issue is to add ultrasonic power to the source solution and mist particles being atomized are transferred by a carrier gas; so a liquid source can be transferred like a gas source.

The schematic of the setup is shown in Fig. 2.2. In the mist CVD method, liquid solution was atomized by ultrasonic power applied to transducers (Honda Electronics, HM2412), where the oscillator voltage and current of an ultrasonic generator were set at 20 V and 1.3 A, respectively. Aerosol or mist particles hence formed are transferred by a carrier gas to the reaction area for the growth of thin films. They are transferred by argon carrier gas to the substrate area. Ozone gas flows to reaction area to react with polysilazane and create silicon oxides on substrates.

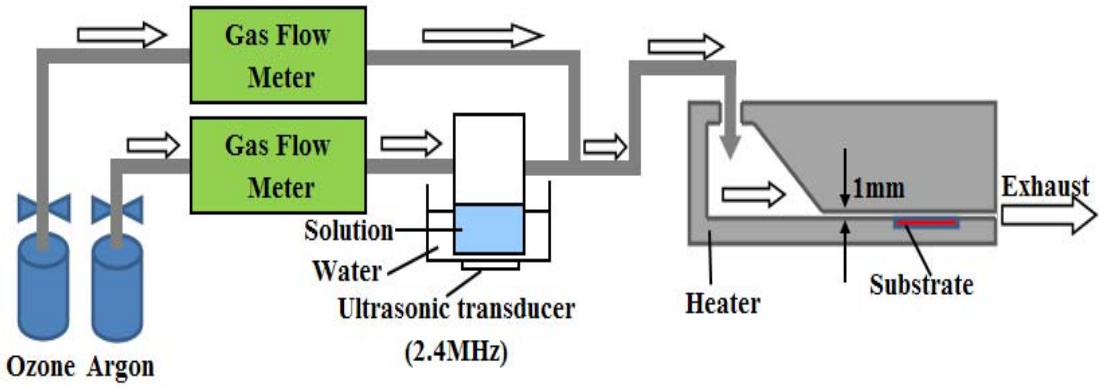


Figure 2.2 Schematic illustration of mist CVD system.

## 2.4 Conclusions

Mist vapor deposition method for thin film fabrication was studied in this chapter. The following conclusions were drawn:

(1) In this chapter, introduced two kinds of mist deposition method. One is called ultrasonic spray-assisted solution based mist deposition technology, mainly be applied to fabricate organic thin films. In chapter 4, will present the details of organic thin film fabrication. Another one is called mist chemical vapor deposition (mist CVD) method, which is applied to deposit silicon oxide thin films. In chapter 5, will present the details of silicon oxide thin film fabrication.

(2) Comparing with spray deposition method, using mist vapor deposition method can deposit thin films which have flat surface. Mist vapor deposition method can be applied to deposit layered structures. However, mist vapor deposition method is a good technology to control the formation of thin films.

## References and notes


2.1) C.H. Jonda, A.B.R. Mayer, U. Stolz, A. Elschner, and A. Karbach: J. Mater. Sci. **35** (2000) 5645.

2.2) C. Bae, S. Lee, S. Choi and G. Kwag: Inorg. Chem. **44** (2005) 7911.

2.3) G. Xu, Y. Tang, C. Tsang, J. Zapien, C. Lee and N. Wong: J. Mater. Chem. **20** (2010) 3006.

2.4) C. Tu, Y. Lai and D. Kwong: IEEE Electron Device Lett. **27** (2006) 354.

2.5) Y. Okabayashi, T. Mitarai, S.Yamazaki, and R.Matsuyama: Appl. Surf. Sci. **244** (2005) 217.

2.6) M. Uchida, Y. Ohmori, T. Noguchi, and T. Ohnishi: Jpn. J. Appl. Phys. **32** (1993) L921.

2.7) T. Takayama, M. Kitamura, Y. Kobayashi, Y. Arakawa, and K. Kudo: Macromol. Rapid Commun. **25** (2004) 1171.

2.8) J. Lu, A.R. Hlil, Y. Meng, A.S. Hay, Y. Tao, M. D'Iorio, T. Maindron, and J. Dodelet: J. Polymer Sci. Part A: **38** (2000) 2887.

2.9) Q. Mei, B. Tong, L. Liang and M. Lua: J. Photochem. Photobiology A: Chem. **191** (2007) 216.

2.10) S. Kawasaki, S. Motoyama, T. Tatsuta, O. Tsuji, S. Okamura, and T. Shiosaki: Jpn. J. Appl. Phys. **43** (2000) 6562.

2.11) T. Kawaharamura, H. Nishinaka, K. Kametani, Y. Masuda, M. Tanigaki, and S. Fujita: J. Soc. Mater. Sci. Jpn. **55** (2006) 153 [in Japanese].

2.12) T. Kawaharamura, H. Nishinaka, Y. Kamada, Y. Masuda, J.G. Lu, and S. Fujita: J. Kor. Phys. Soc. **53** (2008) 2976.

2.13) T. Kawaharamura, H. Nishinaka, and S. Fujita: J. Soc. Mater. Sci. Jpn. **57** (2008) 481 [in Japanese].

2.14) Y. Kamada, T. Kawaharamura, H. Nishinaka and S. Fujita: Jpn. J. Appl. Phys. **45** (2006) L857.

2.15) H. Nishinaka, T. Kawaharamura and S.Fujita: Jpn. J. Appl. Phys. **46** (2007) 6811.

2.16) H. Nishinaka, Y. Kamada, N. Kameyama and S. Fujita: Jpn. J. Appl. Phys. **48** (2009) 121103.

2.17) T. Ikenoue, H. Nishinak and S. Fujita: Thin Solid Films **520** (2012) 1978.

2.18) J. Piao, S. Katori, T. Ikenoue and S. Fujita: Jpn. J. Appl. Phys. **50** (2011) 020204.

2.19) J. Piao, S. Katori, T. Ikenoue and S. Fujita: physica status solidi (a) **8** (2012) 613.

2.20) J. Piao, S. Katori, T. Ikenoue and S. Fujita: MRS Proceedings **1400** (2012).

2.21) Robert J. Lang: J. Acoustical Soc. America **34** (1962) 6.

2.22) D. Shinohara and S. Fujita: Jpn. J. Appl. Phys. **47** (2008) 7311.

# Chapter 3
# Preparation and analysis of source solutions for thin film fabrication

## 3.1 Solution process in thin film fabrication

### 3.1.1 Solution process in organic thin film fabrication

Organic electroluminescence (EL) has now become one of the emerging fields of modern electronics owing to its high potential for a variety of applications to displays and lighting. Because of the strong market demands for low cost and large area devices, together with severe competition with other physics based devices, simple, cost effective, and low energy consumption fabrication processes for EL material thin films and multilayered structures have attracted increased interest. Solution based deposition technologies such as spin coating, dipping, spraying, and inkjet printing can meet the demands and their marked progress has been continuing recently.

However, solution based technologies require the materials to be dissolved in suitable volatile solvents such as alcohol. Actually, it is difficult to find novel solvents for many useful and conventional organic EL materials that are known to exhibit high efficiency and long term EL, such as $Alq_3$, and we must apply vacuum evaporation for the fabrication of their thin films even though it possesses several problems against large area and low cost flat panel devices. Applying high ultrasonic power is effective

method for preparing organic solution, such as a solution of $Alq_3$ in methanol.

### 3.1.2 Solution process in silicon oxide thin film fabrication

Over the past few decades, interest in transparent, thin silicon coatings have increasingly grown for several applications like optics, interlayer dielectrics, and barrier films for the food packaging and medical device industries. Silicon oxide thin films are undoubtedly the most important and widely used insulating films in modern electronic circuit devices. The excellent electrical insulating characteristics of silicon oxide thin films grown by the thermal oxidation of silicon (Si) have supported high performance large scale integrated circuit (LSI) devices. On the other hand, the recent demand for environmentally friendly, lightweight, and mobile devices requires the evolution of device processes at low temperatures in order to use plastic substrates or films. In addition, low temperature grown silicon oxide thin films are also highly expected to be used as barrier films against gas and vapor diffusion in the food packaging and medical device industries [3.1-3.4)], owing to the transparency, recyclability, and microwave-endurance of silicon oxide, as a candidate substituting thin metal (generally aluminum-based metals) coatings.

For the low temperature growth of silicon oxide thin films, vacuum based processes such as vacuum evaporation and sputtering have generally been used, but for electrical applications on large area substrates in mass production, especially on films fabricated by a continuous process such as roll-to-roll process, it is desirable to use vapor phase growth processes such as chemical vapor deposition (CVD).

Since the vapor pressure of source solution is low, it cannot be transferred to the

reaction area in the gas phase, limiting its use as a CVD source. On the other hand, a mist CVD growth technology has been developed in order to use a variety of source materials whose vapor pressure is too low to be transferred in the gas phase [3.5)]. Using this technology, our attempts are reported hereafter for the growth of silicon oxide thin films with reasonably high resistivity and breakdown electric field at the temperatures of as low as 200 $^{o}$C.

## 3.2 Solution preparation in mist vapor deposition method

In our experiments, we applied mist vapor deposition method to thin film fabrication. As introduced at chapter 2, mist deposition method is a good technology to control the formation of thin films. However, this technology has one defect, which is some solvents cannot be atomized.

### 3.2.1 Atomization ability of solvents in mist vapor deposition method

Table 3.1 shows some solvents and their atomizing ability. When discussing atomizing ability, we generally consider surface tension and viscosity as the parameters. Table 3.2 shows surface tension and viscosity with solvents. From table 3.2, we can observe that molecular having smaller viscosity easier to be atomized than having higher viscosity. Relatively, the surface tension less influenced on atomizing ability. However, up to now, we found viscosity is the main parameters related to the atomizing ability when the applied ultrasonic frequency is constant.

| Solvents | Atomizing ability |
|---|---|
| $H_2O$ | Easily be atomized ○ |
| Methanol | Easily be atomized ○ |
| Ethanol | Cannot be atomized × |
| Acetone | Easily be atomized ○ |
| Tetrahydrofuran (THF) | Easily be atomized ○ |
| Dimethylformamide (DMF) | Hardly be atomized △ |
| Toluene | Easily be atomized ○ |
| Chlorobenzene | Hardly be atomized △ |
| o-dichlorobenzene | Hardly be atomized △ |
| o-xylene | Easily be atomized ○ |
| 1-methyl-2-pyrrolidone | Hardly be atomized △ |
| 2-propanol | Cannot be atomized × |
| Acetic acid | Cannot be atomized × |
| Methyl acetate | Easily be atomized ○ |
| Dimethyl sulfoxide (DMSO) | Cannot be atomized × |
| 2-Butanone | Easily be atomized ○ |

Table 3.1 some solvents and their atomizing ability.

| **Solvents** | **Surface tension @ 20°C in mN/m** | **Viscosity @ 20°C in mPa·s** |
|---|---|---|
| $H_2O$ ○ | 72.7 | 1.00 |
| Methanol ○ | 22.6 | 0.59 |
| Ethanol × | 22.5 | 1.20 |
| Acetone ○ | 23.3 | 0.32 |
| Tetrahydrofuran (THF) ○ | 26.4 | 0.48 |
| Dimethylformamide (DMF) △ | 37.1 | 0.92 |
| Toluene ○ | 28.4 | 0.59 |
| Chlorobenzene △ | 33.6 | 0.81 |
| o-dichlorobenzene △ | 36.7 | 1.32 |
| o-xylene ○ | 30.1 | 0.84 |
| 1-methyl-2-pyrrolidone △ | 40.8 | 1.89 |
| 2-propanol × | 23.7 | 1.77 |
| Acetic acid × | 27.7 | 1.22 |
| Methyl acetate ○ | 24.0 | 0.39 |
| Dimethyl sulfoxide (DMSO) × | 43.5 | 1.99 |
| 2-Butanone ○ | 24.6 | 0.40 |

Table 3.2 Surface tension and viscosity with solvents.

### 3.2.2 Solution preparation in mist vapor deposition method

The organic molecular mainly be classified two types, polymer and small molecular (as shown in table 3.3). Small molecular were classified metal complex and small molecular.

Polymer molecular can be dissolved in organic solvents, and thin films can be fabricated by solution process. Small molecular is hard to be dissolved in solvents because of the polymeric structures. In our research, we found that applying high ultrasonic power can make polymeric molecular to be oligomeric molecular. Oligomeric small molecular can exist with solvent molecular in solution. However, after applied high ultrasonic power, the solution was looked uniform. For example, applying high ultrasonic power to the mixture of $Alq_3$ and methanol, polymeric $Alq_3$ molecular was smashed to oligomeric $Alq_3$ molecular (as shown in Fig. 3.1).

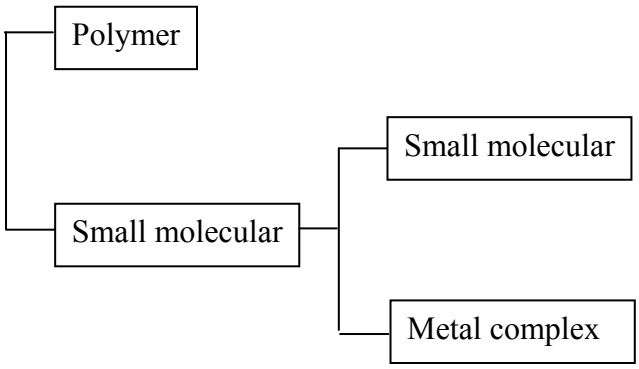


Table 3.3 Organic molecular types.

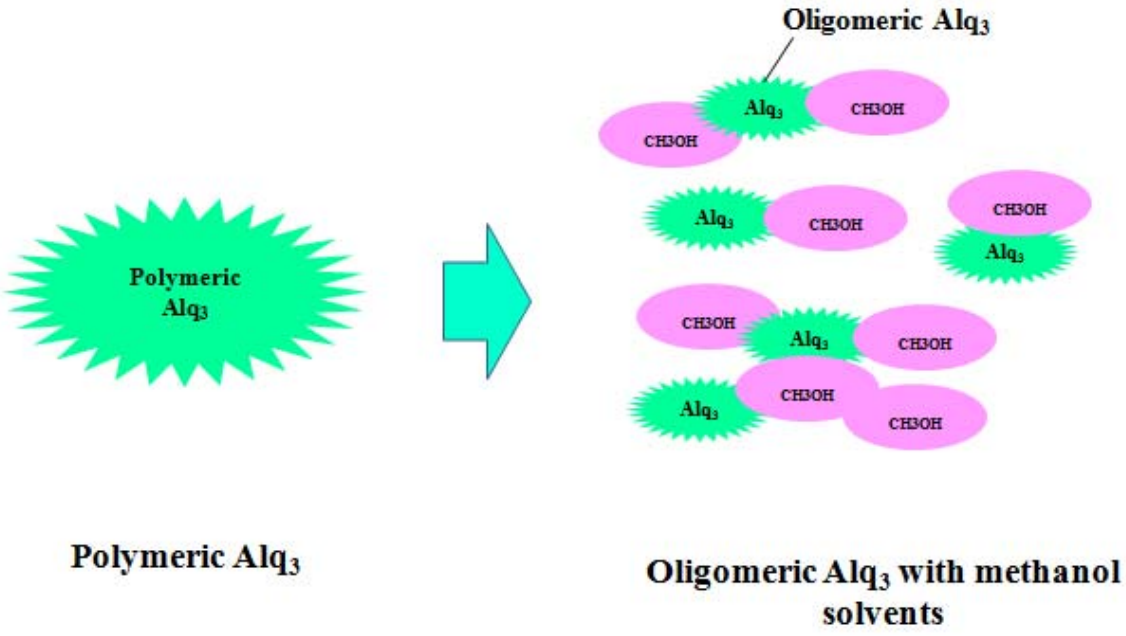


Figure 3.1 $Alq_3$ structure before applying high ultrasonic power, and after applied high ultrasonic power to $Alq_3$/methanol solution.

## 3.3 Preparation of source solutions for thin film fabrication

About two decades have elapsed since $Alq_3$ appeared as a milestone for the development of OLED [3.6]. $Alq_3$ still one of the most stable and fluorescent solid state materials, making it as the emitting material and electron transport layer (ETL).

Except organic materials, we also used inorganic materials, such as insulator materials. In our experiments we used polysilazane, $(R_1R_2Si\text{-}NR_3)_n$, as a source material for the CVD growth of silicon oxide. Polysilazane is inorganic polymer, which can react with oxide atoms, making silicon oxides on substrates.

### 3.3.1 Preparation for $Alq_3$/methanol solution

$Alq_3$ is one of the most stable and fluorescent solid state materials in OLED. Subsequently, quinolate metal complexes have become a very important class of electroluminescent material in OLED [3.7-3.9]. To fabricate OLED by solution, the principal interest in the use of soluble $Alq_3$ complex derivatives lies in the scope for low cost manufacturing, such as spin coating. Soluble $Alq_3$ complex derivatives, such as tris (5-*N*-ethylanilinesulfonamide-8-quinolato) aluminum (Al $(Saq)_3$), tris (4- tridecyl - 8 - quinolinolato) aluminum (TDALQ), and bis (salicylidene - o - aminophenolato) - (dipivaloylmethane) aluminum ((Al (saph) $DPM)_2$) etc. were reported by other groups [3.10-3.12]. Most structurally modified $Alq_3$ derivatives become less stable than $Alq_3$ and these complexes are soluble in commercially available solvents such as tetrahydrofuran (THF), dimethylforamide (DMF), or dimethylsulfoxide (DMSO). However, these materials are not environmentally friendly materials. In our experiments, we used $Alq_3$

as materials and methanol as the solvents.

50 mg of $Alq_3$ (Sigma Aldrich) powder was put into 100 ml methanol, and applied high ultrasonic power for 1 hour. The frequency and power of the ultrasound were 20 kHz and 200 W, respectively. The temperature of methanol was not intentionally controlled, so it rose from room temperature to about 60 $^{o}$C owing to the application of ultrasound. This resulted in a transparent and uniform solution. Fig. 3.2 (a) shows the preparation process for $Alq_3$/methanol solution and Fig. 3.2 (b) shows transparent and uniform solution after applying high ultrasonic power. The solution was then stored in a refrigerator at about 10 $^{o}$C for storage and no precipitates were recognized by the naked eye after two days.

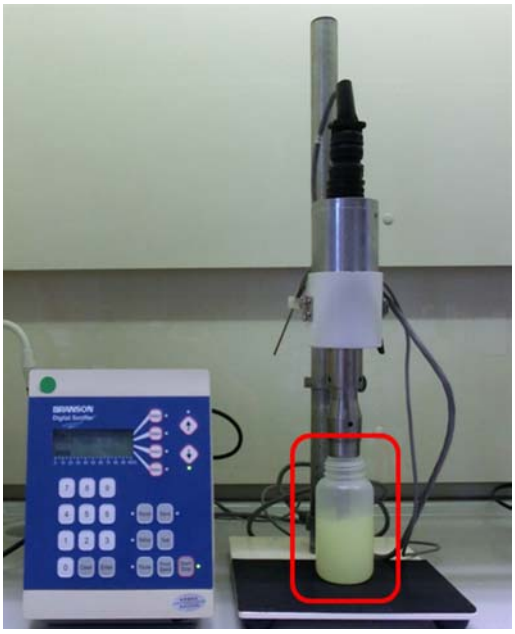

(a)

(b)

Figure 3.2 (a) Preparation process for $Alq_3$/methanol solution and (b) transparent and uniform solution after applying high ultrasonic power.

### 3.3.2 Preparation for polysilazane solution

20% Polysilazane solution were purchased from Exousia Incorporated. The polysilazane were diluted in oxylene and have to pay attention to both polysilazane and oxylene when dilute polysilazane solution in other solvents. Polysilazane is an inorganic polymer, so we firstly chose polymer solvents. Within these solvents, we chose solvents which can be diluted in oxylene and no chemical reaction. Through these steps, chose 1-methyl-2 pyrrolidone, methyl acetate, mesitylene, and methyl ethyl ketone as the solvents for diluting polysilazane solution.

Polysilazane solution was diluted in these solvents in the concentration of 1%. These diluted solutions were looked as transparent and uniform. After deposited thin films on silicon wafers, we decided to choose methyl acetate as the solvents.

## 3.4 Analysis of source solutions for thin film fabrication

$Alq_3$ thin films were fabricated by vacuum evaporation for the difficulty to find suitable solvents. Applying high ultrasonic power can make transparent and uniform $Alq_3$/methanol solution. However, we should argue whether the source $Alq_3$ molecules maintain the original chemical structure without decomposition or combination being affected by the ultrasonic power, because any alteration of chemical structure of $Alq_3$ alter the film properties from those of $Alq_3$. Since we have found that the application of ultrasonic power is effective for other small molecule materials to be solved in various solvents, it is important to confirm that the source materials can keep their original chemical structure in the solution in spite of the application of the high ultrasonic power. The results of nuclear magnetic resonance (NMR) study of the $Alq_3$/methanol solution will show whether the source materials keep their original structures in solution.

### 3.4.1 NMR measurement

Nuclear magnetic resonance (NMR) is a physical phenomenon in which magnetic nuclei in a magnetic field absorb and re-emit electromagnetic radiation. This energy is at a specific resonance frequency which depends on the strength of the magnetic field and the magnetic properties of the isotope of the atoms. NMR allows the observation of specific quantum mechanical magnetic properties of the atomic nucleus. Many scientific techniques exploit NMR phenomena to study molecular physics, crystals, and non-crystalline materials through NMR spectroscopy.

In nuclear magnetic resonance (NMR) spectroscopy, the chemical shift is the resonant frequency of a nucleus relative to a standard. Often the position and number of chemical shifts are diagnostic of the structure of a molecule. Chemical shifts are also used to describe signals in other forms of spectroscopy such as photoemission spectroscopy.

Some atomic nuclei possess a magnetic moment (nuclear spin), which gives rise to different energy levels and resonance frequencies in a magnetic field. The total magnetic field are experienced by a nucleus includes local magnetic fields induced by currents of electrons in the molecular orbitals (note that electrons have a magnetic moment themselves). The electron distribution of the same type of nucleus (e.g. $^{1}H$, $^{13}C$, $^{15}N$) usually varies according to the local geometry (binding partners, bond lengths, angles between bonds, etc.), and with it the local magnetic field at each nucleus. This is reflected in the spin energy levels (and resonance frequencies). The variations of nuclear magnetic resonance frequencies of the same kind of nucleus, due to variations in the electron distribution, are called the chemical shift. The size of the chemical shift is given with respect to a reference frequency or reference sample, usually a molecule with a barely distorted electron distribution.

Chemical shift δ is usually expressed in parts per million (ppm) by frequency, because it is calculated from:

$$\delta = \frac{\text{difference between a resonance frequency and that of a reference substance}}{\text{operating frequency of the spectrometer}}$$

Since the numerator is usually in hertz, and the denominator in megahertz, delta is expressed in ppm. For example, an NMR signal that absorbs at 300 Hz at an applied frequency of 300 MHz has a chemical shift is:

$$\frac{300\,\text{Hz}}{300\times10^{6}\,\text{Hz}} = 1\times10^{-6} = 1\,\text{ppm}$$

Although the frequency depends on the applied field, the chemical shift is independent of it. On the other hand the resolution of NMR will increase with applied magnetic field resulting in ever increasing chemical shift changes.

### 3.4.2 NMR study of the $Alq_3$/methanol solution

In NMR measurement, two basic parameters, chemical shift and line width, provide ligand and coordination information. Aluminum-27 ($^{27}Al$; 100 % abundant, I = 5/2) has a moderately large electric quadrupole moment ($Q=0.149\times10^{-24}$ $cm^2$), and the chemical shift of $^{27}Al$ NMR spectrum is sensitive to aluminium geometry and number [3.13]. Further, the chemical shift of $^{1}H$ spectrum provides the possibility of quinolinol ligand. The NMR spectra of all samples were measured by the UBE analysis centre.

The $^{27}Al$ NMR spectrum of $Alq_3$ solution is shown in Fig. 3.3. For Al coordinated by six oxygen such as $Al(H_2O)_6^{3+}$ show the $^{27}Al$ NMR peak around 0 ppm. Bae et al. [3.14] showed the $^{27}Al$ NMR peak at 31.1 ppm for $Alq_3$ solution and attributed it from

hexa-coordinated Al complexes. The narrow peak at 32 ppm in Fig. 3.3 evidences the existence of $Alq_3$ in the solution. They also pointed out that another peak appear at 57.5 ppm from penta-coordinated Al complexes such as $Alq_2(OCH_3)$. However, we cannot observe penta-coordinated Al complexes except of background from broad peak at 57 ppm in Fig. 3.3. Other peaks, such as tetra-coordinated Al complexes ($Alq(OCH_3)_2$) at 82.3 ppm and $Al^{3+}$ at 0 ppm, were not observed in $^{27}Al$ NMR spectrum of $Alq_3$ solution.

Nevertheless we may infer that even if the ultrasonic power applied to the $Alq_3$ solution is high enough to make new chemical species, such as $Alq_2(OCH_3)$, they will return to $Alq_3$ under the sufficient existence of quinolinol ions.

In order further to clear the possible influence of high ultrasonic power on $Alq_3$ in the solution, we compared the NMR spectra for the following two kinds of solution. One was the mixture of $Alq_3$ and 8-quinolinol in methanol (solution #1: 50 mg $Alq_3$ and 1 g 8-quinolinol was put together into 100 ml methanol and then it was subjected to high ultrasonic power). Another one is the mixture of $Alq_3$ solution and 8-quinolinol solution (solution #2: 50 mg $Alq_3$ was put into 100 ml methanol and it was subjected to ultrasonic power for 1 hour, and then it was mixed with the solution of 1 g 8-quinolinol in 100 ml methanol). The NMR spectra for solution #1 and #2 are shown in Fig. 3.4 (a) and (b), respectively. We cannot observe marked difference between two kinds of solution, suggesting low possibility of formation of $Alq_2(OCH_3)$ from $Alq_3$ due to the ultrasonic power.

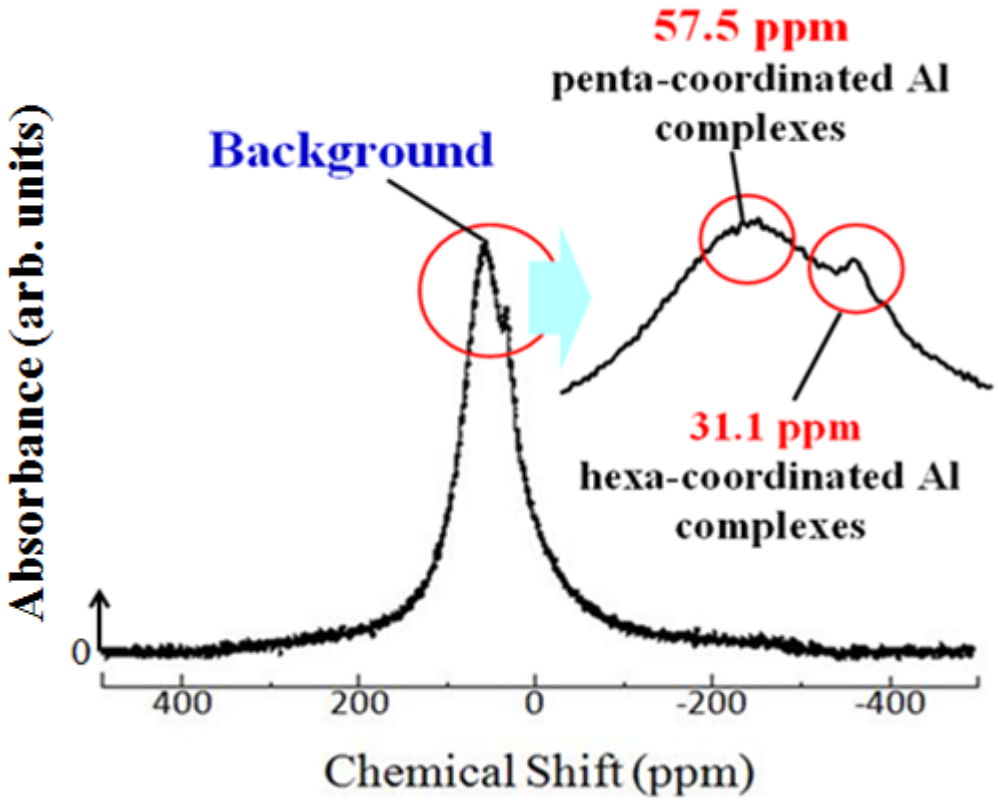


Figure 3.3 $^{27}$Al NMR spectra of $Alq_3$ solution.

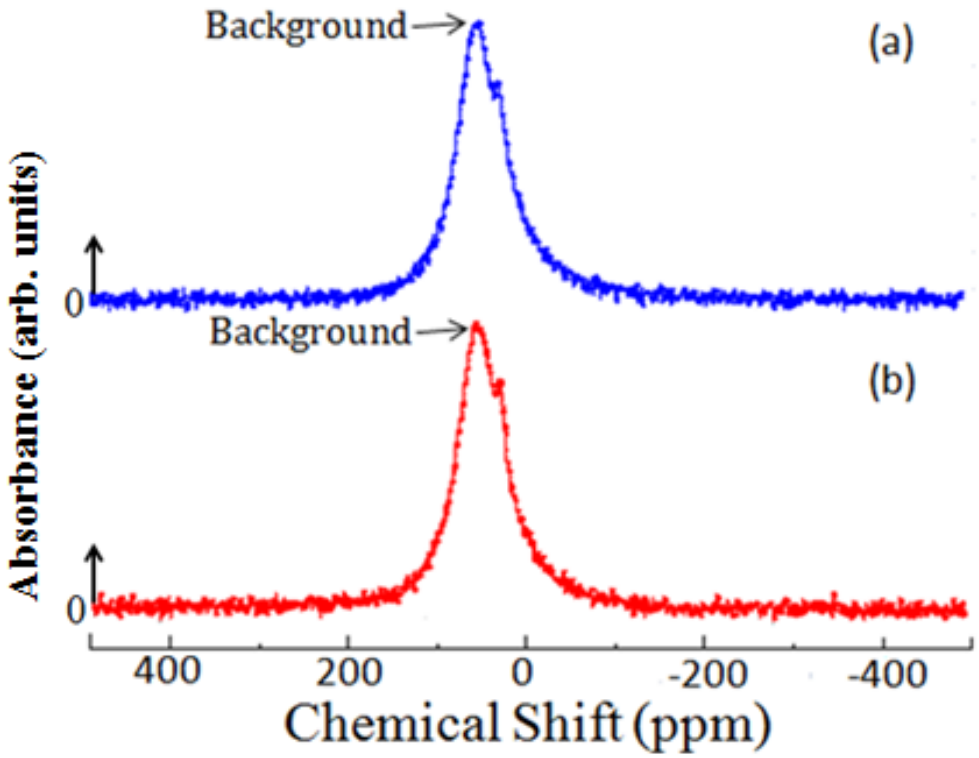


Figure 3.4 $^{27}$Al NMR spectra of (a) mixture of $Alq_3$ and 8-quinolinol in methanol ([50 mg $Alq_3$]+[1 g 8-quinolinol]+[100 ml methanol], and then applying high ultrasonic power) and (b) mixture of $Alq_3$ solution and 8-quinolinol solution ([50 mg $Alq_3$]+[100 ml methanol], subjected to high ultrasonic power for 1 hour, and then mixed with [1 g 8-quinolinol]+[100 ml methanol]).

Fig. 3.5 compares the $^{1}H$ NMR spectra of (a) 8-quinolinol and (b) $Alq_3$ dissolved in methanol. The spectrum (b) is different from those of meridional $Alq_3$ (mer-$Alq_3$) and facial $Alq_3$ (fac-$Alq_3$) reported previously [3.15]. Further the spectrum (b) is definitely different from the spectrum (a). From these observations we can say that $Alq_3$ takes a variety of phases in the methanol solution. It also means the possibility that $Alq_3$ co-crystallizes with clathrate solvents, such as methanol, similar results already published by Kim et al. [3.16].

From these results, we can conclude $Alq_3$ solution can be made by applying high ultrasonic power into the mixture of $Alq_3$ and methanol. The $Alq_3$ atoms in $Alq_3$/methanol solution were not seriously damaged by the high ultrasonic power and the solution can be used as the source of the formation of $Alq_3$ thin films by the mist deposition method.

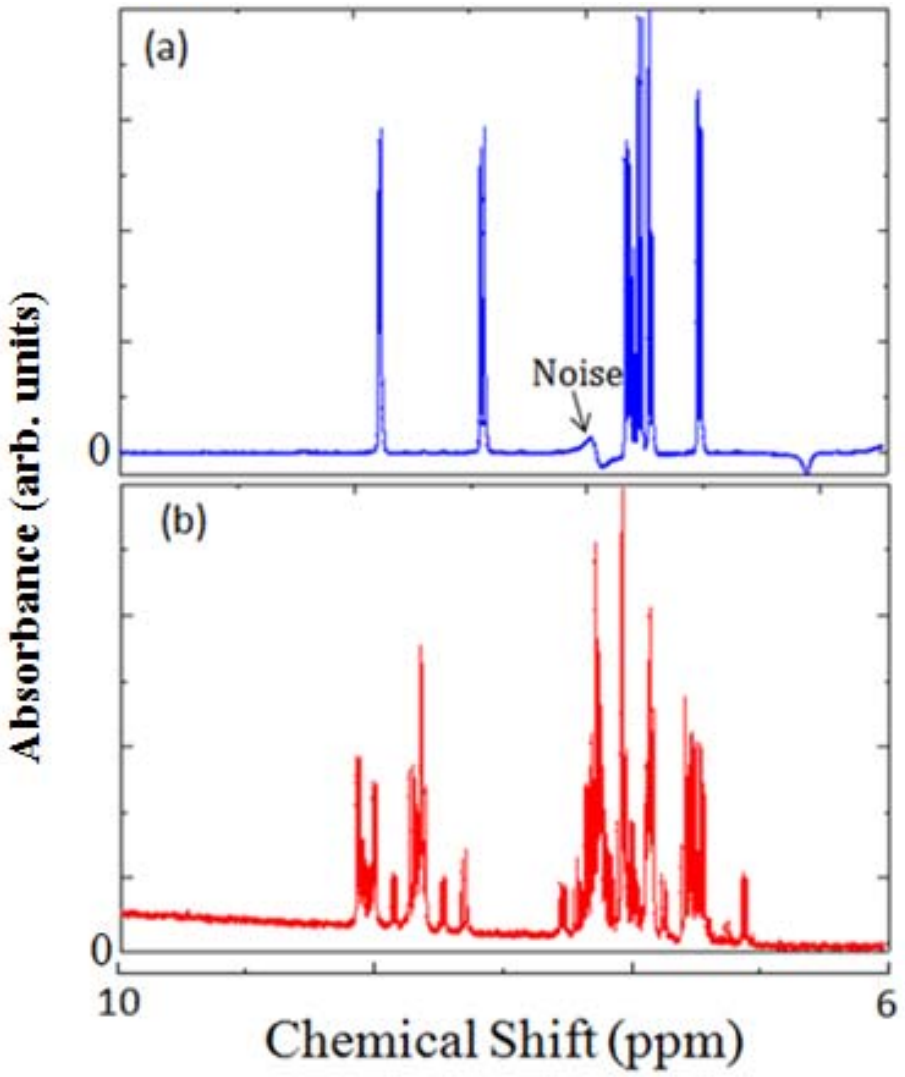


Figure 3.5 $^{1}$H NMR spectra for (a) 8-quinolinol dissolved in methanol and (b) $Alq_3$ dissolved in methanol.

## 3.5 Conclusions

Through applying high ultrasonic power or choosing suitable solvents, we can obtain uniform solutions. When making uniform $Alq_3$/methanol solution, we applied high ultrasonic power to the mixture of $Alq_3$ and methanol solution. The following conclusions were drawn:

(1) Applying high ultrasonic power to the mixture of $Alq_3$ and methanol solution, we obtained transparent and uniform $Alq_3$ solution. The solution was then stored in a refrigerator at about 10 °C for storage, and no precipitates were recognized by the naked eyes after two days.

(2) The $Alq_3$ atoms were not seriously damaged by the high ultrasonic power and therefore the solution were used as the source of the formation of $Alq_3$ thin films by the mist deposition method.

(3) Preparation of uniform polysilazane solution can be classified next three steps. First step is finding polymer solvents; second step is choosing solvents which can be diluted in oxylene and no chemical react with oxylene; third step is deposit thin films and observe whether thin films can be fabricated.

## References and notes


3.1) A. Erlat, R. Spontak, R. Cloarke, T. Robinson, P. Haaland, Y. Tropsha, N. Harvey, and E. Vogler: J. Phys. Chem. B **103** (1999) 6047.

3.2) K. Eun, W. Hwang, B. Sharma, J. Ahn, Y. Lee, and S. Choa: Mod. Phys. Lett. B **26** (2012) 1250077.

3.3) B. Singh, J. Bouchet, Y. Leterrier, J. Manson, G. Rochat, and P. Fayet: Surf. Coatings Technol. **202** (2007) 208.

3.4) D. Howells, B. Henry, J. Madocks, and H. Assender: Thin Solid Films **516** (2008) 3081.

3.5) T. Kawaharamura, H. Nishinaka, K. Kametani, Y. Masuda, M. Tanigaki, and S. Fujita: [J. Soc. Mater. Sci. Jpn.] **55** (2006) 153 [in Japanese].

3.6) C.W. Tang and S.A. VanSlyke: Appl. Phys. Lett. **51** (1987) 913.

3.7) A. Curioni, M. Andreoni, and W. Andreoni: Chem. Phys. Lett. **294** (1998) 263.

3.8) F. Bai, M. Zheng, G. Yu, and D. Zhu: Thin Solid Films **363** (2000) 118.

3.9) D. Ma, G. Wang, Y. Hu, Y. Zhang, L. Wang, X. Jing, F. Wang, C. Lee, and S. Lee: Appl. Phys. Lett. **82** (2003) 1296.

3.10) J. Xie, Z. Ning, and H. Tian: Tetrahedron Lett. **46** (2005) 8559.

3.11) S. Liao, J. Shiu, S. Liu, S. Yeh, Y. Chen, C. Chen, T. Chow, and C. Wu: J. Am. Chem. Soc. **131** (2009) 763.

3.12) L. Duan, L. Hou, T. Lee, J. Qiao, D. Zhang, G. Dong, L. Wang, and Y. Qiu: J. Mater. Chem. **20** (2010) 6392.

3.13) J. Yang, Y. Yu, Q. Li, Y. Li, and A. Gao: J. Polym. Sci. A: Polym. Chem. **43** (2005) 373.

3.14) C. Bae, S. Lee, S. Choi, and G. Kwag: Inorg. Chem. **44** (2005) 7911.

3.15) R. Manju, N. Thomas, C. Tang, C. William, C. Steven, J. David, J. Brian, D. Thomas, Y. Denis, Z. Nicholas, and H. Ralph: Polyhedron **28** (2009) 835.

3.16) T. Kim, D. Kim, H. Im, K. Shimada, R. Kawajiri, T. Okubo, H. Murata, and T. Mitani: Sci. Tech. Adv. Mater. **5** (2004) 331.

# Chapter 4
# Fabrication of organic thin films by solution based deposition process

## 4.1 Fabrication of $Alq_3$ thin films by using ultrasonic spray-assisted vapor deposition method

In chapter 3, the preparation of $Alq_3$/methanol solution was introduced. NMR measurement results mean $Alq_3$ atoms were not seriously damaged. In order to prove impact of making the $Alq_3$-containing solution we proceeded to the fabrication of thin films from the solution. Firstly, we fabricated $Alq_3$ thin films on glass substrates in order to confirm the impact of making $Alq_3$-containing solution. Secondly, we deposited $Alq_3$ thin films on indium tin oxide (ITO) to show the potential application of the mist deposition method for future device fabrication. As deposition technique, we used the ultrasonic spray-assisted vapor deposition method as shown in Fig. 4.1. The details about this method are already introduced at chapter 2.

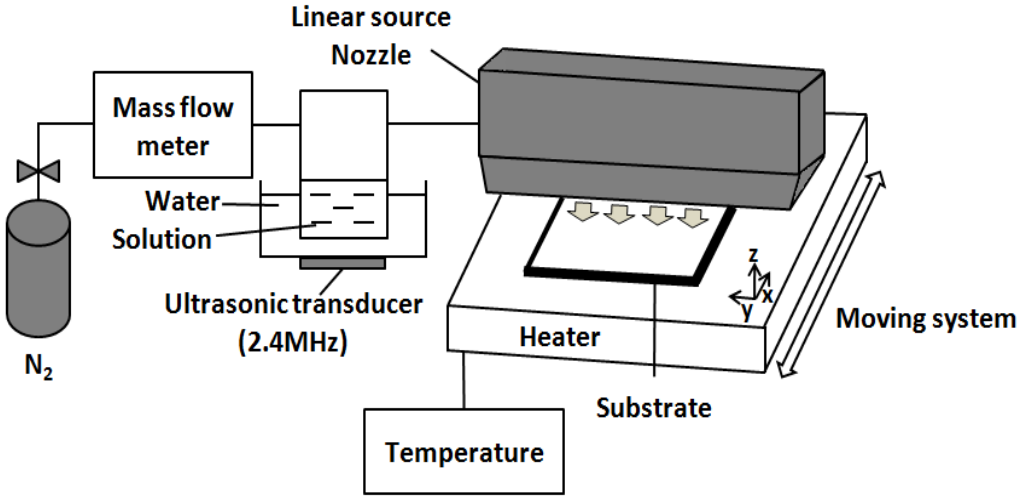


Figure 4.1 Schematic illustration of the mist deposition system.

### 4.1.1 Fabrication of $Alq_3$ thin films on glass substrates

Glass substrates were ultrasonically cleaned in acetone. The $Alq_3$ solution was put into glass container and was atomized by ultrasonic power applied to transducers (Honda Electronics HM2412), where the frequency, oscillator voltage, and current of an ultrasonic generator were set at 2.4 MHz, 26 V, and 1.3 A, respectively. The $Alq_3$ solution was atomized and mist particles of the solution were generated. They were transferred by nitrogen carrier gas with the flow rate of 6.0 L /min to the substrate area. Near the substrate surface, methanol was vaporized by heat and $Alq_3$ was deposited onto the substrate. During the mist deposition process, the nozzle temperature was set at 40 °C in order to preheat the mist and carrier gas. The nozzle moved over the substrate at 1.25 mm/min. The substrate temperature was set at 100, 120, 140, 160, 180, or 200 °C.

Thickness of the films deposited on the substrates was characterized by measuring the height of steps formed by partially scratching off the film from the substrate. A surface profiler (Tencor P-15) was used for the measurement. The optical characterizations were performed using an ultraviolet-visible (UV-vis) transmittance spectrometer (Shimadzu UV-1700) and a photoluminescence (PL) spectrometer (Hitachi F-2500) with the excitation wavelength of 370 nm. The surface morphology of samples was observed with an atomic force microscope (SII SPI-3800N).

Fig. 4.2 shows the thicknesses of the thin films fabricated as a function of the substrate temperatures during deposition process. Below 100 °C, rough powder-like precipitates were left on the glass substrate. We consider that this is because methanol solvent was slowly evaporated and $Alq_3$ molecules dissolved in methanol aggregated into a powder.

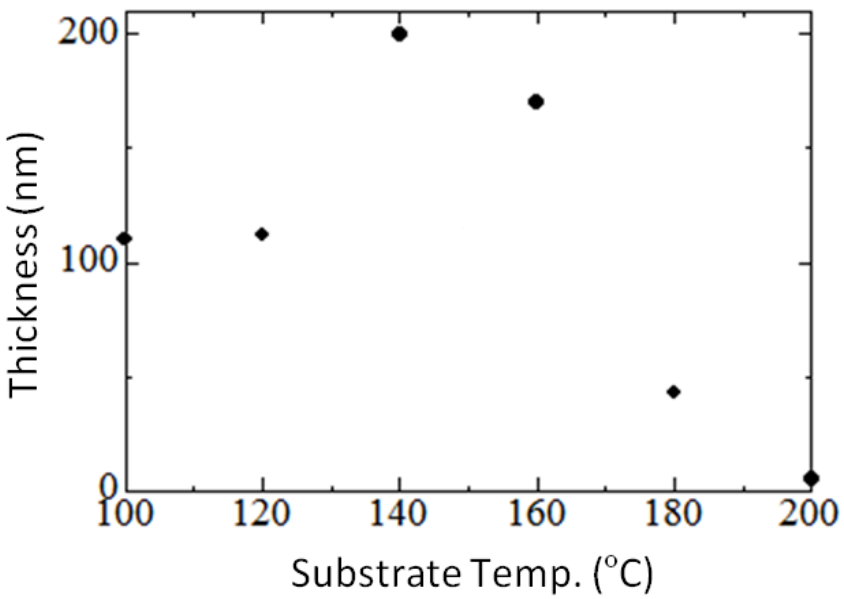


Figure 4.2 Film thicknesses against substrate temperature.

The transmittance of the thin films was measured in the range of 200 - 800 nm using a UV-vis spectrometer. Fig. 4.3 shows the transmission spectra for six samples of thin films deposited onto glass substrates at 100 - 200 °C. It should be noted that the vertical axis represents the measured value, neglecting surface reflection, diffraction, and scattering, and therefore, it does not reflect the real transmission with which a quantitative comparison becomes possible. The characteristic absorption of $Alq_3$ at around 386 nm [4.1, 4.2] is apparently seen for all samples.

Fig. 4.4 shows the PL spectra of the thin films deposited at different substrate temperatures. The $Alq_3$ thin films were excited with 370 nm light. The PL spectra showed broad emission bands ranging from 400 to 650 nm. The emission peaks appeared at around 520 nm, that is, at the green wavelength. A slight difference in the peak wavelength was observed, but at this stage, we have no knowledge that would elicit an explanation. The PL spectra in this wavelength region, together with the absorption spectra, are evidence of the successful formation of $Alq_3$ thin films. Upon comparing with Fig. 4.5, we can see the general tendency that the more intense PL is seen for thicker films, suggesting that the difference in PL intensity is mainly attributable to the thickness of $Alq_3$ thin films.

Fig. 4.5 shows the surface AFM images of $Alq_3$ thin films deposited at different substrate temperatures of (a) 120 °C and (b) 140 °C. Note that the thicknesses of the films were (a) 110 nm and (b) 200 nm, as shown in Fig. 4.2. From the scale showing the vertical height of the films, we can conclude that their surfaces are reasonably flat. The surface roughness may be at a level that allows the formation of layered structures via the deposition of other materials on the surface.

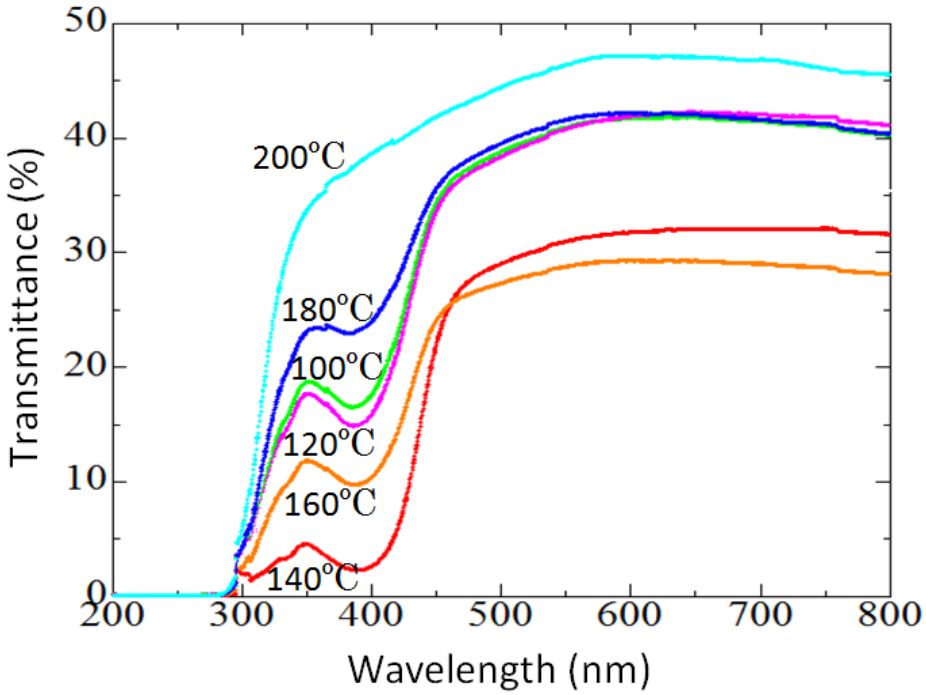


Figure 4.3 Optical transmission spectra of samples deposited at different substrate temperatures.

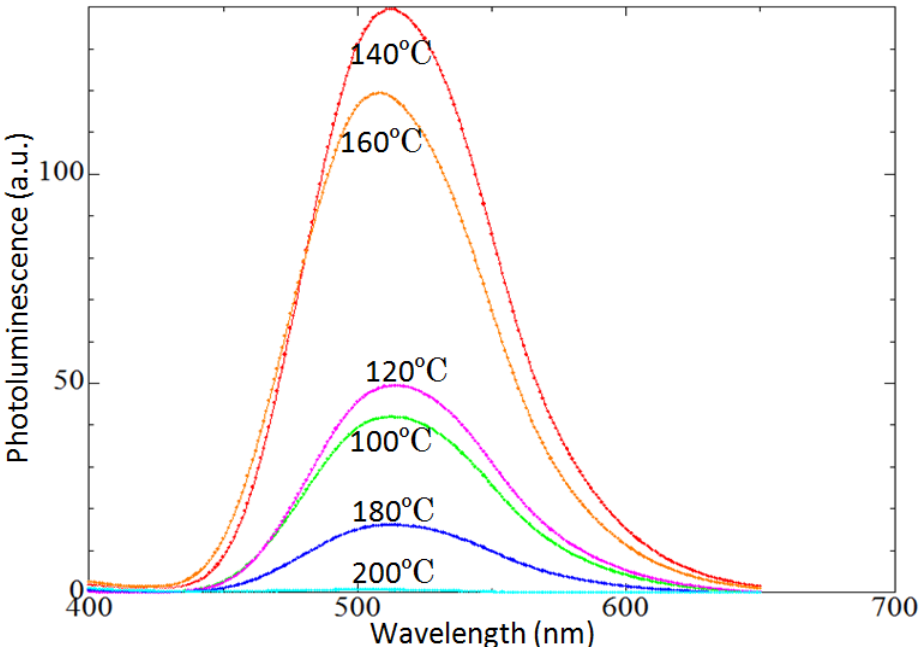


Figure 4.4 PL spectra of samples deposited at different substrate temperatures.

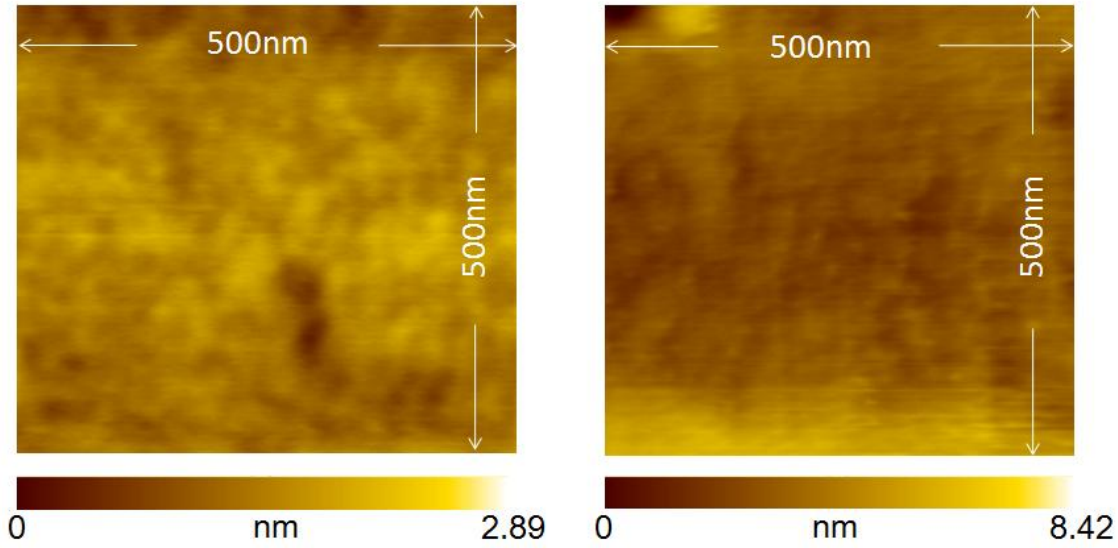


Figure 4.5 Surface AFM images of samples deposited at (a) 120 °C and (b) 140 °C.

### 4.1.2 Fabrication of $Alq_3$ thin films on ITO substrates

As the substrate, we used ITO (10 Ω/sq, thickness = 200 nm) on glass (GEOMATEC Corporation). ITO/glass substrates were cleaned in purified water (10 minutes), acetone (10 minutes), and ozone (15 minutes), successively. The $Alq_3$ solution was atomized by ultrasonic power applied to transducers (Honda Electronics HM2412), where the frequency, oscillator voltage, and current of an ultrasonic generator were set at 2.4 MHz, 26 V, and 1.3 A, respectively. The $Alq_3$ solution was atomized and mist particles consisted with the solution was generated, and transferred by nitrogen carrier gas with the flow rate of 6.0 L/min to the substrate area. Near the substrate surface methanol was vaporized by heat and $Alq_3$ deposits onto the substrate. During the mist deposition process, the nozzle temperature was set at 40 °C in order to preheat the mist and carrier gas. The nozzle moved on the substrate at 1.25 mm/min. The substrate temperatures were changed around 200 °C to optimize the deposition condition.

The optical characterizations were performed by using photoluminescence (PL) spectrometer (Hitachi F-2500), and the surface morphology of sample was observed by an atomic force microscope (SII, SPI-3800N). In order to characterize the electrical properties, we fabricated a diode structure as shown in Fig. 4.6, where a $Alq_3$ layer was sandwiched between cathode (Al, 300 nm), deposited by vacuum evaporation, and transparent anode (ITO, 200 nm) electrodes on glass fabricated in a metal cross-linked configuration. The current-voltage characteristics were measured by using a Keithley source meter (2600 series).

In the fabrication of $Alq_3$ thin films on ITO substrates, poor morphology was resulted for the substrate temperature below 200 $^{o}$C and the marked decrease in deposition rate

was recognized for the substrate temperature above 200 $^{o}$C. This means that the optimum substrate temperature is 200 $^{o}$C under the present values of other deposition conditions (concentration of $Alq_3$, gas flow rate, etc.). The optimum substrate temperature is quite different, that is, higher, compared to that (140 - 160 $^{o}$C) for the deposition on glass substrates [4.3)]. Referring the model proposed as the deposition process, it is considered that the rougher substrate surface of ITO comparing with glass obstructed migration of $Alq_3$ sources on the substrate surface.

Fig. 4.7 shows the PL spectrum of an $Alq_3$ thin film on an ITO substrate under the excitation of the 350 nm light. The emission peaks appeared at 505 nm together with a broad emission. The green PL evidences the formation of $Alq_3$ thin films.

Fig. 4.8 shows the surface AFM image of $Alq_3$ thin films on ITO substrate above 200 $^{o}$C. In this result, RMS (Root Mean Square) of surface is 1.1 nm. From the scale showing the vertical height of the films, we can claim that the surface is reasonably flat.

To evaluate the electrical defects in the $Alq_3$ thin film, we measured the characteristics of current density-applied voltage as shown in Fig. 4.9. The low leakage current suggests well defined $Alq_3$ thin films without significant electrical defects such as pinholes. The result encourages the successive deposition of other thin films on the $Alq_3$ thin film toward the formation of OLED devices, suggesting potential of the mist deposition method for fabrication of layered structures.

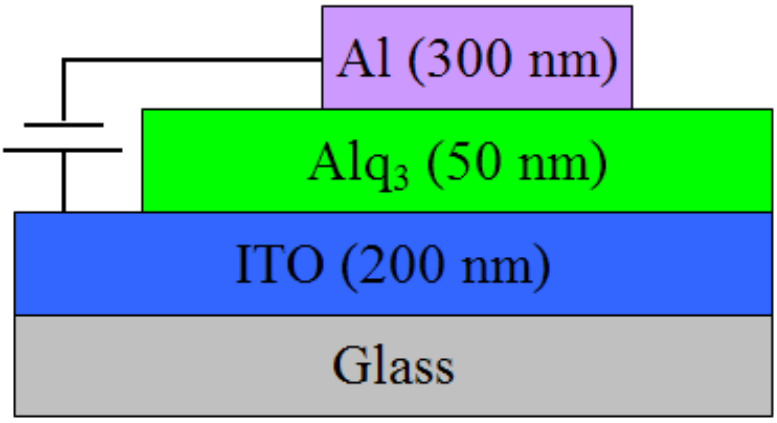


Figure 4.6 Schematic drawing of the $Alq_3$ diode structure for electrical characterization.

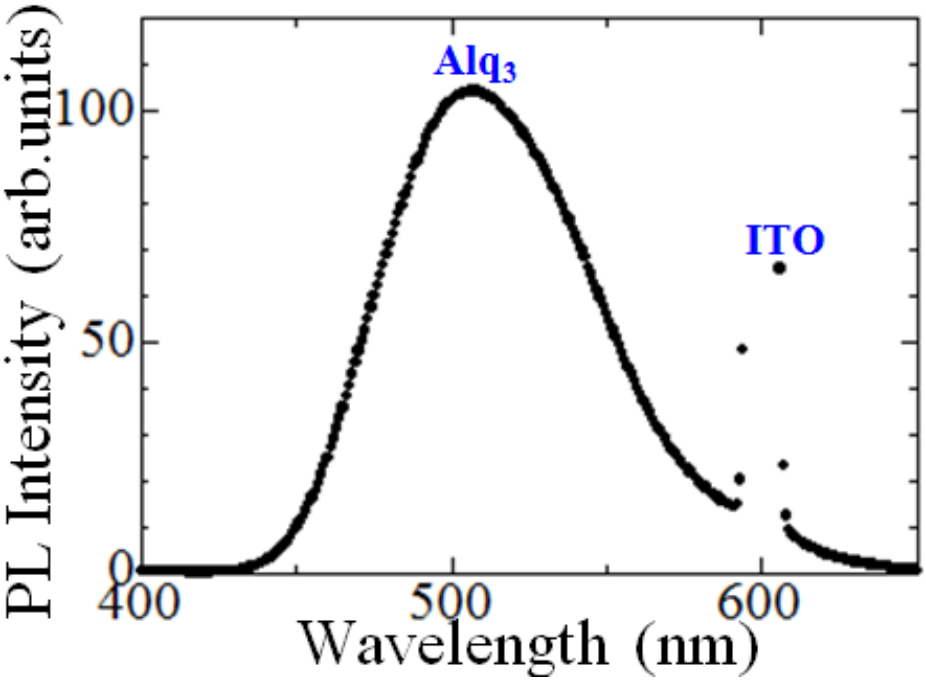


Figure 4.7 PL spectra of $Alq_3$ thin film deposited on ITO substrate.

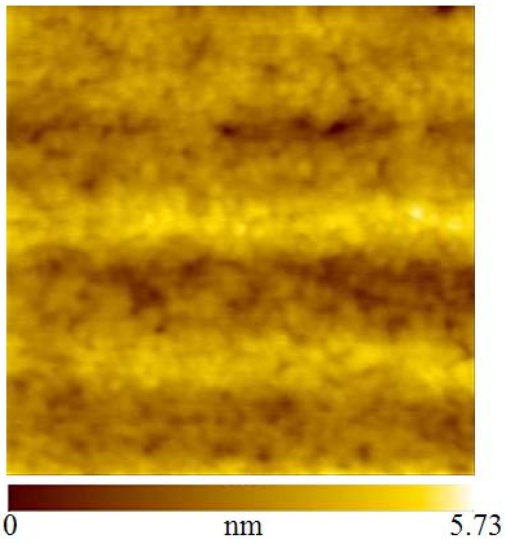


Figure 4.8 Surface AFM image of the sample. Here the scanning area is 1μm×1μm.

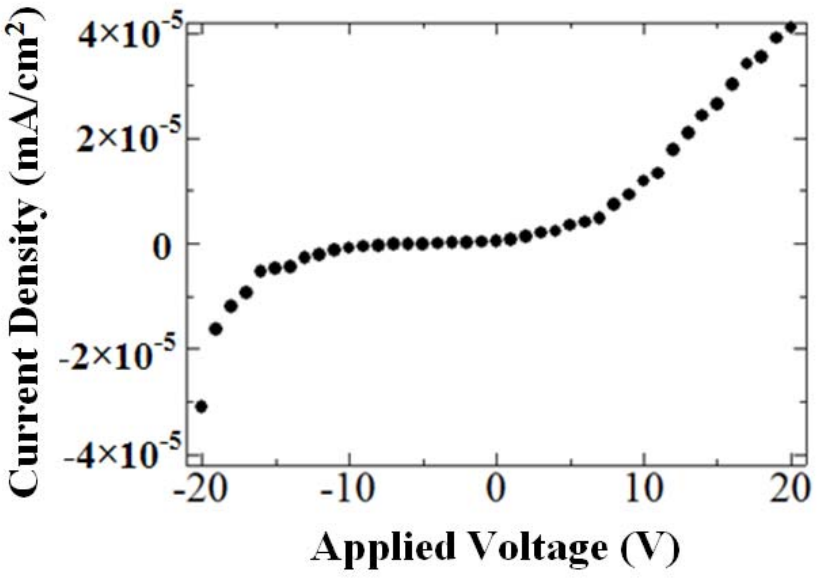


Figure 4.9 Current density-applied voltage characteristics of the sample.

### 4.1.3 Deposition mechanism

The deposition temperature was not only influenced by solvent evaporation temperature also influenced by substrate materials, because of the different material properties, such as surface energy, hydrophilic properties, and surface roughness and so on. When using glass substrates, below 100 °C, rough powder-like precipitates were left on the glass substrate. We consider that this is because methanol solvent was slowly evaporated and $Alq_3$ molecules dissolved in methanol aggregated into a powder. A schematic model for the process is shown in Fig. 4.10 (a). On the other hand, above 200 °C, the film thickness was measured to be smaller than 10 nm, and no deposition was observed at higher temperatures. This is probably because $Alq_3$ was evaporated far above the substrate surface along with the solvent (methanol), as shown in Fig. 4.10 (c). In the intermediate temperature range, that is, between 100 and 200 $^{o}$C, the vaporization of solvent (methanol) and the deposition of solute ($Alq_3$) were well balanced, and films with of mirror-like surfaces were formed, as shown in Fig. 4.10 (b).

When using ITO substrates, the temperature has become higher than glass substrates. Below 150 °C, rough powder-like precipitates were left on the glass substrate. In the intermediate temperature range, that is, between 150 and 320 °C, the vaporization of solvent (methanol) and the deposition of solute ($Alq_3$) were well balanced, and films with of mirror-like surfaces were formed. Above 320 °C, no deposition was observed.

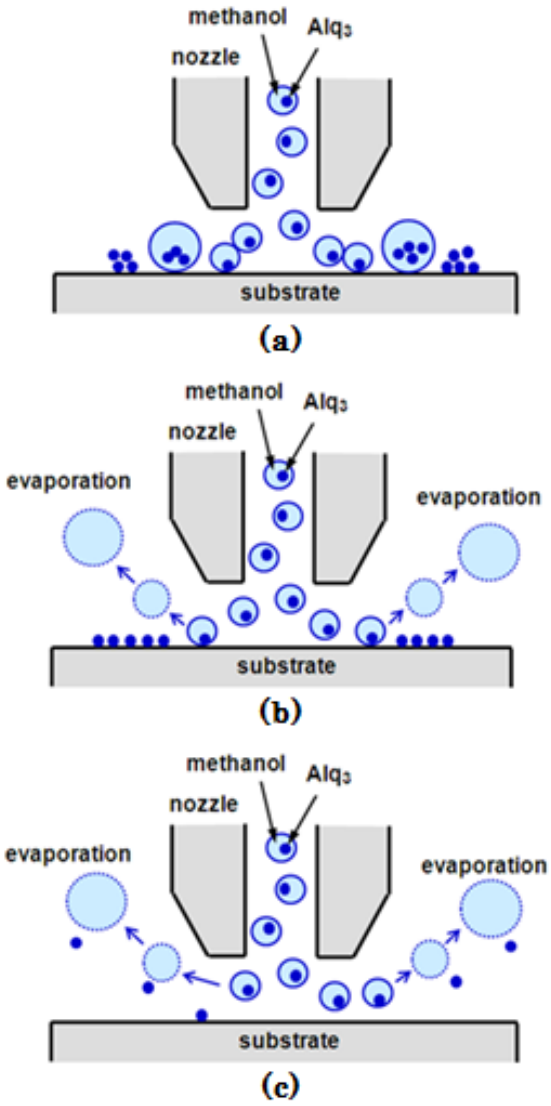


Figure 4.10 Schematic models of formation of thin films below the nozzle in different substrate temperature regimes (a) low temperature, (b) intermediate temperature and (c) high temperature.

### 4.1.4 Discussions

Despite of the flat surface, the current density in $Alq_3$ thin films is low. Maybe it is caused by low carrier density because the energy diagram of Al/$Alq_3$/ITO diode ($Alq_3$ diode) structure shows high potential barriers of 0.9 eV and 1.1 eV, as shown in Fig. 4.11 (a), both for electrons and holes, respectively, resulting in low carrier injection in the films. If the above was the case, the property was similar to that of well known vacuum evaporation fabricated $Alq_3$ thin films ever reported. This seems to guarantee the good electrical performance of the mist deposited $Alq_3$ thin films. However we should take into account of another reason for high resistivity, that is, poor film structure originating from the mist deposition technology. This is also the same for TPD. Therefore, we continued the two sets of experiments, that is, the fabrication and electrical characterization of a MEH-PPV thin film and $Alq_3$/TPD structure, which is equivalent to organic light emitting diode (OLED) structure. MEH-PPV was successfully deposited as an emitting layer (EL) using solution process by other groups [4.4].

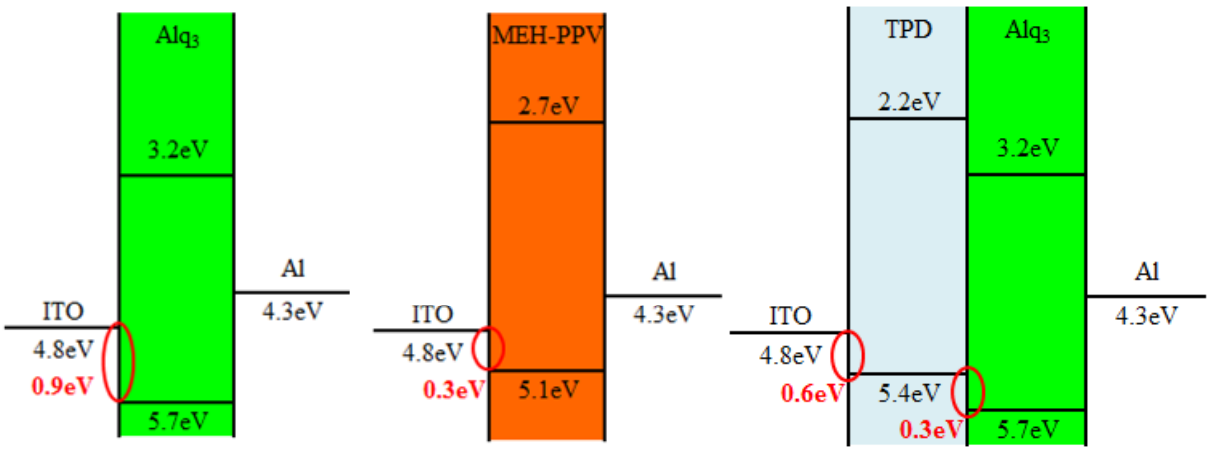


(a) (b) (c)

Figure 4.11 Energy diagrams of (a) $Alq_3$, (b) MEH-PPV, and (c) TPD/$Alq_3$ together with Al and ITO.

## 4.2 Fabrication of TPD thin films

TPD has been widely used as a hole transporting material in multilayer OLEDs [4.5]. Generally, TPD is deposited in OLED devices using vacuum evaporation [4.6]. On the contrary, some groups tried to make TPD layers using spin coating, which is categorized as solution processing [4.7]. However, spin coating is not always suitable for large area devices and results in so many material losses. In our experiments, we applied solution based vapor deposition method to fabricate TPD thin films on ITO substrates, without the use of any dopant or other materials to make precursor solution.

### 4.2.1 Experiments

ITO (10 Ω/sq, thickness = 200 nm) on glass substrates (GEOMATEC Corporation) were cleaned in purified water (10 minutes), acetone (10 minutes), and ozone (15 minutes), successively. 100 mg TPD (Sigma Aldrich) was dissolved in the mixture of 50 ml tetrahydrofuran (THF; not stabilized) and 200 ml methanol. TPD, THF, and methanol were used without further purification. To obtain homogenously dispersion of TPD solution, the solution was mixed for 2 hours by ultrasonic stirring.

TPD organic films were deposited by using ultrasonic spray-assisted vapor deposition method, that is, the mist deposition (as shown in Fig. 4.1). The solution was atomized and mist particle of the solution were generated. They were transferred by nitrogen carrier gas with the flow rate of 6.0 L/min to the substrate area. Near the substrate surface, solvents were vaporized by heat and TPD was deposited onto the substrate.

Organic thin films were deposited on the substrate, and this means the structure of

thin films were influenced by the substrate surface. Surface energy is the most important parameter for thin film deposition. The particle diffusion on substrate is given by

$$\tau_d = \tau_0 \exp (E_b/kT) \quad (4.1)$$

where $\tau_0$ is a constant, $E_b$ is the surface potential, $k$ is the Boltzmann constant, $T$ is the absolute temperature and $\tau_d$ is the residence time on substrate surface [4.8-4.12]. In order to keep the reasonable diffusion $\tau_d$, we need to increase the temperature. But when the surface temperature exceeds 100 ºC, the TPD thin films will be beginning to incinerate by heating [4.13]. Therefore the substrate temperature was set at 100 ºC for optimum vaporization of the solvent, and the nozzle temperature was set at 100 ºC in order to preheat the mist and carrier gas.

The nozzle moved over the substrate at 1.25 mm/min. In the present deposition experiments, the nozzle was scanned on the substrates once, twice, or three times in order to change the thickness of the films and investigate the effects of film thickness on the properties of the films.

Surface morphology of samples was observed with an atomic force microscope (AFM; SII SPI-3800N). Thickness of the thin films deposited on substrates was characterized by measuring the height of steps formed by partially scratching off the thin film from the substrate. A surface profiler (Tencor P-15) was used for the measurement. The optical characterizations were performed using ultraviolet-visible (UV-vis) transmittance spectrometer (Shimadzu UV-1700) and photoluminescence (PL) spectrometer (Hitachi F-2500).

In order to characterize the electrical properties, we fabricated a diode structure as shown in Fig. 4.12, where a TPD layer was sandwiched between cathode (Al, 50 nm) and transparent anode (ITO, 200 nm) on glass fabricated in a metal cross-linked configuration. The current-voltage characteristics were measured between the Al and ITO electrodes using a Keithley source meter (2600 series).

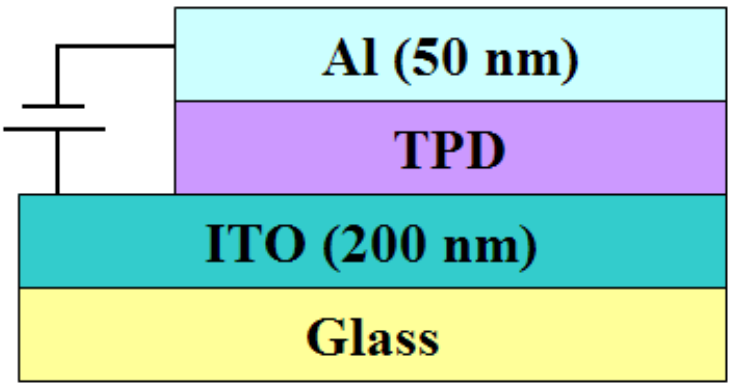


Figure 4.12 Schematic drawing of the TPD diode structure for electrical characterization.

### 4.2.2 Experimental results and discussion

Fig. 4.13 shows the thickness of the thin films against the number of nozzle scanning on the substrates, which from now on we refer as "deposition sequence". The thickness was nearly proportional to the deposition sequence because of the repeated deposition on the underlying films owing to the double and triple scanning of the nozzles. Let us denote the samples (a), (b), and (c), as shown in Fig. 4.13, for the deposition sequence of one, two, and three. The high transmittances of deposited thin films were showed by Fig. 4.14, and the characteristic absorption of TPD at around 365 nm is apparently seen for all samples.

Fig. 4.15 shows the PL spectra of the samples (a), (b), and (c), under the excitation of the 300 nm light. All spectra showed broad emission bands ranging from 350 to 500 nm. The emission peaks appeared at 403 nm, and a broad band in the long wavelength part of the spectrum ($\lambda$ > 390 nm) is observed. These samples showed long wavelength emission. Thus, the long wavelength emission band is not due to the formation of a new chemical species. The photophysical characteristics described above are consistent with excimer formation in the PL of TPD films observed and discussed in the previous studies [4.14)], and therefore we assigned the film actually as TPD. We can see the general tendency that the more intense PL is seen for thicker films, suggesting that the difference in PL intensity is mainly attributable to the thickness of TPD thin films.

Fig. 4.16 shows the surface AFM images of the TPD thin films of (a), (b), and (c). In these results, root-mean-square (RMS) roughness of the surface is 1.56, 3.11, and 2.47 nm for the samples (a), (b), and (c), respectively. This means that, although the

surface RMS roughness tends to be increased for thicker films, it may be at a level that allows the formation of layered structure via the deposition of other materials on the surface.

Fig. 4.17 depicts the current density-applied voltage of characteristics TPD thin films of (a), (b), and (c). The characteristics of sample (a) may include leakage current component, since this is the thinnest sample. On the other hand, those of samples (b) and (c) seem to be dominated by the different film thickness. This suggests the formation of TPD thin films of low leakage current.

These results mean under the proper control of the deposition conditions as well as the proper choice of organic materials, we can expect the formation of OLED devices using the mist deposition method by the layered structures.

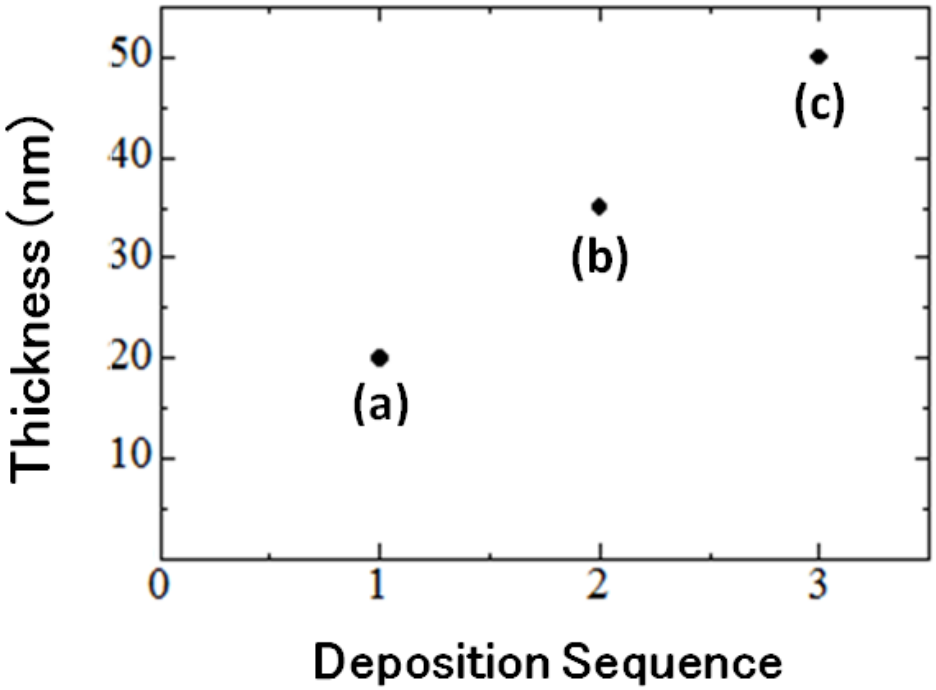


Figure 4.13 Film thicknesses against the different deposition sequence (number of nozzle scanning on the substrates for repeated deposition under the same deposition conditions). Three samples are denoted as (a), (b), and (c) in order for successive characterization.

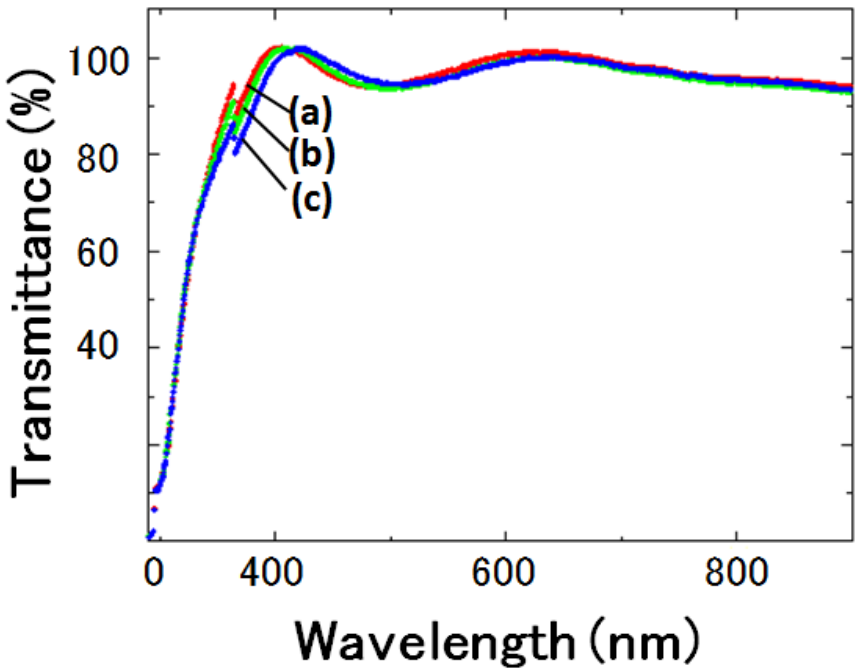


Figure 4.14 Optical transmission spectra of the samples deposited at different deposition conditions.

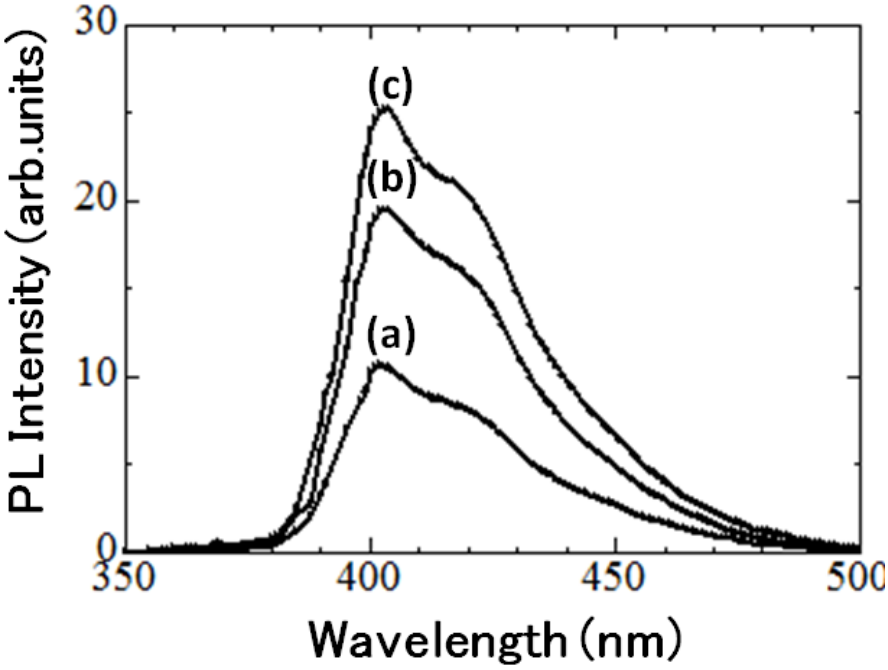


Figure 4.15 PL spectra of the samples (a), (b), and (c).

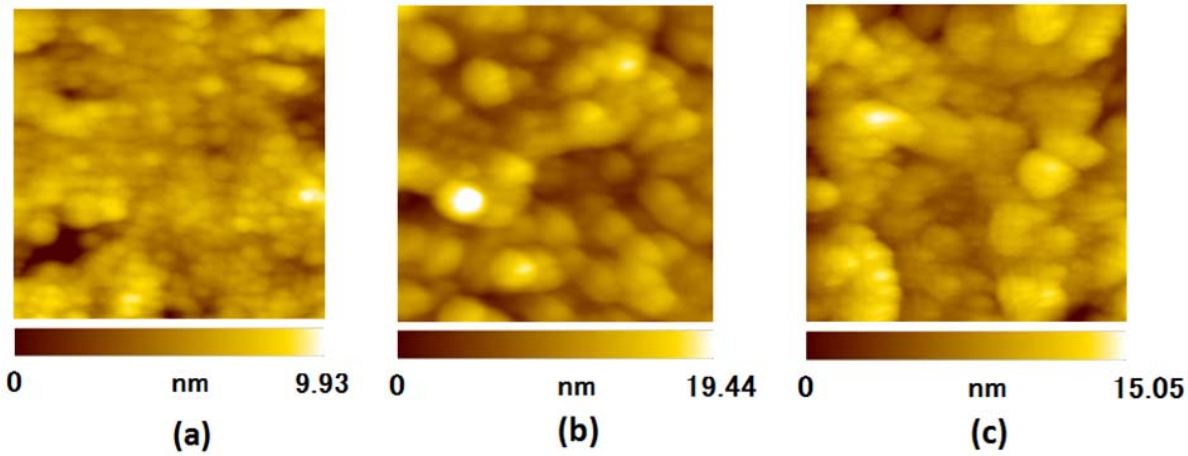


Figure 4.16 Surface AFM images of the samples (a), (b), and (c). Here the scanning area is 1 μm × 1 μm.

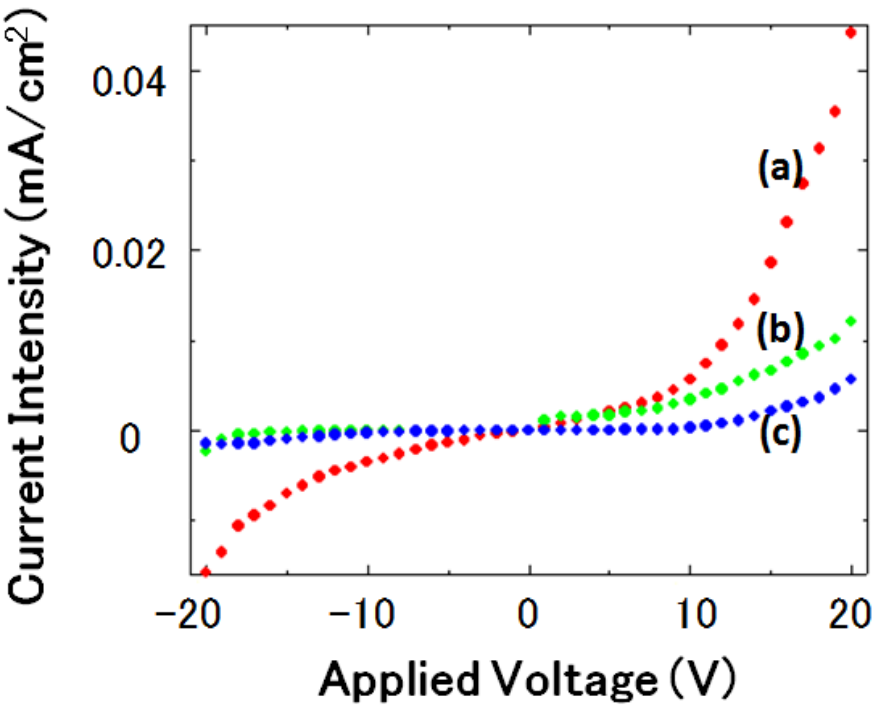


Figure 4.17 Current density-applied voltage characteristics of the samples (a), (b), and (c).

### 4.2.3 Fabrication of ITO/TPD/$Alq_3$/Al structure

20 nm thick TPD thin films were deposited on ITO substrates, and 50 nm thick $Alq_3$ thin films were fabricated on TPD thin films. 11 $mm^2$ Aluminum electrodes were deposited by vacuum evaporation. The thickness is about 50 nm. The schematic illustrations of the diode samples for electrical characterization are shown in Fig. 4.18.

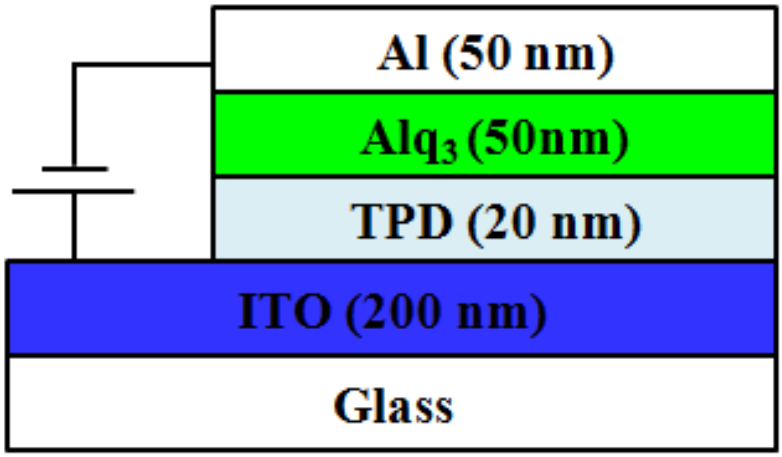


Figure 4.18 Schematic illustrations of $Alq_3$/TPD diode structures for electrical characterization.

Fig. 4.19 shows the characteristics of current density versus applied voltage of $Alq_3$/TPD diode. In $Alq_3$/TPD diode, marked increase of current was observed, in spite of high resistivity measured for $Alq_3$ and TPD diodes. This result means the enhanced carrier injection by taking the $Alq_3$/TPD structure, which was well evidenced by vacuum evaporated samples, and suggests that the high resistance of $Alq_3$ or TPD diodes is not due to poor electrical properties of $Alq_3$ or TPD but due to high barrier height at the metal or ITO junctions.

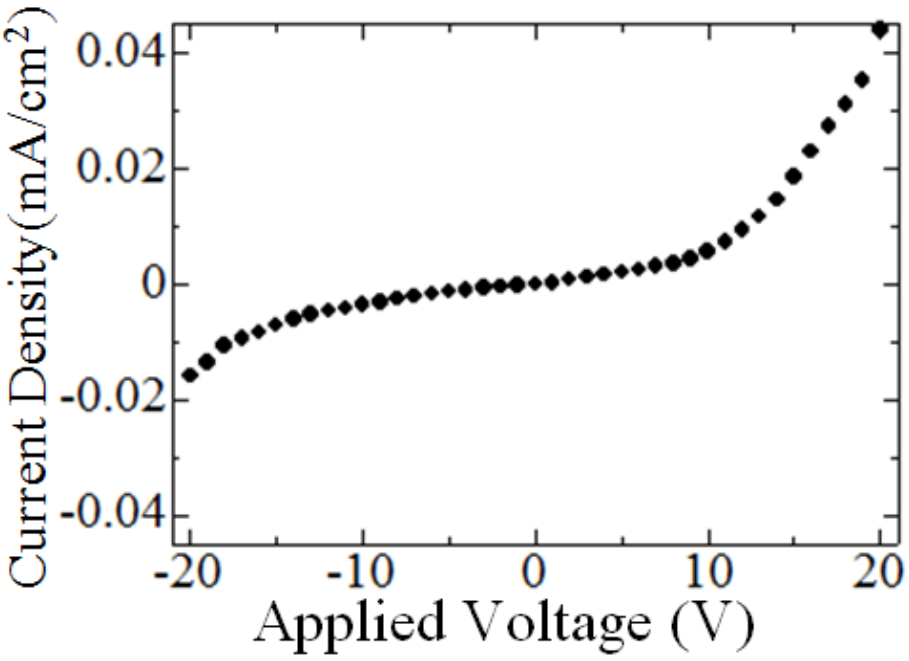


Figure 4.19 Current density versus applied voltage characteristics of $Alq_3$/TPD diode.

## 4.3 Fabrication of MEH-PPV thin films at low temperature

Electroluminescence in conjugated polymer was initially discovered by Burroughes et al in 1990 [4.15] by using poly (p-phenylene vinylene) or PPV which produces green emission. OLED consists of a multilayer structure of an emitting layer sandwiched between a transparent anode, and metallic cathode [4.16]. MEH-PPV as the emitting layer used in this work is a very attractive conjugated polymer that can be used in the application of display technology [4.17]. This material produces orange color when an electric field is applied across the active layer. One of the advantages of this conjugated polymer is its solubility in common organic solvent and its ability to produce a good optical quality film through a simple processing technique such as spin coating. However, spin coating is not always suitable for large area devices and results in so many material losses. In our research, we deposited MEH-PPV thin films by using ultrasonic spray-assisted vapor deposition method (as shown in Fig. 4.1).

As a source solution, 100 mg MEH-PPV (Sigma Aldrich) was dissolved in 100 ml methyl ethyl ketone (2-butanone). ITO (10 Ω/sq, thickness = 200 nm) on glass substrates (GEOMATEC Corporation) were cleaned in purified water (10 minutes), acetone (10 minutes), and ozone (15 minutes), successively.

The source solutions were put into a container shown in Fig. 4.1 and were atomized by ultrasonic power (2.4 MHz). The mist particles formed were transferred by nitrogen carrier gas with the flow rate of 6.0 L/min to the substrate area. In this mist deposition process, the nozzle and substrates temperature was set at 80 °C and 100 °C for the deposition of MEH-PPV thin films, respectively. MEH-PPV thin films were successfully deposited on ITO substrates, and the thickness is about 50 nm, and 50 nm

thicknesses Al electrodes were evaporated on MEH-PPV thin films. This structure is equivalent to OLED structure. The schematic illustration of the diode samples for electrical characterization is shown in Fig. 4.20.

Fig. 4.21 shows the characteristics of current density versus applied voltage of MEH-PPV diode. For the MEH-PPV diode fairly good conductivity was realized, which was supported by the low barrier height for holes of 0.3 eV, as shown in Fig. 4.11 (b), at the ITO/MEH-PPV interface. This suggests that the mist deposition does not cause poor electrical characteristics, originating from electrical defects, of the deposited films, at least for MEH-PPV.

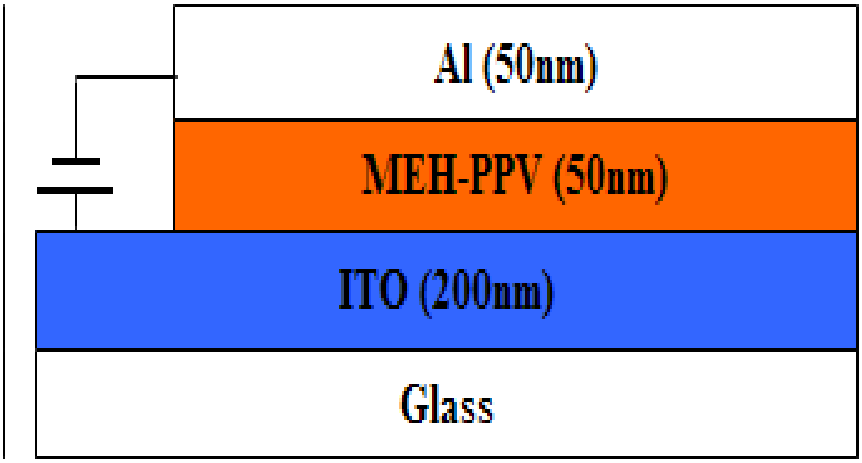


Figure 4.20 Schematic illustrations of MEH-PPV diode structures for electrical characterization.

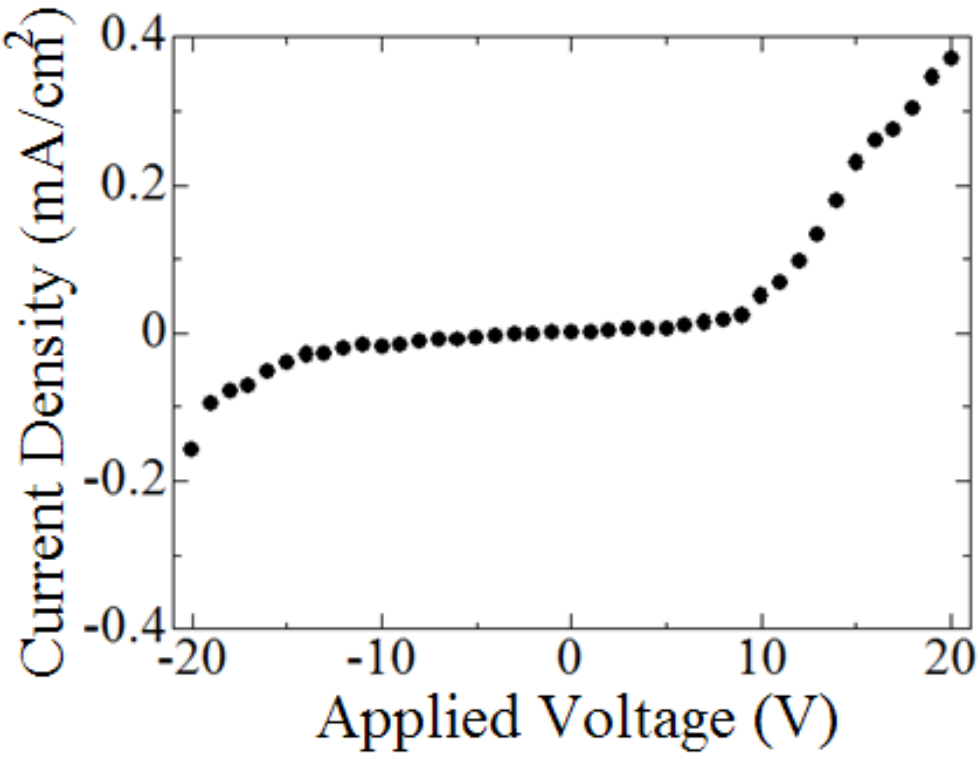


Figure 4.21 Current density versus applied voltage characteristics of MEH-PPV diode.

## 4.4 Discussions

From the characteristics of current density-applied voltage as shown in Fig. 4.9, Fig. 4.19, and Fig. 4.21, we can observe current density is easier to flow when ITO voltage is positive than negative. These results can be explained by potential barriers (as shown in Fig. 4.22). Fig. 4.22 (a) shows $Alq_3$ diodes. When ITO voltage is positive, hole and electron potential barriers are 0.9 eV and 1.1 eV, respectively. When the ITO voltage is negative, the hole potential barrier is 1.6 eV, which is higher than 0.9 eV, resulting in low carrier injection in the films. Other two type diodes, TPD/$Alq_3$ and MEH-PPV, also can be explained by potential barriers.

From the above experiments and discussions we can claim that the mist deposition can form organic thin films without poor electrical properties, that is, without severe electrical defects such as deep levels, interface traps, and wavy mobility edges. This encourages the successive application of the mist deposition for the actual device fabrications.

However at the present stage we have not observed electroluminescence both for MEH-PPV and $Alq_3$/TPD diodes. This is probably caused by air deposition conditions. Humidity, oxygen, or other concentrations in air maybe caused the low carrier density. It also suggests the improvement of nozzle, and can fabricate high quality organic thin films.

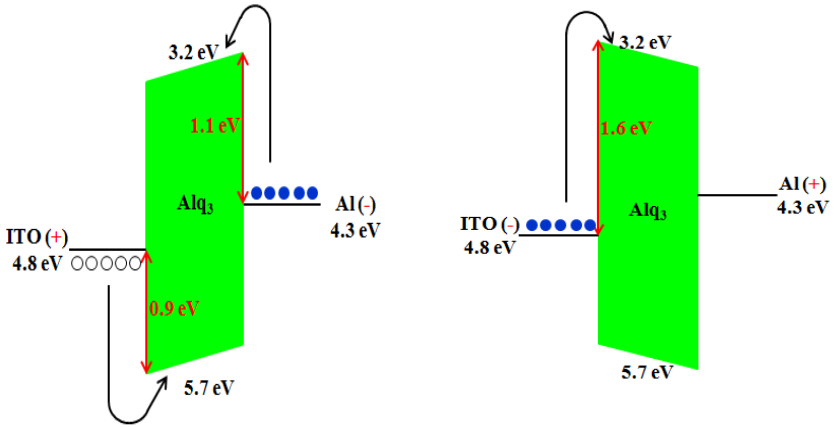


(a)

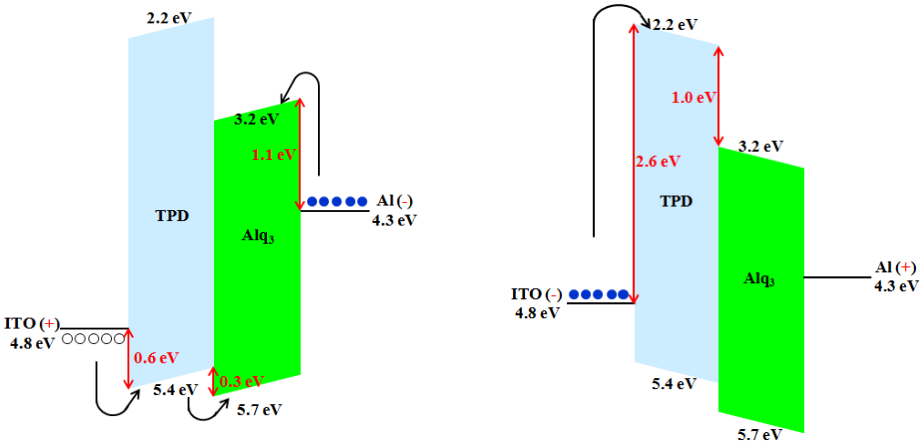


(b)

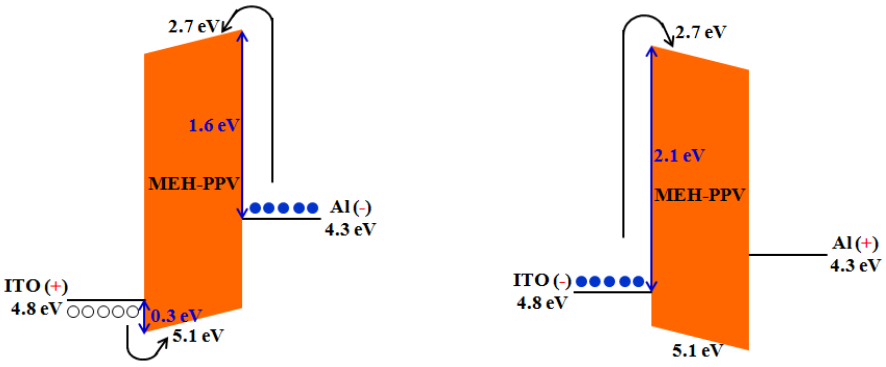


(c)

Figure 4.22 Energy diagrams of (a) $Alq_3$, (b) TPD/$Alq_3$, and (c) MEH-PPV together with Al and ITO.

## 4.5 Conclusions

In this chapter, we successfully demonstrated the formation of organic thin films such as $Alq_3$, TPD, and MEH-PPV by using the ultrasonic spray-assisted mist vapor deposition method. The following conclusions were drawn:

(1) Using ultrasonic spray-assisted mist vapor deposition method, we successively fabricated $Alq_3$ thin films. The surface of $Alq_3$ thin films is reasonably flat, and low leakage current suggests well defined $Alq_3$ thin films without significant electrical defects such as pinholes.

(2) Despite of the flat surface, the current density in $Alq_3$ thin films is low. Maybe it is caused by low carrier density because the energy diagram of Al/$Alq_3$/ITO diode ($Alq_3$ diode) structure shows high potential barriers of 0.9 eV and 1.1 eV. Or maybe it is caused by high resistivity, that is, poor film structure originating from the mist deposition technology. Therefore, we continued the two sets of experiments, that is, the fabrication and electrical characterization of a MEH-PPV thin film and $Alq_3$/TPD structure, which is equivalent to organic light emitting diode (OLED) structure. The improvement of current density means, low current density in $Alq_3$ diode was caused by high potential barriers.

(3) The mist deposition method may be extended to fabricate other materials which have been deposited by other solution based method (for example, spin coating, or dip coating methods) or by vacuum evaporation. This method will offer a simple, large area, and cost effective solution based deposition technique possessing high potential for device formation.

## References and notes


4.1) V.R. Kishore, A. Aziz, K.L. Narasimhan, N. Periasamy, P.S. Meenakshi, and S. Wategaonkar: Synth. Met. **126** (2002) 199.

4.2) D.Z. Garbuzov, V. Bulovic, P.E. Burrows, and S.R. Forrest: Chem. Phys. Lett. **249** (1996) 433.

4.3) J. Piao, S. Katori, T. Ikenoue, and S. Fujita: Jpn. J. Appl. Phys. **50** (2011) 020204.

4.4) Dinh, L.Chi, T. Thuy, T. Trung and H. Kim, J. Physics **187** (2009) 012029.

4.5) J. Shinar, in: Organic Light-Emitting Devices, Springer-Verlag, New York, 2003.

4.6) H. Mu, H. Shen, and K. David: Solid State Electron. **48** (2004) 2085

4.7) P.K. Nayak, M.P. Patankar, K.L. Narasimhan, and N. Periasamy: J. Lumin. **130** (2010) 1174.

4.8) K.E. Ziemelis, A.T. Hussain, D.D.C. Bradley, R.H. Friend, J. Ruhe, and G. Wegner: Phys.Rev.Lett. **66** (1991) 2231.

4.9) G. Horowitz and M.E. Hajlaoui: Synth. Met. **122** (2001) 185.

4.10) A. Salleo, M.L. Chabinyc, M. Yang, and R.A. Street: Appl.Phys. Lett. **81** (2002) 4383.

4.11) F. Heringdorf, M. Reuter, and R. Tromp: Nature **412** (2001) 517.

4.12) S. Hoshino, T. Kamata, and K. Yase: J. Appl. Phys. **92** (2002) 6028.

4.13) T. Yasuda, K. Fujita, and T. Tsutsui: Jpn. J. Appl. Phys. **43** (2004) 7731.

4.14) M. Nagai and H. Nozoye: J. Electrochem. Soc. **154** (2007) J239.

4.15) W.Stampor: Chem. Phys. **256** (2000) 351.

4.16) H. Burroughes, D.D.C. Bradlley, A.R. Brown, R.N. Marks, K. Mackay, R.H. Friend, P.L. Burns and A.B. Holmes: Nature **347** (1990) 539.

4.17) J. Liu, Y. Shi, L. Ma, and Y. Yang: J. Appl. Phys. **88** (2000) 605.

# Chapter 5
# Fabrication of silicon oxide thin films from polysilazane solution at low temperature

Over the past few decades, interest in transparent, thin silicon coatings have increasingly grown for several applications like optics, interlayer dielectrics, and barrier films for the food packaging and medical device industries. Silicon oxide thin films are undoubtedly the most important and widely used insulating films in modern electronic circuit devices. Excellent electrical insulating characteristics of silicon oxide thin films grown by thermal oxidation of silicon (Si) have supported high performance large scale integrated circuit (LSI) devices. On the other hand recent demands for environmentally friendly, lightweight, and mobile devices require evolution of device processes at low temperature in order to meet the required use of plastic substrates or films. In addition, low temperature grown silicon oxide thin films are also highly expected as barrier films against gas and vapor diffusion for food-packaging and medical device industries [5.1-5.4], owing to the transparency, recyclability, and microwave-endurance of silicon oxide, as a candidate substituting thin metal (generally aluminum-based metals) coating.

## 5.1 Materials

Generally, the silicon oxide films are deposited by thermal oxidation with a high temperature of nearly 1000 °C. An excessively high deposition temperature would lead to defect formation and diffusion, such as vacancies, self-interstitial atoms and dislocation [5.5]. Therefore, it is necessary to applying low temperature deposition method for fabrication of silicon oxide films.

For low temperature growth of silicon oxide thin films, vacuum based processes such as vacuum evaporation and sputtering have generally been used, but for electrical applications on large area substrates in mass production, especially on films by a continuous process flow like a roll-to-roll process, it is desirable to use vapor phase growth processes like chemical vapor deposition (CVD). In the CVD process, silane ($SiH_4$) and tetra ethyl ortho silicate (TEOS) have been the well known source materials for the growth of silicon oxide thin films. However, $SiH_4$ is flammable and dangerous in use, and TEOS, though it is a relatively inexpensive and safe source for silicon, requires high temperature, for example, 600 $^{o}$C, which does not meet the growth on plastic substrates.

In our experiments we used polysilazane, $(R_1R_2Si\text{-}NR_3)_n$, as a source material for the CVD growth of silicon oxide. Fig. 5.1 (a) shows the chemical structure of polysilazane, where we can observe no carbon atoms. Polysilazane can react with oxide atoms, making silicon oxides on substrates as shown in Fig. 5.1 (b). Growth of silicon oxide thin films from polysilazane has been reported by thermal decomposition and spin coating, but thermal decomposition needs high temperature and spin coating requires other additional processes such as plasma, vacuum, or heating treatments after

the deposition [5.6-5.11]. In our experiments, we focused on low temperature growth using a mist CVD process, without other additional processes.

## 5.2 Fabrication of silicon oxide thin films at low temperature

### 5.2.1 Deposition method for silicon oxide thin films

Since the vapor pressure of polysilazane is low, it cannot be transferred to the reaction area in gas phase, limiting the use as a CVD source. On the other hand, a mist CVD growth technology has been developed in order for using a variety of source materials even if the vapor pressure is too low to be transferred in gas phase [5.12-5.14]. The key issue is to add ultrasonic power to the source solution and mist particles being atomized are transferred by a carrier gas; so a liquid source can be transferred like a gas source. With this technology our attempts are reported hereafter for the growth of silicon oxide thin films with reasonably high resistivity and breakdown electric field at the lowest temperature of 200 °C.

The schematic of the setup is shown in Fig. 5.2. In the mist CVD method, liquid solution was atomized by ultrasonic power applied to transducers (Honda Electronics, HM2412), where the oscillator voltage and current of an ultrasonic generator were set at 20 V and 1.3 A, respectively. Aerosol or mist particles hence formed are transferred by a carrier gas to the reaction area for the growth of thin films. They are transferred by argon carrier gas with the flow rate of 7.0 L/min to the substrate area. Ozone gas flow rate was set at $5.0\times10^{-4}$ mol /min and the substrate temperature was set at 150 - 350 °C.

The size of mist particles based on experimental data is given by $d=0.34(8\pi\sigma/\rho f^2)$, where $d$ is the number of median particle diameter in cm, $\sigma$ is the surface tension, $\rho$ is the liquid density, and $f$ is the frequency of the waves on the surface of liquid. When $f$ is 3 MHz, $d$ is about 2 μm [5.15].

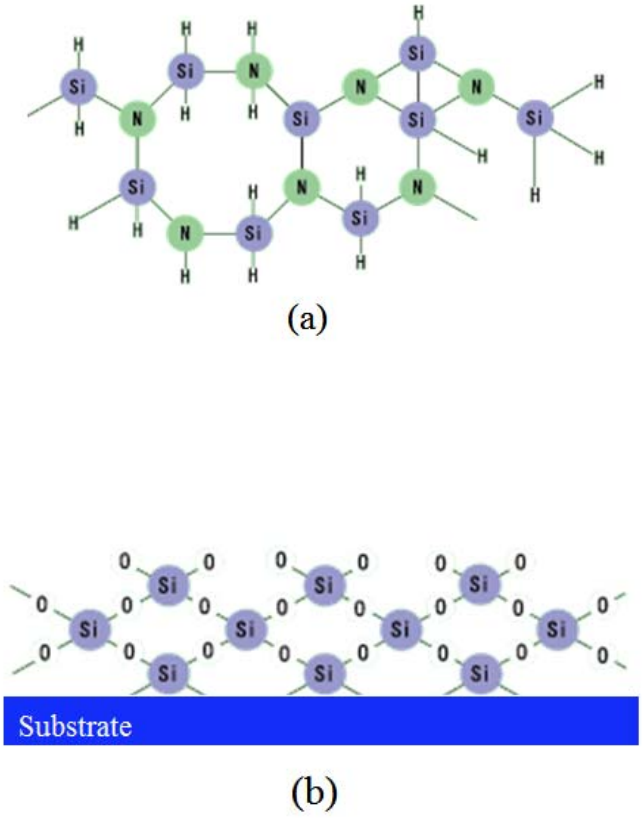


(a)

(b)

Figure 5.1 Chemical structures of (a) polysilazane and (b) silicon oxide on a substrate.

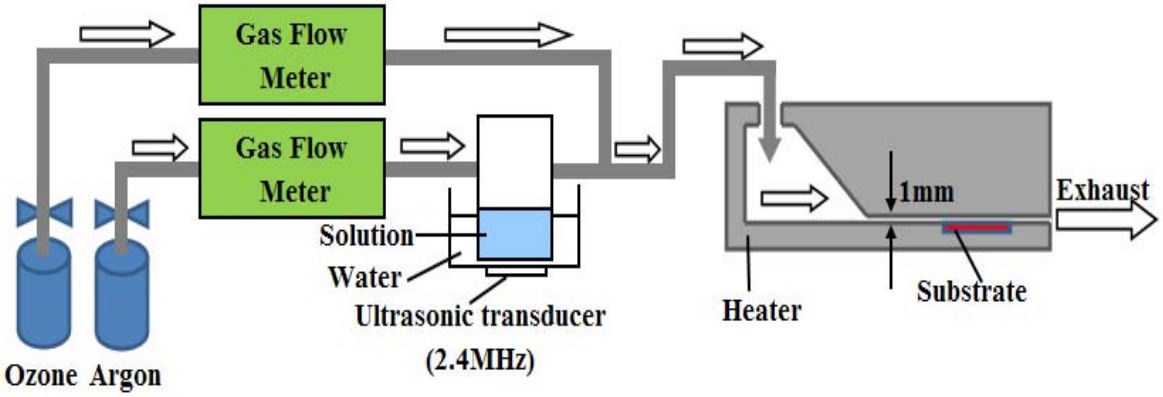


Figure 5.2 Schematic illustration of mist CVD system.

### 5.2.2 Experimental preparation

P-type <100> silicon wafers and indium-tin-oxide (ITO) substrates were used in our experiments. Hydrofluoric acid (HF) was used to remove native silicon dioxide from wafers. ITO (10 Ω /sq, thickness = 200 nm) on glass substrates (GEOMATEC Corporation) were cleaned in purified water (10 minutes), acetone (10 minutes), and ozone (15 minutes), successively. Polysilazane solution (Exousia Inc.) was diluted in methyl acetate (Tokyo Chem. Industry Co. Ltd.) in the concentration of 1%. The thickness and refractive index were determined by ellipsometry (J. A. Woollam JAPAN, WVASE32), and configurations of chemical bonds were characterized by Fourier-transform infrared absorption (FT-IR) spectra (JASCO Corporation, FT/IR-6300). The surface morphology of samples was observed by an atomic force microscope (SII, SPI-3800N). Electrical characterization was made by measuring the current-voltage characteristics with a source meter (Keithley, 2600 series).

### 5.2.3 Results and discussion

Fig. 5.3 shows (a) the growth rate, calculated from the film thickness, and (b) refractive index measured by ellipsometry as a function of the substrate temperature during the growth of silicon oxide ($SiO_x$) films. Since the film composition was not the stoichiometric silicon dioxide ($SiO_2$), hereafter we describe the silicon oxide as $SiO_x$, with which the composition is given by $x$. The growth time was set at either 10 or 5 minutes. At the substrate temperature of 150 °C, the growth ratio was under 0.1 nm/min. The growth rate markedly increased above 200 °C, almost proportional to the

substrate temperature. Despite the different growth time, the growth rate showed no big change, suggesting successive growth on the underlying layer. Comparing with the refractive index of silicon dioxide ($SiO_2$), 1.46, and that of silicon, 3.85, the deposited films tend to silicon-rich films ($x$<2). In our experiments, the refractive index of the film was close to 1.46 at the growth temperature of 200 °C, while increased at higher growth temperature. This suggests that the film composition was close to $SiO_2$ at the growth temperature of 200 °C, while became more silicon-rich as higher growth temperature. This seemed to be caused by more decomposition of polysilazane at higher growth temperatures and there was no enough ozone to complete chemical reactions to deposit silicon oxides, especially at the growth temperature of 350 °C. Component shift is defined as eq. (5.1)

$$\delta = (R_{SiOx} - R_{SiO2}) / (R_{Si}-R_{SiO2}) \quad (5.1)$$

where δ is component shift, $R_{SiOx}$ is refractive index of SiOx, $R_{SiO2}$ is refractive index of $SiO_2$, and $R_{Si}$ is refractive index of Si. Component shift of thin films which deposited at 200 °C, 250°C, and 300 °C, are around 1 %; at 350 °C, the component shift is 5 %. From these results, we can observe the component shift has significant increase at 350 °C.

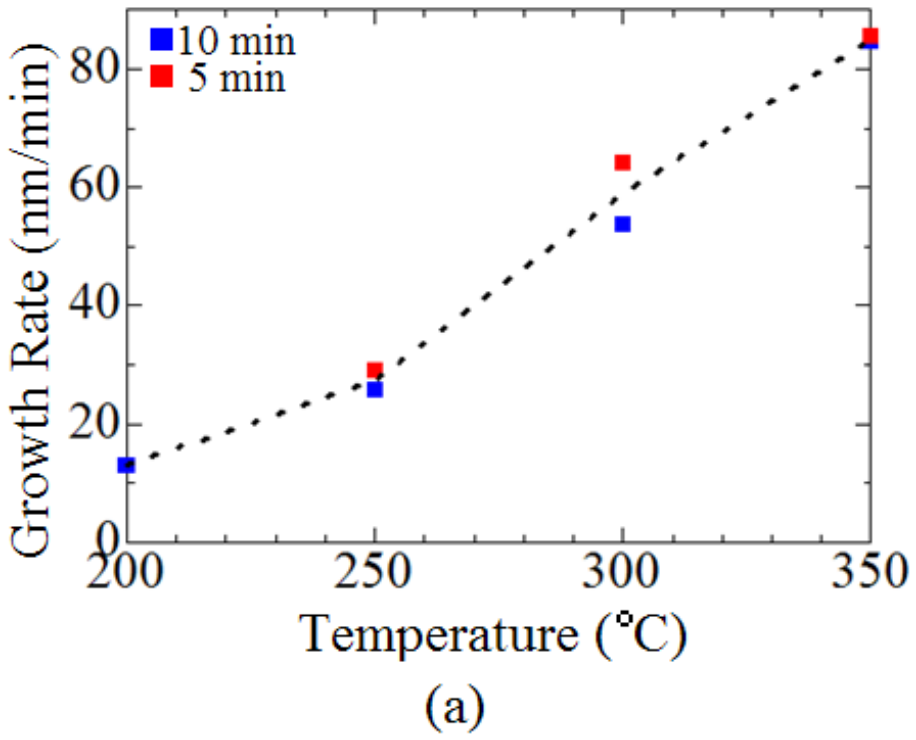


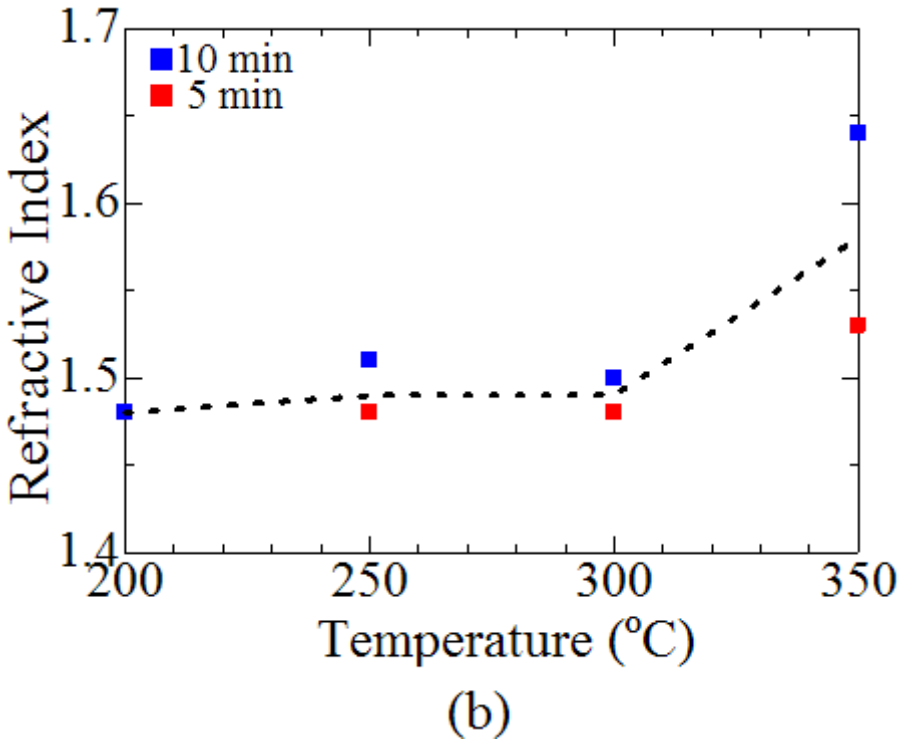


Figure 5.3 (a) Growth rate and (b) refractive index of $SiO_x$ thin films in terms of their growth temperature.

In order to analyze the chemical bond configurations in the deposited films, we prepared about 100 nm thick $SiO_x$ thin films at different growth temperature and characterized them by the FT-IR measurement. Fig. 5.4 shows the FT-IR spectrum for the samples prepared at 200 °C. At the different growth temperatures, 250, 300, and 350 °C, the FT-IR spectra showed the same absorbance peaks as those seen at 200 °C. The absorbance peak at 1060 $cm^{-1}$ can be assignable to the stretching vibration of Si-O groups. The small peaks at 800 and 3400 $cm^{-1}$ can be attributed to the stretching vibration of $Si-CH_3$ groups and of Si-OH groups, respectively [5.16-5.19], suggesting incorporation of unintentional impurities of carbon (C) and hydrogen (H). The origin of these impurities may be caused by chemical reactions between polysilazane and solvents, or be OH bases in polysilazane remained without decomposition; in the future study the influence of these impurities on the film properties should be clarified.

Fig. 5.5 shows the surface of SiOx thin films on p-type <100> silicon wafers deposited at 200, 250, 300, and 350 °C grown for 10 minutes. In these results, RMS (Root Mean Square) of surface is 0.8, 0.5, 0.4, and 1.5 nm, respectively. From the scale showing the vertical height of the films, we can claim that the surface is reasonably flat.

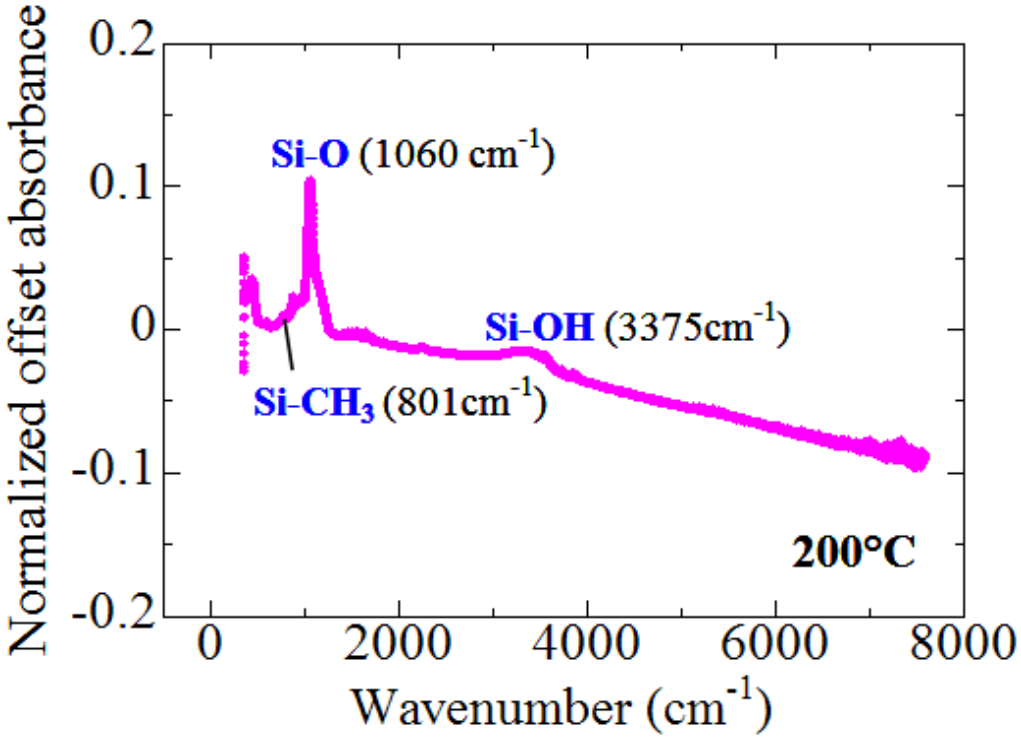


Figure 5.4 An FT-IR spectrums for the film whose $SiO_x$ layer was grown at 200 °C.

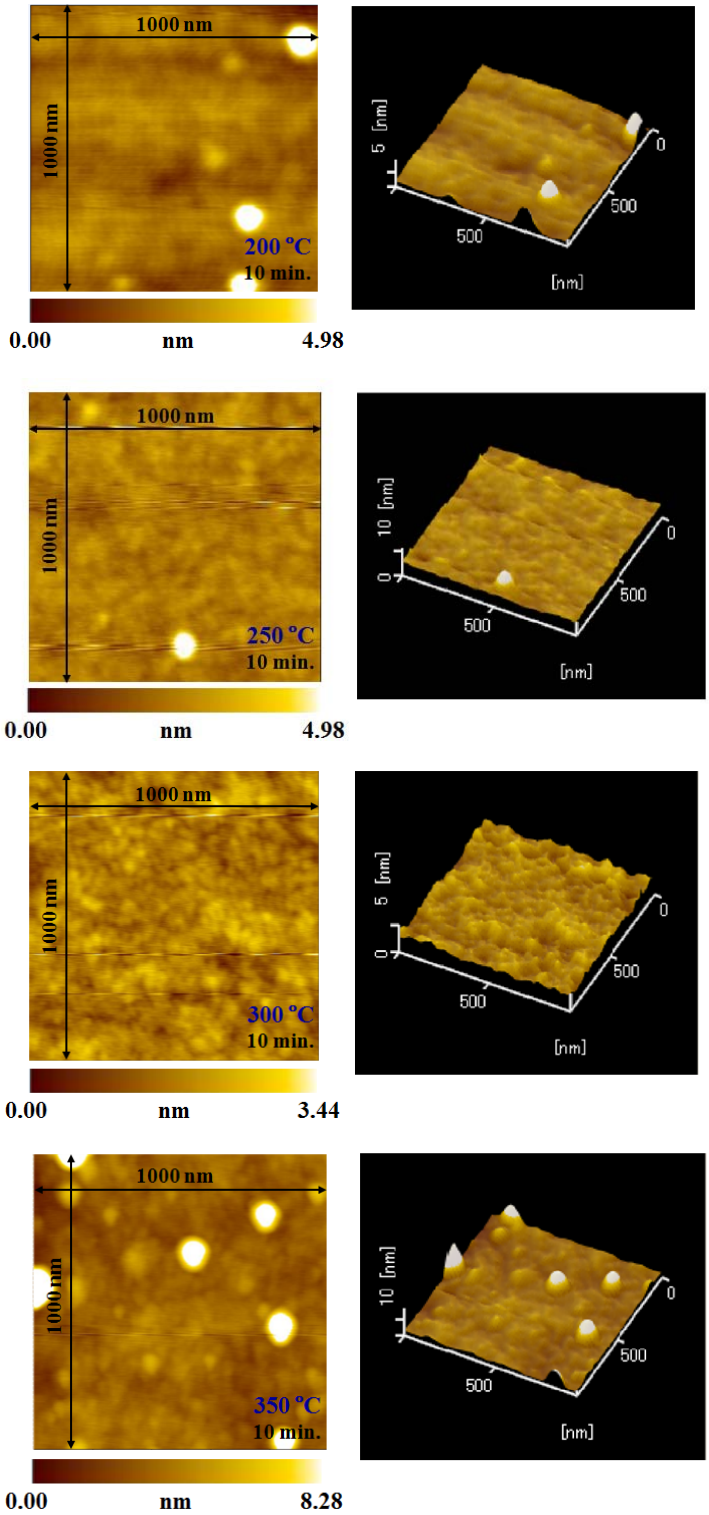


Figure 5.5 Surface AFM images of samples deposited at 200, 250, 300, and 350 °C grown for 10 minutes.

In order to characterize electrical properties, we fabricated 100 nm thick $SiO_x$ thin films on ITO substrates at different temperatures, 200, 250, 300, and 350 °C. Aluminum electrode (50 nm) was deposited by vacuum evaporation on the $SiO_x$ layer to fabricate the samples, as shown in Fig. 5.6, for the electrical characterization. The contact area was 0.4 $mm^2$. Fig. 5.7 (a) - (d) shows the characteristics of current density ($J$) versus applied voltage ($V$) for the samples whose $SiO_x$ layers were grown at 200, 250, 300, and 350 °C, respectively. The differential resistivity at low voltage, for example, $|V| < 10$ V, was as large as $(2\text{-}8)\times10^{15}$ Ω·cm for all samples. The resistivity at $V = 30$ V, obtained from the resistance per unit area $V/J$ at $V = 30$ V, was $(4\text{-}9)\times10^{15}$ Ω·cm for all samples. The breakdown field is higher than 3.5 MV/cm. In spite of the low temperature growth, we can claim that the resistivity is relatively high. Generally improvements of electrical properties are expected for the samples grown at higher temperatures, but in the present experiments the higher growth temperature results in more silicon-rich stoichiometry, as discussed from Fig. 5.3 (b), which seems to obstruct the expected improvements of electrical properties. The present results also suggest the formation of well defined $SiO_x$ thin films without significant electrical defects such as pinholes.

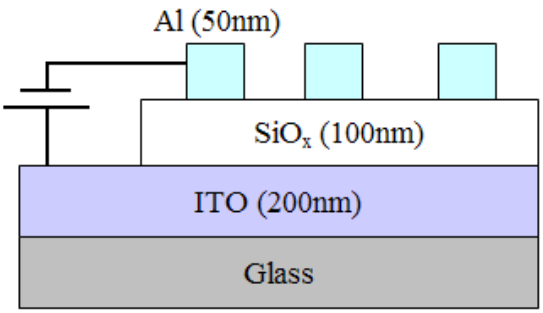


Figure 5.6 Schematic drawing of the $SiO_x$ sandwich structure for electrical characterization.

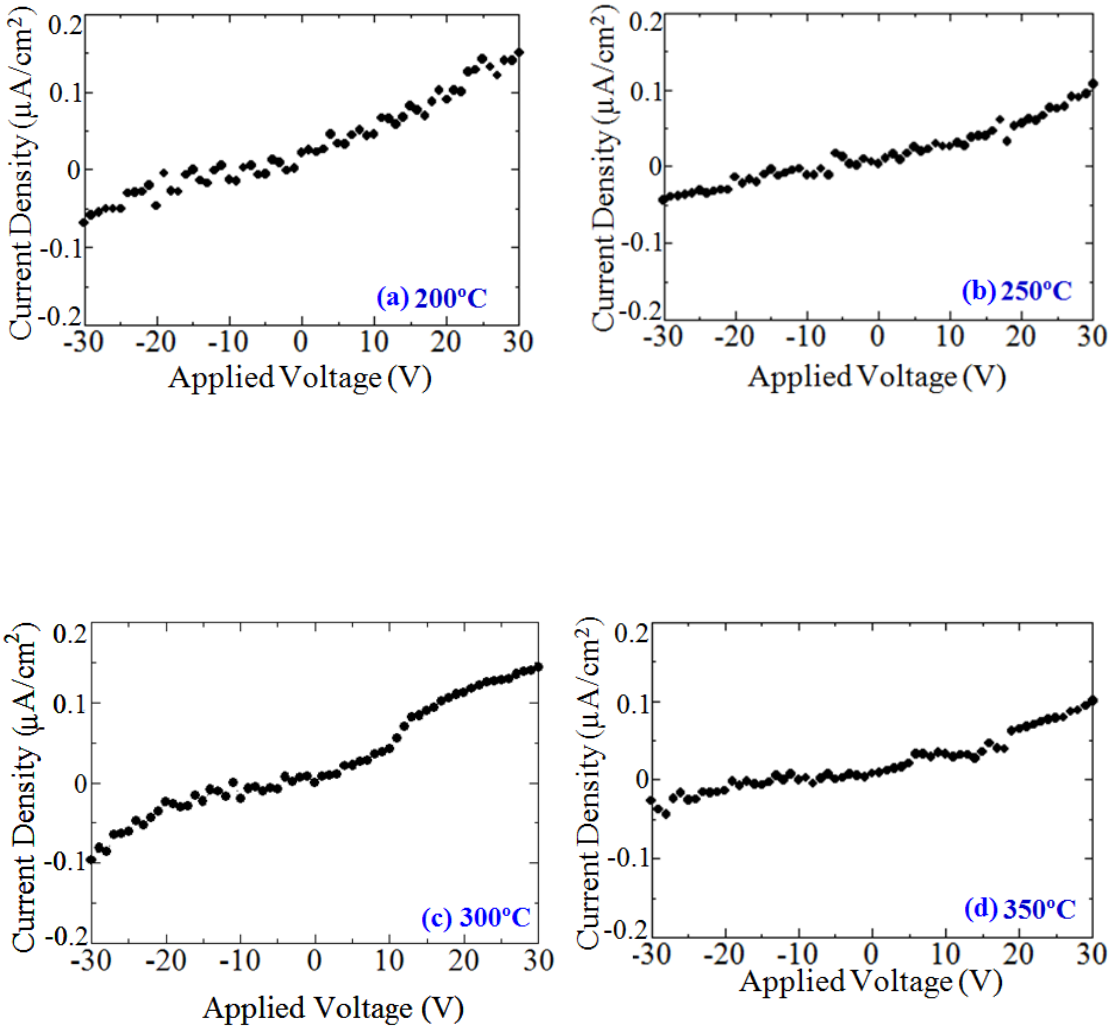


Figure 5.7 Characteristics of current density versus applied voltage for the sample whose $SiO_x$ layer was grown at different temperatures.

### 5.2.4 Additional experiments

As mentioned before, more silicon-rich SiOx thin films as higher growth temperature. Maybe it is caused by more decomposition of polysilazane at higher growth temperatures and there was no enough ozone to complete chemical reactions to deposit silicon oxides, especially at the growth temperature of 350 °C (as shown in Fig. 5.3).

To resolve silicon-rich problems, we increased the ozone gas flow rate and observed the change of refractive index and chemical bond configurations. We deposited silicon oxide thin films on Si <100> wafers. P-type <100> silicon wafers were cleaned by using hydrofluoric acid (HF), and then the native silicon dioxide was removed from wafers. The growth temperature and time were set at 300 °C and 5 minutes, respectively.

Fig. 5.8 shows the refractive index with photon energy as a function of the different ozone gas flow rate set at $5.0\times10^{-4}$, $5.3\times10^{-4}$, and $5.6\times10^{-4}$ mol/min. When ozone gas flow rate was set at $5.3\times10^{-4}$ or $5.6\times10^{-4}$ mol/min, the refractive index is lower than set at $5.0\times10^{-4}$ mol/min, but still be around 1.48, which is higher than silicon dioxide refractive index, 1.46. FT-IR spectrum in Fig. 5.9 means samples still have impurities caused by chemical reactions between polysilazane and solvents.

From mentioned above, we can conclude that increasing ozone gas flow rates can decrease the refractive index, but cannot have significant improvements. So, we tried other treatments, such as annealing treatments.

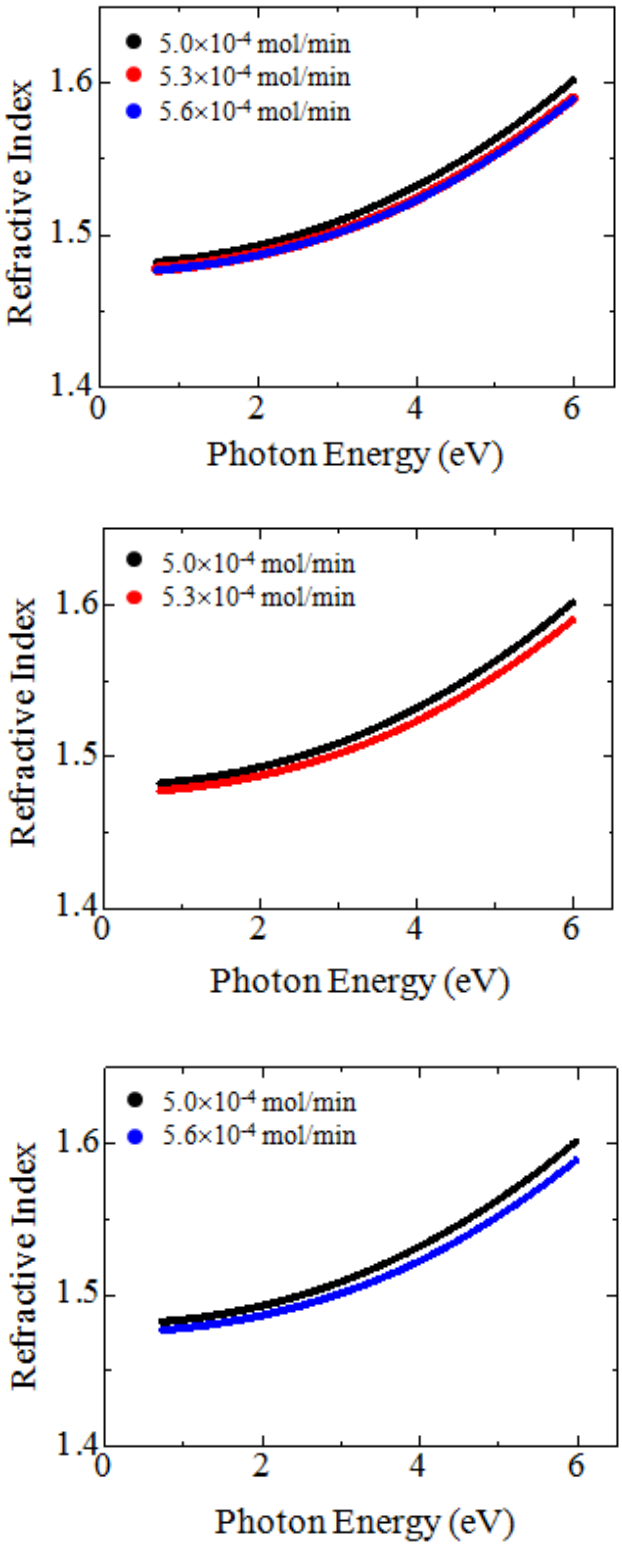


Figure 5.8 Refractive index of SiOx thin films with photon energy set at different ozone gas flow rate.

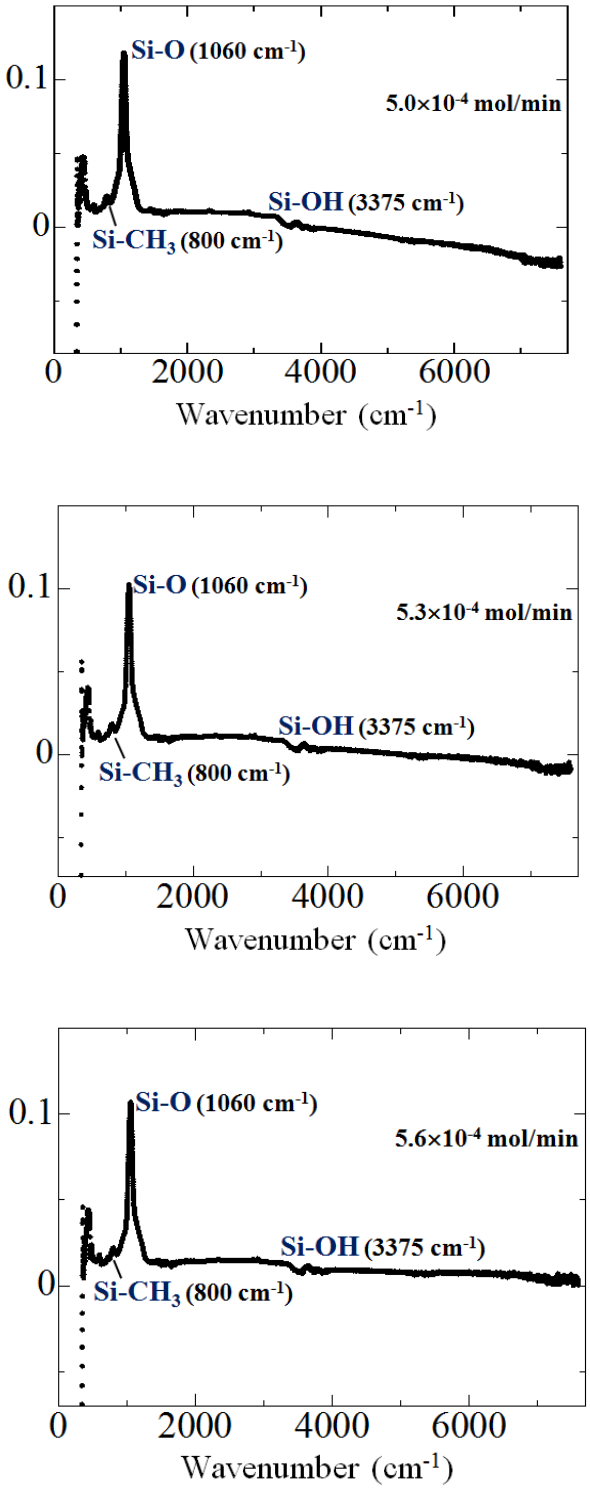


Figure 5.9 FT-IR spectrum of SiOx thin films set at different ozone gas flow rate.

## 5.3 Annealing treatments for silicon oxide thin films

Recently it becomes possible to fabricate silica glass coatings onto various kinds of materials by heating coated polysilazane films. This technique attracts much interest in side area of industry for making protective hard coatings, electrical insulating layers, thermal or chemical resistive films, highly transparent or anti-refraction coatings, and gas barrier coatings. To produce high quality silica glass coatings from the polysilazane precursor, heating processes above 600 °C are necessary. Many research groups demonstrated a room temperature photochemical fabrication of silica glass coatings by utilizing a vacuum ultraviolet (VUV) light irradiation or soaking in hot water process. These processes have one typical problem need long reaction time, even over 6 hours [5.20-5.22)].

In our experiments, we deposited silicon oxide thin films at 200, 250, 300, and 350 °C. As the annealing temperature, the substrate temperature was set at 350 °C, and the time is set at 1 hour and 20 minutes, respectively. If we can resolve the silicon-rich problems through these annealing treatments, means it is possible to improve the quality of silicon oxide films by increasing annealing time, or increasing carrier gas flow rates. In this section, I mainly discuss about the ozone annealing and hot water annealing treatments. Through annealing treatments, the refractive index decreased from 1.48 to 1.45-1.46. These experimental results suggest the silicon-rich silicon oxide problems were improved.

### 5.3.1 Ozone annealing treatments

V.S. Kortov et al. performed with $SiO_2$ samples through the thermal decomposition of polysilazane in air [5.20]. Heating of polysilazane to T = 600 °C for 48 hours in air resulted in the chemical reaction

$$H_xC_yN_zSi + O_2 \rightarrow SiO_2 + \text{gaseous phase.}$$

Our annealing treatments were performed through ozone gas flowing; silicon-rich silicon oxide thin films can react with ozone gas and create silicon dioxide thin films.

$$\text{Silicon-rich SiOx} + O_3 \rightarrow SiO_2 \qquad (5.2)$$

The schematic of the ozone annealing setup is shown in Fig. 5.10. Ozone gas flow to substrate area and the rate was set at $5.0\times10^{-4}$ mol/min. The substrate temperature was set at 350 °C and the annealing time was set at 1 hour.

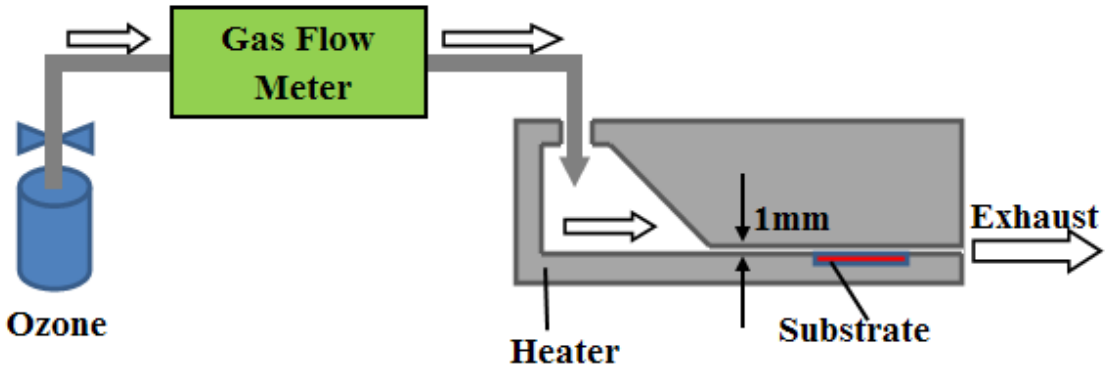


Figure 5.10 Schematic illustration of ozone annealing process.

### 5.3.2 Hot water annealing treatments

In our experiments, we deposited silicon oxide thin films at 300 °C for 5 minutes. 5 minutes is a short time, and we can suppose the possibility that the source materials, polysilazane, were left inside thin films. Polysilazane is also the source materials can react with humidity in air and create silicon oxide thin films. So, we pay attention to the water annealing treatments.

T. Kubo et al. reported that soaking polysilazane coated substrates in hot water, the coatings can be converted to silica films [5.21)]. In their experiments, soaking polysilazane films in 25 °C water for 24 hours can create silica films. 24 hours is a very long time for depositing thin films, and we a little arranged this experiment.

Fig. 5.11 shows the schematic of hot water annealing setup. In this process, water was atomized by ultrasonic power applied to transducers (Honda Electronics, HM2412), where the oscillator voltage and current were set at 20 V and 1.3 A, respectively. Mist particles hence formed are transferred by carrier gas to the substrate area. In this process, the argon carrier gas flow rate is set at 7.0 L/min. The substrate temperature and time were set at 350 °C and 20 minutes, respectively.

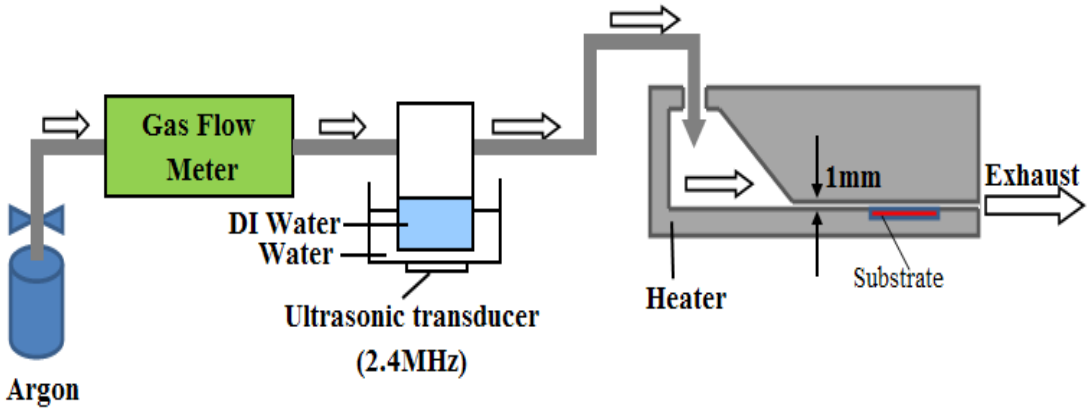


Figure 5.11 Schematic illustration of hot water annealing process.

### 5.3.3 Results and discussion

P-type <100> silicon wafers were used in experiments. Hydrofluoric acid (HF) was used to remove native silicon dioxides from wafers. Polysilazane solution (Exousia Inc.) was diluted in methyl acetate (Tokyo Chem. Industry Co. Ltd.) in the concentration of 1%. Polysilazane is soluble not only in methyl acetate but also in tetrahydrofuran or dichloroethane. However, paying attention to the safety issue, we chose methyl acetate as the proper solvents in our experiments, though physical properties of $SiO_2$ might be better by diluting in other solvents.

Fig. 5.12 shows the refractive index of SiOx thin films with photon energy before and after annealing when the ozone gas flow rate set at (a) $5.0\times10^{-4}$ mol/min, (b) $5.3\times10^{-4}$ mol/min, and (c) $5.6\times10^{-4}$ mol/min. Before annealing, the refractive index is about 1.48; after ozone or hot water annealing, the refractive index decreased to 1.45-1.46. This suggests that the silicon-rich thin films have become to close silicon dioxide films through annealing treatments. With the increasing of photon energy, the refractive index tends to increasing. However, the component shift is still around 2 %, and we can claim that refractive index of silicon oxide thin films are close to silicon dioxide thin films.

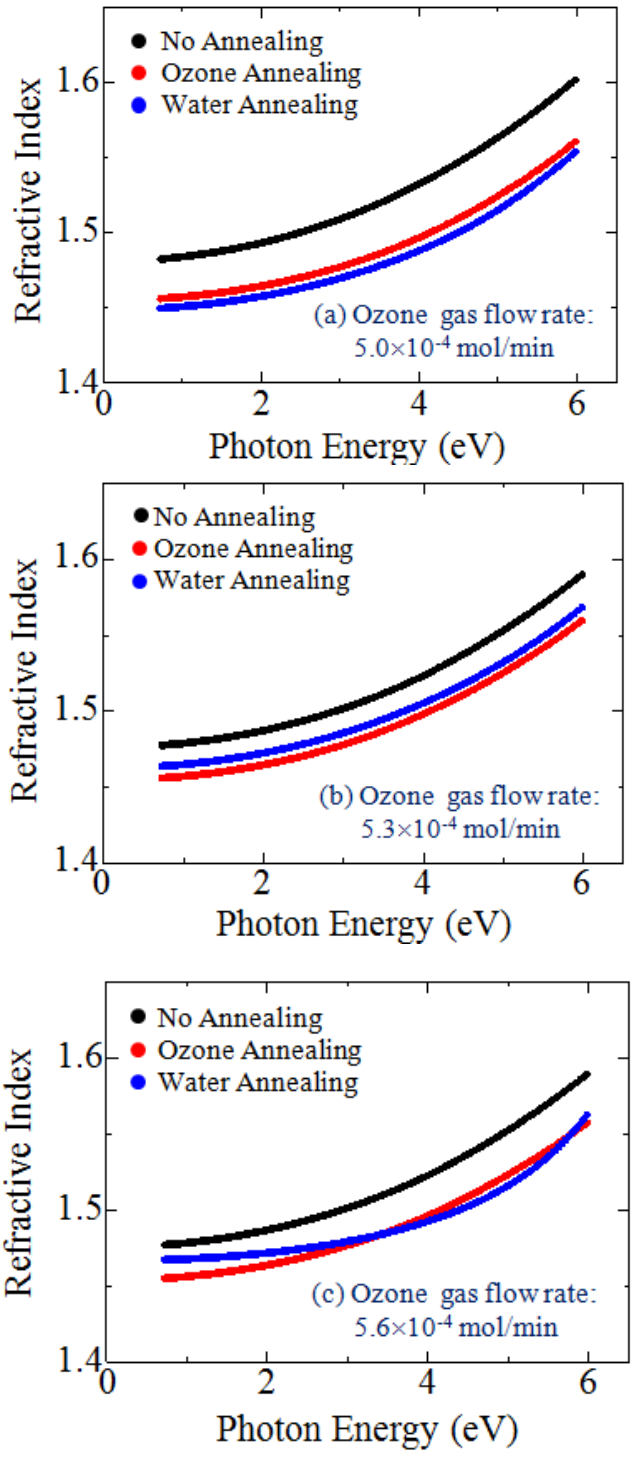


Figure 5.12 Refractive index of SiOx thin films with photon energy before and after annealing when the ozone gas flow rate set at (a) $5.0\times10^{-4}$ mol/min, (b) $5.3\times10^{-4}$ mol/min, and (c) $5.6\times10^{-4}$ mol/min.

In order to analyze the chemical bond configurations and impurities after ozone and hot water annealing treatments, we characterized samples by the FT-IR measurement. Fig. 5.13 shows the FT-IR spectrum of SiOx thin films after (a) ozone annealing and (b) water annealing treatments. After annealing treatments, the impurities of carbon (C) and hydrogen (H) were still be observed. Impurities are unavoidable problems in fabrication of silicon oxide thin films, even using TEOS as the source materials [5.23-5.27]. Comparing with other groups' research, we guess this appearance of impurities maybe caused by short annealing time or insufficient carrier gas flow rates [5.20-5.21].

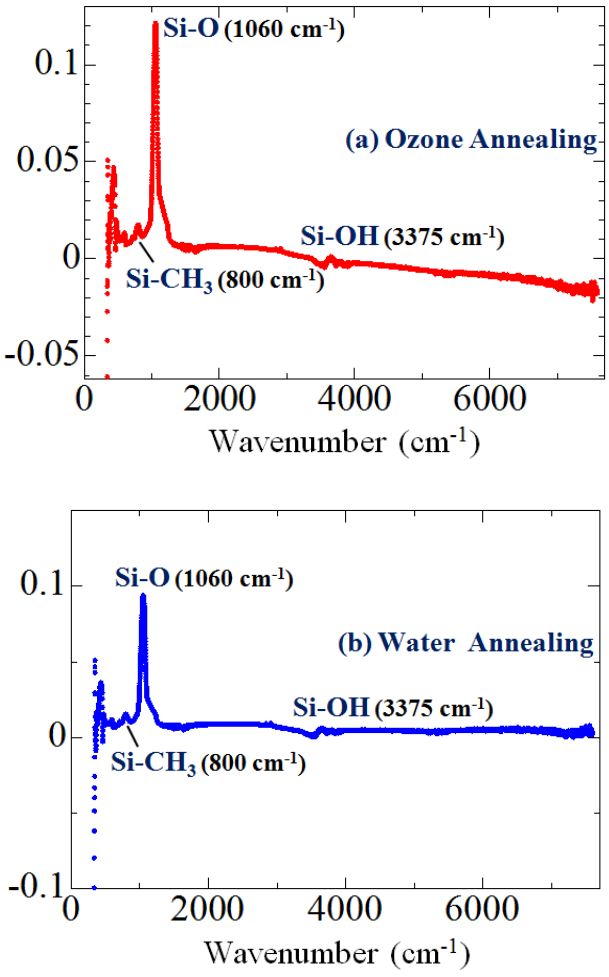


Figure 5.13 FT-IR spectrum of SiOx thin films after (a) ozone annealing and (b) water annealing.

In order to characterize electrical properties, we fabricated thin SiOx thin films at 300 °C for 5 minutes. To obtain accurate resistivity, we deposited thin SiOx thin films on p-Si <100> substrates (0.01-0.02 Ω/sq, thickness = 0.5 mm). Using p-Si <100> substrates, we can measure thicknesses for all samples and also can have relatively accurate resistivity. Circular aluminum electrodes (0.4 $mm^2$ in contact area and 50 nm in thickness) were deposited by vacuum evaporation on the SiOx layer to fabricate the samples, as shown in Fig. 5.14 (a), for the electrical characterization. Fig. 5.15, Fig. 5.16, and Fig. 5.17 show the characteristics of current density (J) versus applied voltage (V) for the samples whose SiOx layers were grown at different ozone gas flow rates of (a) $5.0\times10^{-4}$ mol/min, (b) $5.3\times10^{-4}$ mol/min, and (c) $5.6\times10^{-4}$ mol/min, before annealing, after ozone annealing, and after hot water annealing, respectively.

The resistivity at V=50 V, obtained from the resistance per unit area V/J at V=50 V, was $(2\text{-}3)\times10^{16}$ Ω·cm for all samples. The breakdown field is higher than 4 MV/cm. When the Al electrode is positive, current density is almost same as the Al electrode is negative. These results can be explained by energy diagram is shown in Fig. 5.14 (b). The potential barrier between Al electrode and silicon oxides is same as the potential barrier between silicon wafers and silicon oxides. Same potential barrier resulted in same current density in Al/SiOx/Si diodes.

However, in spite of the low temperature growth, we can claim that the resistivity is relatively high. Further, the low leakage current suggests the formation of well defined SiOx thin films without significant electrical defects such as pinholes.

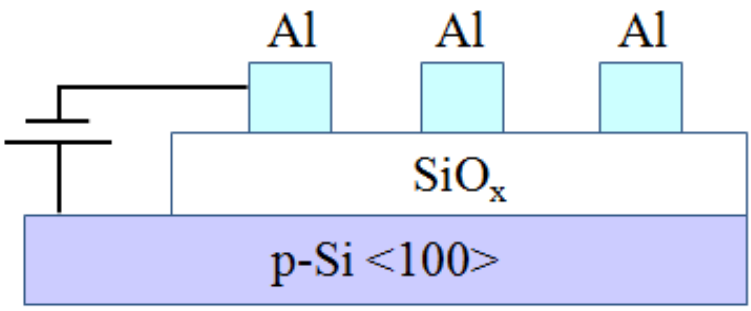


(a)

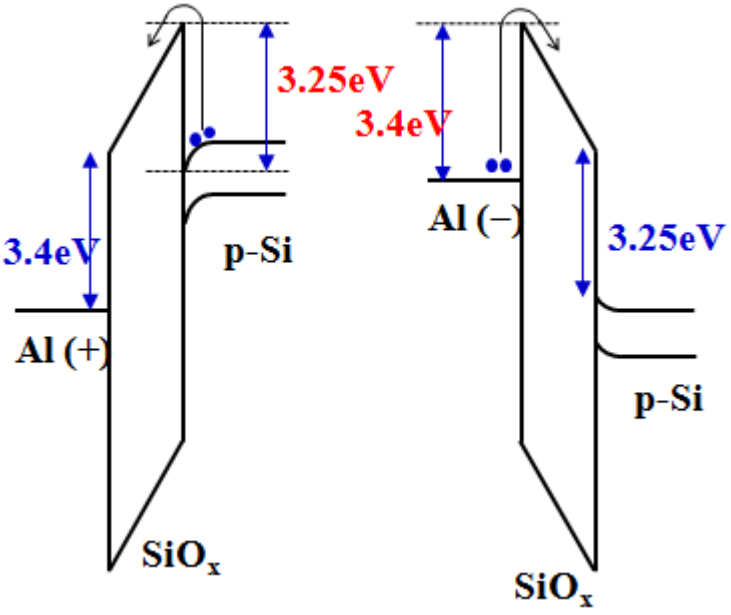


(b)

Figure 5.14 (a) Schematic drawing of the $SiO_x$ sandwich structures, and (b) energy diagrams of Al/SiOx/Si.

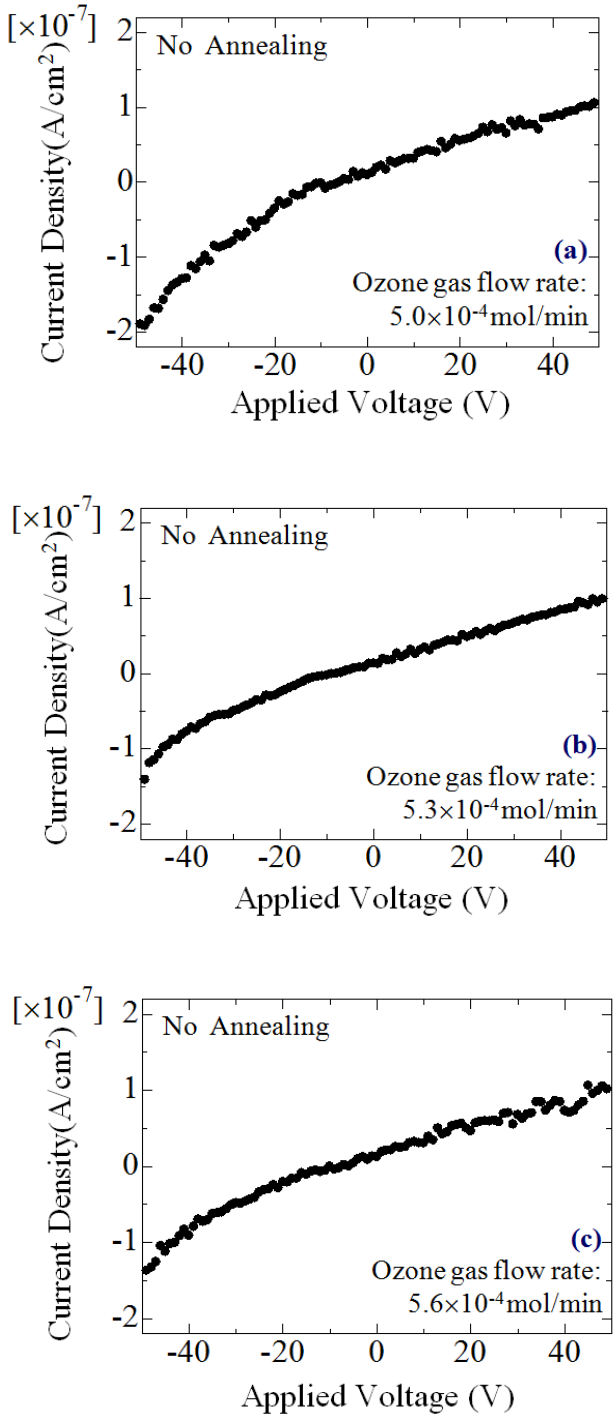


Figure 5.15 Characteristics of current density versus applied voltage for the sample whose $SiO_x$ layer was grown at different ozone gas flow rates (before annealing).

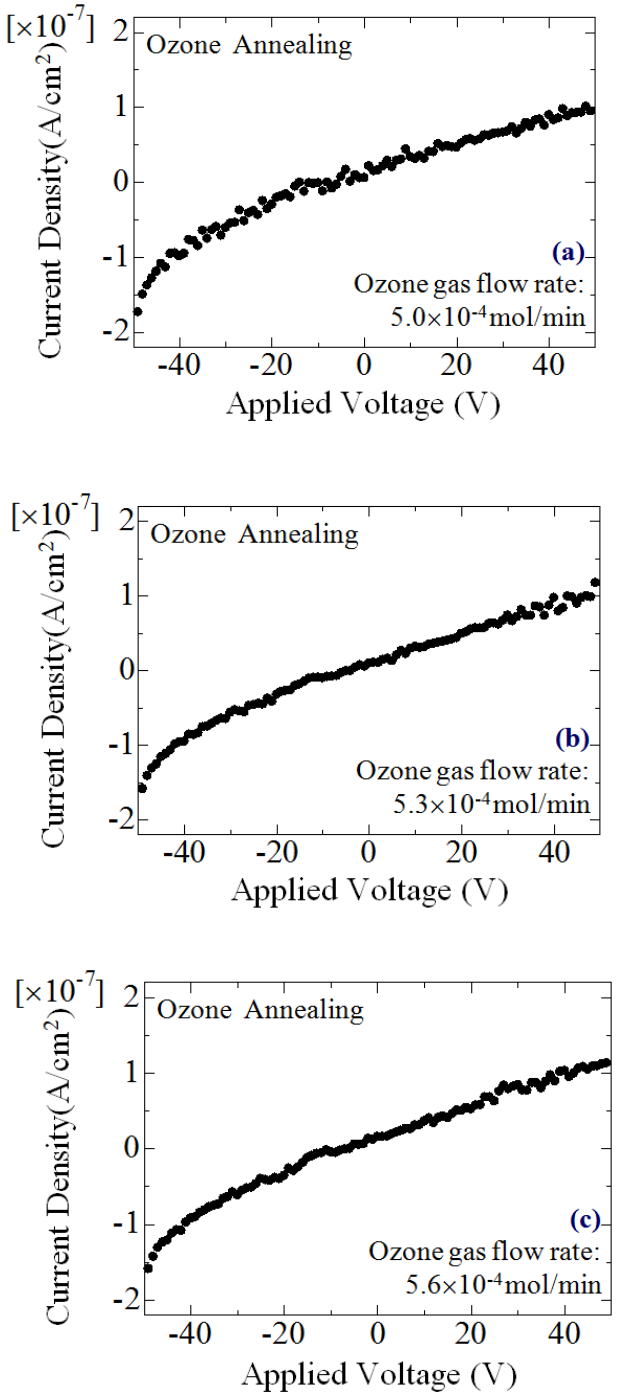


Figure 5.16 Characteristics of current density versus applied voltage for the sample whose $SiO_x$ layer was grown at different ozone gas flow rates (after ozone annealing).

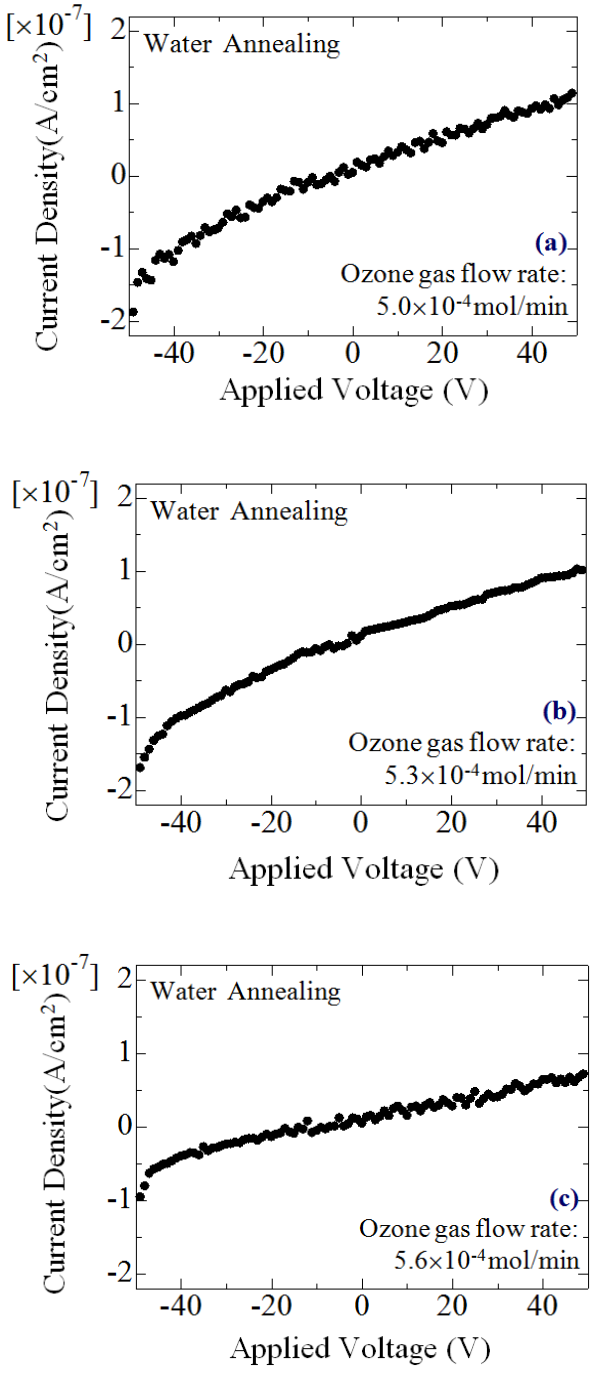


Figure 5.17 Characteristics of current density versus applied voltage for the sample whose $SiO_x$ layer was grown at different ozone gas flow rates (after hot water annealing).

## 5.4 Conclusions

Using polysilazane as the source material of silicon, we demonstrated the successful formation of $SiO_x$ thin films with the mist CVD deposition method at the lowest temperature of 200 °C. With the further research on detailed physical and chemical properties we expect the extended use of mist CVD method for fabrication of $SiO_x$ thin films as barrier films on plastic films.

In this chapter, we successfully demonstrated the formation of silicon oxides thin films with the mist CVD deposition method from polysilazane and ozone as sources. The following conclusions were drawn:

(1) Using polysilazane as the sources materials of silicon, we demonstrated the successful formation of silicon oxides thin films with the mist CVD deposition method at the lowest temperature of 200 °C. The reasonably high electrical insulating characteristics encourage us the application of mist CVD method for fabrication of SiOx thin films as gate or interlayer insulation layer in electrical circuits on plastic substrates.

(2) Increasing the ozone gas flow rates when depositing silicon oxides films can decrease the refractive index, but still have no significant improvements. The silicon oxide thin films still tend to silicon-rich films, and need other additional treatments.

(3) Annealing treatments can decrease refractive index from 1.48 to 1.45-1.46. This suggests that through ozone annealing or hot water annealing treatments, the silicon-rich films can tend to silicon dioxide films. Despite of the improvements of refractive index, the silicon oxide thin films still have the

impurities of carbon (C) and hydrogen (H). With the increasing of the annealing time or carrier gas flow rates, can expect to decrease the impurities in silicon oxide thin films.

## References and notes


5.1) A. Erlat, R. Spontak, R. Cloarke, T. Robinson, P. Haaland, Y. Tropsha, N. Harvey, and E. Vogler: J. Phys. Chem. B **103** (1999) 6047.

5.2) K. Eun, W. Hwang, B. Sharma, J. Ahn, Y. Lee, and S. Choa: Modern Phys. Lett. B **26** (2012) 1250077.

5.3) B. Singh, J. Bouchet, Y. Leterrier, J. Manson, G. Rochat, and P. Fayet: Surf. Coat. Technol. **202** (2007) 208.

5.4) D. Howells, B. Henry, J. Madocks, and H. Assender: Thin Solid Films **516** (2008) 3081.

5.5) X. Xu, L. Li, S. Wang, L. Zhao, and T. Ye, Plasma Sources Sci. Technol. **16** (2007) 372.

5.6) V. Kortov, A. Zatsepin, S. Gorbunov, and A. Murzakaev: Phys.Solid State **48** (2006) 1273.

5.7) C. Kato, S. Tanaka, Y. Naganuma, and T. Shindo: J. Photopolym. Sci. Technol. **16** (2003) 163.

5.8) V. Kortov, A. Zatsepin, V. Guseva, V. Vazhenin, and M. Artyomov: Mater. Sci. Eng. **15** (2010) 012066.

5.9) T. Kubo, E. Tadaoka, and H. Kozuka: J. Mater. Res. **19** (2004) 635.

5.10) C. Vakifahmetoglu, I. Menapace, A. Hirsch, L. Biasetto, R. Hauser, R. Riedel, and P. Colombo: Ceramics Int. **35** (2009) 3281.

5.11) L. Hu, M. Li, C. Xu, Y. Luo, and Y. Zhou: Surf. Coat. Technol. **203** (2009) 3338.

5.12) S. Kawasaki, S. Motoyama, T. Tatsuta, O. Tsuji, S. Okamura, and T. Shiosaki: Jpn. J. Appl. Phys. **43** (2004) 6562.

5.13) T. Kawaharamura, H. Nishinaka, Y. Kamaka, Y. Masuda, J. Lu, and S. Fujita: J. Korean Phys. Soc. **5** (2008) 2976.

5.14) D. Shinohara and S. Fujita: Jpn. J. Appl. Phys. **47** (2008) 7311.

5.15) R. J. Lang: J. Acoustical Soc. America **34** (1962) 6.

5.16) B. Frank, D. Ulrich, D. Andreas, E. Horst, H. Roswitha, L. Hubert, and M. Reiner: Prog. Org. Coat. **53** (2005) 183.

5.17) K. Kusova, O. Cibulka, K. Dohnalova, I. Pelant, J. Valenta, A. Fucikova, K. Zidek, J. Lang, J. Englich, P. Stepanek, and S. Bakardjieva: ACS Nano **4** (2010) 4495.

5.18) C.A. Canaria, I.N. Lees, A.W. Wun, G.M. Miskelly, and M. J. Sailor: Inorg. Chem. Commun. **5** (2002) 560.

5.19) J. E. Bateman, R.D. Eagling, B.R. Horrock, and A.A. Houlton: J. Phys. Chem. B **104** (2000) 5557.

5.20) V.S. Kortov, A.F. Zatsepin, S.V. Gorbuno, and A.M. Murzakae: Phys. Solid State **48** (2006) 1273.

5.21) T. Kubo, E. Tadaoka, and H. Kozuka: J. Mater. Res. **19** (2003) 635.

5.22) C. Kato, S. Tanaka, Y. Naganuma, and T. Shindo: J. Photopolymer Sci. Technol. **16** (2003) 163.

5.23) A.M. Coclite, A. Milella, R. d'Agostino, and F. Palumbo: Surf. Coat. Technol. **204** (2010) 4012.

5.24) D. Rieger and F. Bachmann: Appl. Surf. Sci. **54** (1992) 99.

5.25) J. Lee, E. Chung, W. Moon, and D. Suh: Microelectronic Eng. **83** (2006) 2001.

5.26) J. Kim, S. Jeong, B. Kim, and S. Shim: J. Phys. D: Appl. Phys. **37** (2004) 2425.

5.27) K. Ikeda, S. Nakayama, and M. Maeda: Jpn. J. Appl. Phys. **34** (1995) 2182.

# Chapter 6

# Conclusions and outlook

## 6.1 Conclusions

This chapter is conclusions and outlook for the main result of previous mentioned solution based thin film fabrication at low temperature. I gave successful demonstration of device-element thin film fabrication at low temperature. At the future progress, in order to more detailed study for the materials and deposition method, fabrication of thin films on plastic substrates to create flexible and lightweight devices will become possible. Before going to future scope, here I summarized my thesis as follows:

In Chapter 1, in order to clarify the purpose for the study of device-element thin film formation at low temperature based on solution based formation, I overviewed backgrounds and introductions of materials in devices. Looking back the recent trend of the development of organic and inorganic materials in devices, I stressed the importance of the thin film fabrication at low temperature.

In Chapter 2, I introduced two kinds of mist vapor deposition method. To fabricate large size and flexible thin films, solution based deposition method was mainly used. Mist vapor deposition technology is a solution based method; ultrasonic spray-assisted

mist vapor deposition method and mist chemical vapor deposition (CVD) method were introduced in my thesis. Ultrasonic spray-assisted mist vapor deposition method was used in the fabrication of organic thin films and mist CVD method was used in fabrication of silicon oxide thin films.

In Chapter 3, I demonstrated the preparation of $Alq_3$/methanol solution and polysilazane solution. When preparing $Alq_3$/methanol solution, we applied high ultrasonic power to the mixture of $Alq_3$ and methanol. Through nuclear resonance (NMR) study, can conclude $Alq_3$ atoms have no serious damages even applied high ultrasonic power to $Alq_3$/methanol solution. When preparing polysilazane solution, pay attention to solubility in oxylene and polysilazane, stability in solution, and environmentally friendly, we chose methyl acetate as the solvents.

In Chapter 4, I presented organic thin film fabrication by using mist vapor deposition methods. In order to confirm the impact of making the $Alq_3$ containing solution, we deposited $Alq_3$ thin films on glass and ITO substrates. Despite of the flat surface, the current density in $Alq_3$ thin films is low. Maybe it is caused by low carrier density, or maybe caused by poor film structure originating from the mist deposition technology. To clear these reasons, we continued the two sets of experiments, that is, the fabrication and electrical characterization of a MEH-PPV thin film and $Alq_3$/TPD structure. The improvement of current density means, low current density in $Alq_3$ diode was caused by high potential barriers.

In Chapter 5, I reported silicon oxide thin film fabrication by using mist CVD method.

Polysilazane, inorganic polymer, was used as source material. Polysilazane can react with oxide atoms and create silicon oxide thin films on substrates. Comparing with $SiH_4$ and TEOS, polysilazane is a safe material and can have chemical react at low temperature. Using mist CVD method, silicon oxide thin films were already successfully deposited on flexible polyimide (PI) substrates at 200 °C. The refractive index of the silicon oxide thin films is about 1.48 at the growth temperature of 200 °C, while gradually increased at higher growth temperature up to 300 °C, without other treatments. Marked increase of the refractive index was seen at the growth temperature of 350 °C, together with large sample-to-sample variation. These results mean the silicon oxide thin films have become more silicon-rich films as higher growth temperature. In order to decrease the refractive index, annealing treatments, ozone annealing and hot water annealing, were applied. Through annealing treatments, the refractive index was controlled at 1.45-1.46.

In Chapter 6, I concluded my thesis as described above.

## 6.2 Future outlook

Through this study, approaches for solution based formation of device-element thin films at low temperature were established. However, there are still remaining issues to be solved to improve the formation of organic thin films and silicon oxide thin films.

**Improvement of organic thin film formation:**

In chapter 4, we successfully deposited organic thin films by using solution based mist vapor deposition method at low temperature. However, at present stage we have not observed electroluminescence both for MEH-PPV and TPD/$Alq_3$ diodes. This is probably caused by air deposition conditions, humidity, oxygen, or other concentrations in air maybe caused the low carrier density. It also suggests the improvement of nozzle, and can fabricate high quality organic thin films. Our proposal about the nozzle is shown Fig. 6.1.

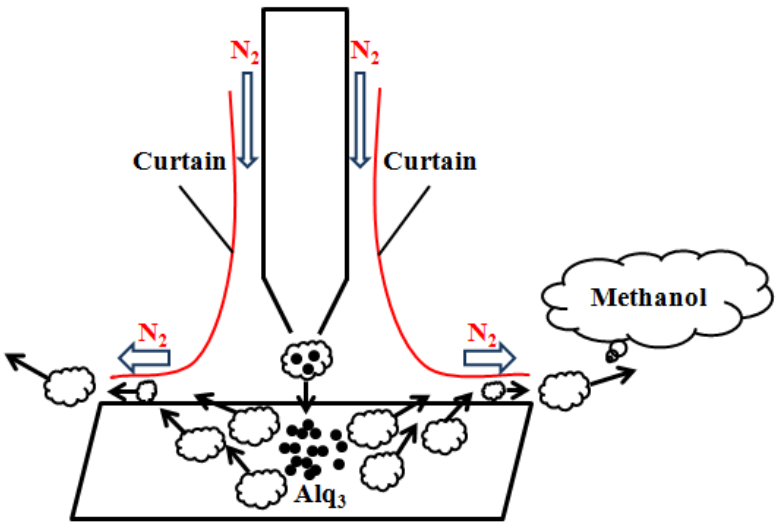


Figure 6.1 Proposal of nozzle improvements

**Improvement of silicon oxide thin film formation:**

In chapter 5, we successfully decreased refractive index by applying annealing treatments. However, the component of impurities not yet be solved. In our experiments, we applied one annealing condition both ozone and water annealing treatments. Additional annealing treatments, such as increasing argon gas flow rates and annealing time in water annealing treatments, or increasing ozone gas flow rates and annealing time in ozone annealing treatments, are necessary to improve silicon oxide thin film formation.

Finally, the author sincerely hopes the formation of device-element thin films based on the technology developed in this study, can be applied to deposit layered structures. Author also hopes this technology can be extended to thin film fabrication on plastic substrates to create flexible, lightweight, and environmentally friendly.

# Acknowledgements

This thesis is a summary of my work conducted at the laboratory of Advanced Electronic Materials, Department of Electronic Science and Engineering, Kyoto University, from 2009 to 2012. Three years went so quickly. I thought my desire was too big when I first decided to come to Japan and also decided to quit my job in China. After starting my life in Japan, there were many times that I lost self-confidence, felt down. Without kind advices and help, I think I cannot finish my doctor course in Japan.

I would like to give my gratitude and acknowledgement to Prof. Shizuo Fujita, Professor of the Department of Electronic Science and Engineering, Kyoto University, for his excellent and persistent supervision together with constant support throughout this work. Undoubtedly, the work could not be completed smoothly without his constructive suggestion and valuable comments. Under his instruction, I have learned the knowledge and skills of being a researcher from conducting a research project, implementing experiments and writing scientific papers. Therefore, again, I would like to express my sincere appreciation to Prof. Fujita.

It is my great pleasure and honor to have two assistant supervisors of this thesis, Prof. Gikan Takaoka and Prof. Yoichi Kawakami, Professors of the Department of Electronic Science and Engineering, Kyoto University. I would like to express my deep gratitude for their critical and careful proofreading of my original manuscript. The valuable remarks and important corrections given by the professors guided me to substantially improve this thesis.

I would like to express my sincere appreciation to Dr. Shigetaka Katori, Department of Electronic Science and Engineering, Kyoto University, for helping to create new idea of research topics and to solve the problems in experiments. Through the friendly discussion with him, I have obtained much significant advice of this work. I also like to show my great gratitude to Dr. Takumi Ikenoue, Department of Electronic Science and Engineering, Kyoto University, for his kind instructions on the operation of the experimental devices.

It is a great honor for me to have research collaboration with the research group of Dr. Toshiyuki Kawaharamura and Dr. Chaoyang Li, Assistant Professor and Associate Professor at Institute for Nanotechnology, Kochi University of Technology. I am sincerely thankful to Dr. Kawaharamura for his great support on providing the experiments apparatus and giving the critical suggestions of the research work in Chapter 5. I would also like to show my honest appreciation to the Dr. Li, for the great help on appointment of comfortable guest house in Kochi University of Technology.

I wish to give many thanks to officers in Rohm Plaza, and the members of the Fujita's Laboratory. Because of their mental and physical support, the life in Japan becomes more colorful and brilliant since first five months as a research student. Without their kind association and warm fellowship, I certainly cannot concentrate on the research.

It is my great fortune to have several nice friends who always give me happiness and encouragement. I will memorize the time being with them; even we are not in same country.

Finally, I would like to express my deepest appreciation to my parents, my brother and his families, and of course, my husband, for their understanding and affectionate support. I will never forget the love they give.

# List of Publications

1. Jinchun Piao, Shigetaka. Katori, Takumi. Ikenoue, and Shizuo Fujita
   "Ultrasonic Spray-Assisted Solution-Based Vapor-Deposition of Aluminum Tris(8-Hydroxyquinoline) Thin Films"
   *Japanese Journal of Applied Physics*, Vol. 50 No. 020204 (2011) pp. 1~3.
2. Jinchun Piao, Shigetaka Katori, Takumi Ikenoue, and Shizuo Fujita
   "Formation of Aluminum Tris (8-Hydroxyquinoline) Solution in Methanol and Fabrication of Thin Films by Ultrasonic Spray-Assisted Vapor-Deposition"
   *Physica Status Solidi (a)*, Vol. 209 No. 7 (2012) pp.1298-1301.
3. Jinchun Piao, Shigetaka Katori, Takumi Ikenoue, and Shizuo Fujita
   "Fabrication of Organic Small Molecular Thin Films based on Ultrasonic Spray-Assisted Vapor-Deposition Method"
   *Materials Research Society Proceedings*, Vol. 1400 No. 201218 (2012) pp.1~6.
4. Jinchun Piao, Shigetaka Katori, and Shizuo Fujita
   "Ultrasonic Spray-Asssisted Mist Vapor Deposition Method for Organic Thin Films Fabrication"
   *J. Nanoscience and Nanotechnology*, submitted.
5. Jinchun Piao, Shigetaka Katori, Toshiyuki Kawaharamura, Chayang Li, and Shizuo Fujita
   "Fabrication of silicon oxide thin films by mist chemical vapor deposition method from polysilazane and ozone as sources"
   *Japanese Journal of Applied Physics,* Vol. 51 No. 9 (2012) 090201.
6. Jinchun Piao, Shigetaka Katori, Toshiyuki Kawaharamura, Chayang Li, and Shizuo Fujita
   "Annealing effects on properties of silicon oxide thin films deposited at low temperature by mist chemical vapor deposition method"
   in preparation.

# Conferences

## International Conferences

1. Jinchun Piao, Shigetaka Katori, Takumi Ikenoue and Shizuo Fujita
   "Ultrasonic Spray-Assisted Solution-Based Vapor-Deposition of Functional Thin Films and Their Applications"
   2011 Materials Research Society Fall Meeting, Boston, USA, (Nov.28-Dec.2, 2011) #S6.19 [poster, Nov.30].
2. Jinchun Piao, Sam-Dong Lee, Shigetaka Katori, Takumi Ikenoue, Kentaro Kaneko and Shizuo Fujita
   "Spray-Assisted Vapor-Deposition Method as a Cost-Effective and Environmental-Friendly Technology for Fabrication of Novel Devices"
   2012 European Materials Research Society Spring Meeting, Strasbourg, France (May 14-18, 2012) #Q2.6 [oral, May 14].
3. Jinchun Piao, Shigetaka Katori, Takumi Ikenoue and Shizuo Fujita
   "Ultrasonic Spray-Assisted Mist Vapor Deposition Method for Organic Thin Films Fabrication"
   2012 European Materials Research Society Spring Meeting, strasbourg, France (May 14-18, 2012) #H13.4 [oral, May 17].

## Domestic Conferences

1. Jinchun Piao, Shigetaka Katori, Takumi Ikenoue and Shizuo Fujita
   "Spin-coating deposition and characterization of Alq3 thin films"
   2010 Fall Meeting Japan Society of Applied Physics, Nagasaki, Japan (Sept. 14-17, 2010), #17a-K-1 [oral, Sept. 17].